GENETIC CODE EXPANSION OF PLASTIC-DEGRADING ENZYMES FOR DETECTION OF
MICROPLASTICS

Miss Jariya Jitdee

จุฬาลงกรณ์มหาวิทยาลัย
CHULALONGKORN UNIVERSITY

A Thesis Submitted in Partial Fulfillment of the Requirements

for the Degree of Master of Science in Chemistry

Department of Chemistry

FACULTY OF SCIENCE

Chulalongkorn University

Academic Year 2021

การขยายรหัสพันธุกรรมของเอนไซม์ย่อยสลายพลาสติกเพื่อการตรวจวัดไมโครพลาสติก

น.ส.จริยา จิตรดี

Thesis Title	GENETIC CODE EXPANSION OF PLASTIC-DEGRADING ENZYMES FOR DETECTION OF MICROPLASTICS
By	Miss Jariya Jitdee
Field of Study	Chemistry
Thesis Advisor	Associate Professor WORAWAN BHANTHUMNAVIN, Ph.D.
Thesis Co Advisor	Chayasith Uttamapinant, Ph.D.

Accepted by the FACULTY OF SCIENCE, Chulalongkorn University in Partial Fulfillment of the Requirement for the Master of Science

.... Dean of the FACULTY OF SCIENCE

(Professor POLKIT SANGVANICH, Ph.D.)

THESIS COMMITTEE

.... Chairman

(Professor VUDHICHAI PARASUK, Ph.D.)

.... Thesis Advisor

(Associate Professor WORAWAN BHANTHUMNAVIN, Ph.D.)

.... Thesis Co-Advisor

(Chayasith Uttamapinant, Ph.D.)

.... Examiner

(Assistant Professor NAWAPORN VINAYAVEKHIN, Ph.D.)

.... External Examiner

(Assistant Professor Chutima Jiarpinitnun, Ph.D.)

จริยา จิตรดี : การขยายรหัสพันธุกรรมของเอนไซม์ย่อยสลายพลาสติกเพื่อการตรวจวัด
ไมโครพลาสติก . (GENETIC CODE EXPANSION OF PLASTIC-DEGRADING
ENZYMES FOR DETECTION OF MICROPLASTICS) อ.ที่ปรึกษาหลัก : รศ. ดร.วรว
รรณ พันธุมนาวิน, อ.ที่ปรึกษาร่วม : ดร.ชยสิทธิ์ อุตมาภินันท์

งานวิจัยนี้มีจุดประสงค์เพื่อสังเคราะห์กรดอะมิโนที่ไม่มีอยู่ในธรรมชาติคือ สารประกอบ
อนุพันธ์ของ 2,3-ไดอะมิโนโพรพิโอนิก แอซิด และนำไปใช้ในเทคนิคขยายรหัสทางพันธุกรรมเจ
เนติกโคดเอ็กซ์แพนชัน ลงบนเอนไซม์ย่อยสลายพลาสติก เพื่อเปลี่ยนแปลงสมบัติของเอนไซม์จาก
ย่อยสลายพลาสติกให้จับกับพลาสติกโดยไม่เกิดการย่อยสลายใด ๆ ทำให้สามารถใช้ประโยชน์จาก
สมบัตินี้ได้หลากหลายมากขึ้น โดยการใช้กรดอะมิโนที่ไม่มีอยู่ในธรรมชาติเข้ารหัสแทนที่กรดอะมิโน
ที่มีหน้าที่ที่บริเวณเร่งในเอนไซม์ ซึ่งการสังเคราะห์อนุพันธ์ของ 2,3-ไดอะมิโนโพรพิโอนิก แอซิด
สามารถทำได้ตามกระบวนการทดลองของ นิโคลัส เดซอท และคณะ ที่ได้รายงานไว้เมื่อปี พ.ศ
2562 อย่างไรก็ตามในการทดลองบางขั้นตอนมีการปรับเปลี่ยนสารที่ใช้เข้าทำปฏิกิริยา และทุก
ขั้นตอนมีการปรับเปลี่ยนเวลาที่ใช้ดำเนินการทดลอง ซึ่งทั้งหมดนี้เพื่อปรับปรุงเงื่อนไขของปฏิกิริยา
ให้สำเร็จและเหมาะสมมากที่สุด โดยจะมีทั้งหมด 7 ขั้นตอน และสามารถทำปริมาณผลได้ของ
ผลิตภัณฑ์รวมทุกขั้นตอนทั้งสิ้น 7 % สารที่ได้สามารถตรวจสอบยืนยันโครงสร้างได้จากเทคนิค
เอ็นเอ็มอาร์สเปกโทรสโกปี จากนั้นทดสอบระบบของการขยายรหัสทางพันธุกรรมของเอนไซม์ย่อย
สลายพลาสติกเพทเอส โดยการนำยีนส์เพทเอส เอนไซม์อะมิโนเอซิล ทีอาร์เอ็นเอ ซินทีเทส และที
อาร์เอ็นเอ ซึ่งต้องมีความจำเพาะต่อกรดอะมิโนที่ไม่มีอยู่ในธรรมชาติเข้าสู่เอสเชอริเชีย โคไล เซลล์
โดยผลคือระบบที่ได้พัฒนาขึ้นสามารถเหนี่ยวนำเซลล์แบคทีเรียให้ผลิตโปรตีนที่ต้องการได้ และ
สามารถจะต่อยอดนำไปปรับใช้กับกรดอะมิโนที่ไม่มีอยู่ในธรรมชาติตัวอื่น ๆ เพื่อเปลี่ยนแปลง
สมบัติของโปรตีน นำมาซึ่งการใช้งานและประโยชน์ที่จะได้รับแตกต่างกัน ทั้งนี้เป้าหมายในอนาคต
หรือการศึกษาเพิ่มเติมต่อยอดสามารถทำได้ทั้งในด้านของการนำไปใช้เป็นตัวตรวจวัดพลาสติก
ควบคู่กับเทคนิคการเรืองแสง การศึกษาโครงสร้าง และความจำเพาะเจาะจงหรือรูปแบบของการ
เกิดปฏิกิริยาระหว่างเอนไซม์และพลาสติก

สาขาวิชา	เคมี	ลายมือชื่อนิสิต ....
ปีการศึกษา	2564	ลายมือชื่อ อ.ที่ปรึกษาหลัก ....
		ลายมือชื่อ อ.ที่ปรึกษาร่วม ....

6172121923 : MAJOR CHEMISTRY

KEYWORD: PLASTIC-DEGRADING ENZYMES, PETase, GENETIC CODE EXPANSION, DAP, UNNATURAL AMINO ACID, PET

Jariya Jitdee : GENETIC CODE EXPANSION OF PLASTIC-DEGRADING ENZYMES FOR DETECTION OF MICROPLASTICS. Advisor: Assoc. Prof. WORAWAN BHANTHUMNAVIN, Ph.D. Co-advisor: Chayasith Uttamapinant, Ph.D.

Petrochemical plastics can degrade into the size level of microplastics. One source of microplastics is polyethylene terephthalate (PET or PETE). Enzymes used to degrade PET have been reported. In our work, we wish to repurpose the activity of PET-degrading enzymes, into PET-detecting enzymes, and use the engineered enzyme for microplastic detection, *via* enzyme engineering to create enzyme variants which can form covalent adducts with microplastic particles. The enzyme-microplastic adduct is generated *via* the use of 2,3-diaminopropionic acid (DAP) derivative, which we will incorporate in place of the catalytic serine residue at the active site of *I. sakeinesis*—PETase *via* the genetic code expansion technique. Working toward this goal, we have successfully synthesized 2,3-diaminopropionic acid (DAP) derivative. The synthetic methods were carried out with improvements to the protocols previously reported in literature, in seven steps and an overall yield of 7 %. The compound was structurally characterized by nuclear magnetic resonance (NMR) spectroscopy. Moreover, we cloned an expression vector for PETase, in which its catalytic serine codon is replaced with an amber stop codon—marking it as a site for unnatural amino acid incorporation and demonstrated the expression of the PETase protein bearing an unnatural amino at the active site serine in *Escherichia coli* using amber-suppressor pyrrolysyl tRNA and its corresponding pyrrolysyl-tRNA synthetase enzyme.

Field of Study:	Chemistry	Student's Signature ....
Academic Year:	2021	Advisor's Signature ....
		Co-advisor's Signature ....

ACKNOWLEDGEMENTS

Jariya Jitdee

TABLE OF CONTENTS

จุฬาลงกรณ์มหาวิทยาลัย

CHULALONGKORN UNIVERSITY

LIST OF FIGURES

จุฬาลงกรณ์มหาวิทยาลัย
CHULALONGKORN UNIVERSITY

LIST OF ABBREVIATIONS

Boc-DAP-OH	N^{α}-BOC-(S)-β-aminoalanine
br	broad signal (NMR)
brs	broad singlet (NMR)
$CDCl_3$	deuterated chloroform
CH_3COOH	acetic acid
d	doublet (NMR)
dd	doublet of doublet (NMR)
DCM	dichloromethane
DMSO	dimethyl sulfoxide
EtOAc	ethyl acetate
Et_3SiH	triethylsilane
eq.	equivalent
g	gram
Hz	hertz
J	coupling constant
kDa	kilodaltons
m	multiplet (NMR)
M	molar
MeCN	acetonitrile

MeOH	methanol
mg	milligram
MHz	megahertz
mL	milliliter
mm	millimolar
mmol	millimole
mol	mole
MS	mass spectrometry
m/z	mass-to-charge ratio
NMR	Nuclear Magnetic Resonance
OD_{600}	Optical density (wavelength of 600 nm)
ppm	Part per million
q	quartet (NMR)
R_f	retention factor
s	singlet (NMR)
SDS-PAGE	Sodium dodecyl-sulfate polyacrylamide gel electrophoresis
t	triplet (NMR)
Temp.	temperature
THF	tetrahydrofuran
TLC	thin layer chromatography
UV	ultraviolet

wt.   weight

[M$^+$]   molecular ion

[M-H$^+$]   protonated molecular ion

δ chemical shift

°C   degree Celsius

μL   microliter

%   percent

CHAPTER I

INTRODUCTION

1.1.   Plastic

Plastics are organic polymers whose monomers are mostly derived from fossil fuel-based natural resources, particularly crude oil and natural gas. Due to their high thermostability and plasticity, plastic polymers can be adapted to produce a wide range of consumer products, including clothes, bags, food packaging, and scaffolds for appliances and devices. Heavy consumption of plastic-based products and their integration into everyday life result in the generation of large amount of plastic waste. Such global surplus of plastic waste is a grave environmental problem, which is exacerbated by the fact that all frequently used fossil fuel-based plastics cannot be naturally degraded in a short time span.

Plastics raise many complexes, which the aquatic organisms are highly variable spatially, even within relatively enclosed bodies of water.[1] More than 700 marine species animals were reported to feed on marine debris worldwide.[2] Microplastics can have a chemical, physical, and biological effect on organisms that ingest them directly and on organisms that indirectly consume contaminated prey. In addition, plastics can degrade to small pieces called microplastics.[3]

Microplastics are small pieces of plastic, less than 5 mm (0.2 inches) in length, that are present in the environment due to plastic pollution. Microplastics come from various sources, including larger plastic debris that degrades into smaller pieces.[4] Some investigations of microplastics focused on microbeads in personal-care products and pellets of virgin plastic, along with fragments that slowly erode from discarded bottles and other large debris. All these have been washed into rivers and oceans. In 2015, oceanographers estimated that between 15 trillion and 51 trillion microplastic particles were floating in surface waters worldwide. [5]

Microplastics are divided into two types: primary and secondary. Primary microplastic are those already existing in less than 5 mm in size. Examples of primary microplastics include microbeads found in personal care products, plastic pellets used in industrial manufacturing, and plastic fibers used in synthetic textiles. Secondary microplastics form from the breakdown of larger plastics. One type of plastic majorly contributing as a source of microplastics is polyethylene terephthalate (PET), which is primarily used in clothes, packaging, and drink bottles. PET is a condensation polymer produced by the esterification of ethylene glycol (EG) with terephthalic acid (TPA) or dimethyl terephthalate (DMT). PET is a clear, strong, and lightweight plastic widely used for packaging foods and beverages, especially convenience-sized soft drinks, juices, and water.[6] PET can be biochemically degraded with many hydrolytic enzymes. Therefore, degradation or even detectable process of PET microplastics are highly desirable.
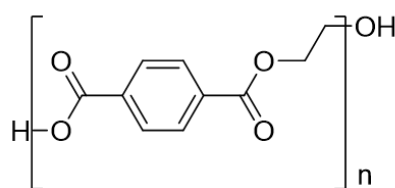
Polyethylene terephthalate (PET)
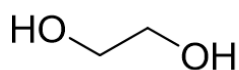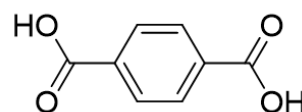
Ethylene glycol (EG)   Terephthalic acid (TPA)

Figure 1.1 Polyethylene terephthalate (PET) structure and their monomers.

1.2. Identification methods of microplastic

The detection of microplastics in environmental samples by visual inspection is cheap and relatively easy, but the results could be full of errors.[7] Large microplastics

in the range from 1 to 5 mm, mainly plastic pellets from the raw material in plastic production, were identified since the earliest studies during ocean surface water sampling or in beach sediments by visual identification with the naked eye based on the plastic color and shape.[8] Sometimes, the colors of the plastic material are similar to those of natural particles or other materials such as glass. Moreover, portions of plastic particles are not easily visible. This is a high probability of missing these particles or overestimating the microplastic pollution by false-positive identification without other analytical methods.

More highly reliable techniques employ spectroscopic means. Currently used methods for identification of microplastic are as follows:

1.2.1. Microscopy

The stereomicroscope is useful and widely used to identify microplastics whose dimensions fall within the range of hundreds of microns. The stereo microscope allows three-dimensional analysis by observing the sample from two slightly different angles to obtain the two images significant for stereoscopic vision.[9] The first fast-screening method allows rapid identification of the particles' shape, size, and color. However, this method cannot confirm the type of the plastic.

1.2.2. FTIR spectroscopy

Most molecules absorb light in the infrared region of the electromagnetic spectrum.[10] FTIR spectroscopy takes advantage of the infrared radiation that excites molecular vibrations when interacting with a sample.[11] This absorption is characteristic of the nature of the chemical bonds present in a sample. FTIR is able to confirm functional group present in microplastics. The technique can also detect small plastic particles (lower than 20 μm in size) with μ-FTIR.

1.2.3. Scanning Electron Microscopy (SEM)

Scanning electron microscopy (SEM) is a microscopic technique that provides information about the morphological surface structure of microplastics, generating high-resolution images of the surface state. Furthermore, it can give data on the chemical composition of the samples.[9] The advantage is clear and high-resolution images of particles. On the other hand, this method is expensive and time-consuming. In addition, problems on lack of information on the type of polymer still exist.

1.2.4. Raman Spectroscopy

Raman Spectroscopy is a non-destructive chemical analysis technique that provides information about chemical structure, phase, polymorphism, crystallinity, and molecular interactions. It is based upon the interaction of light with the chemical bonds within a material. [12] A Raman microscope couples a Raman spectrometer to a standard optical microscope, allowing high magnification visualization of a sample and Raman analysis with a microscopic laser spot. Analysis of samples in solution, gas, film, surface, solids, and single crystals is possible. However, the disadvantage is detection needs sensitive and highly optimized instrumentation. Fluorescence of impurities or of the sample itself can hide the Raman spectrum. Some compounds fluoresce when irradiated by the laser beam.[13]

1.2.5. Staining technique

In 2019, Erni-Cassola and coworkers[14] reported a protocol that allowed high-throughput detection and automated quantification of small microplastic particles (20–1000 μm). The method utilized a combination of Nile red dye, fluorescence microscopy, and image analysis software. Commonly applied methods separate synthetic microparticles from nonsynthetic materials *via* density separation techniques before visually sorting the particles and finally confirming their identity *via* spectroscopy.

Their study presents the application of a fluorescence-based protocol using Nile red to detect and quantify small microplastics in environmental samples. Nile red had been suggested as a tool for fluorescently labeling microplastics. Staining efficacy and automated particle detection were tested on nine polymer types: PE, PET, PVC, nylon-6, PP, PS, PC, PUR, and black tire rubber.

They tested the fluorescence of these polymers stained with Nile red on PC track-etched filter membranes (PCTE) in green and red. The result showed fluorescence-based automated detection of microplastics on PCTE membranes was 100% for four polymer types (i.e., PE, PP, PS, and nylon-6). All 10 particles of each respective polymer were detected with ImageJ using appropriate threshold for pixel brightness.

As fluorescence intensity varied with polymer type and thickness, the original setting for the pixel brightness threshold in macro for ImageJ was optimized to capture all particles with strong fluorescence. This could also represent particle size accurately, using bright-field images as size references. Examples are illustrated in Figure 1.2.
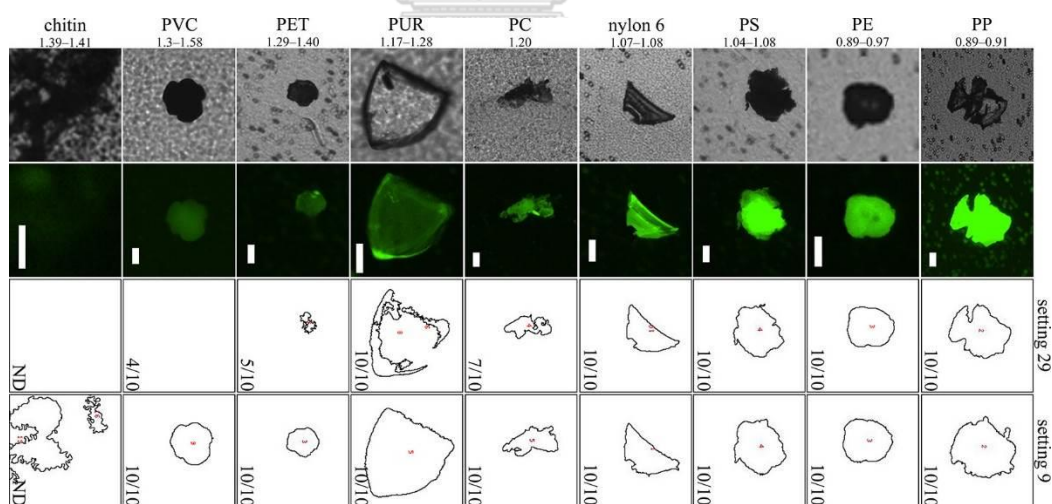
Figure 1.2 Microscope and ImageJ images of microparticles of different polymer types on PCTE filter membranes stained with Nile red at various pixel brightness settings. [14]

1.3. Advantages and disadvantages of identification methods

In 2015, Song and coworkers[15] compared microscopic and spectroscopic identification methods to analyze microplastics in environmental samples. The microscope method for the identification of microplastics is easier and faster than FT-IR. Nevertheless, microplastics <1 mm in size are possible to be missed. Many translucent or white fragments were identified as synthetic polymers, such as polyethylene and polypropylene by FTIR but were not counted as microplastics using the microscope (Figure. 1.3).
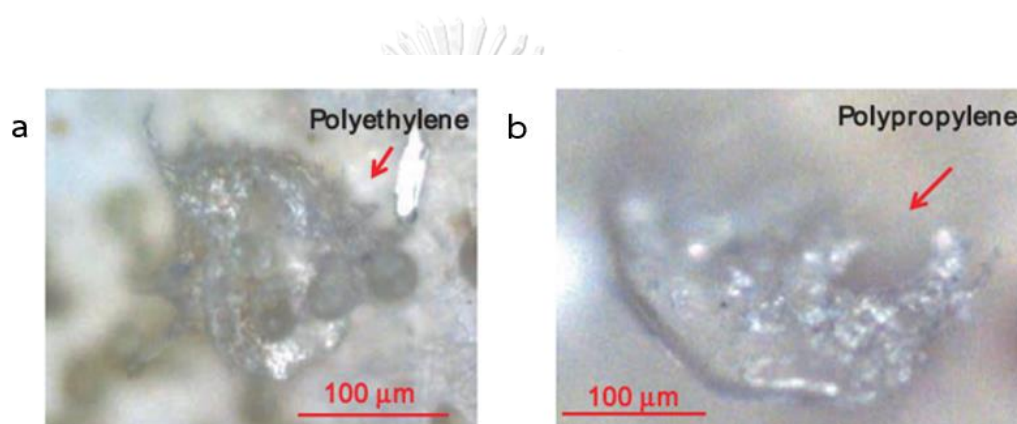
Figure 1.3 Pictures of transparent (a) polyethylene and (b) polypropylene fragments on filter paper.[15]

On the other hand, the spectroscopic method was more accurate than the microscopic counterpart, reducing the missing and miscount rates. Especially, tiny microplastics (<1 mm) were detected by FT-IR.[15] The most significant advantage is the ability of FT-IR to confirm the polymer types of microplastics. This can also provide additional information such as origin and other behaviors. However, FT-IR is time-consuming to identify the microplastic-like particles one by one.

It is challenging yet problematic to identify microplastics of different types of polymer, various sizes, and shapes by a single analytical technique. Therefore, combinations of two or more analytical methods are commonly used. For instance, in 2019 Gniadek and coworkers[16] presented a characterization of marine nano- and microplastics by Scanning Electron Microscopy - Energy Dispersive X-Ray

Spectroscopy (SEM-EDS). SEM can give fast information of morphology, aging, and origin of the examined samples.

However, EDS measurement on non-conducting samples has some drawbacks. Higher electron beam energy caused electric charging of the sample surface. Due to this effect, the results of quantitative analysis can be disturbed, and this technique also cannot provide information on the type of polymer.

In the case of Raman spectroscopy, in 2018, Araujo and coworkers[17] reported the identification of microplastics using Raman spectroscopy. Raman is an indispensable tool for the analysis of very small microplastics (<20 μm). Compared with FTIR spectroscopy, Raman techniques show better spatial resolution (down to 1 μm while FTIR is 10-20 m), broader spectral coverage, higher sensitivity to non-polar functional groups, lower water interference, and narrower spectral bands. While both techniques proved equally capable for particles larger than 20 μm, the detection success rate of μ-FTIR lagged behind for smaller particles.

Likewise, even though μ-FTIR did succeed in identifying some microplastics in the 11-20 μm range, the quality of the spectra suffered because of a low signal-to-noise ratio, a direct after effect of the size of the particle approaching that of the instrument's diffraction limit. Figure 1.4 shows a comparing the FTIR and Raman spectra of a small (15-20 μm) polypropylene (PP) particle, where a clear Raman spectrum (left) contrast with a weak and noisy FTIR spectrum (right).

On the downside, Raman spectroscopy is prone to fluorescence interference. Raman also has an inherently low signal to noise ratio, and might cause sample heating due to the laser light source, leading to polymer degradation.

The use of microscopy technique identification provides a high risk of producing both false positive and false negative results in analyses of small microplastics. It is unable to provide the chemical data. In the same way, the spectroscopy methods (such as FTIR, Raman, SEM) are an expensive and long time to effort for analysis. For this reason, there is a need to improve and develop new methods to reduce identification time and effort to detect microplastics. Combining the easier and faster visual identification method (e.q., microscope) with the staining method to increase the specificity of detecting polymers or polymer types is challenging and interesting.
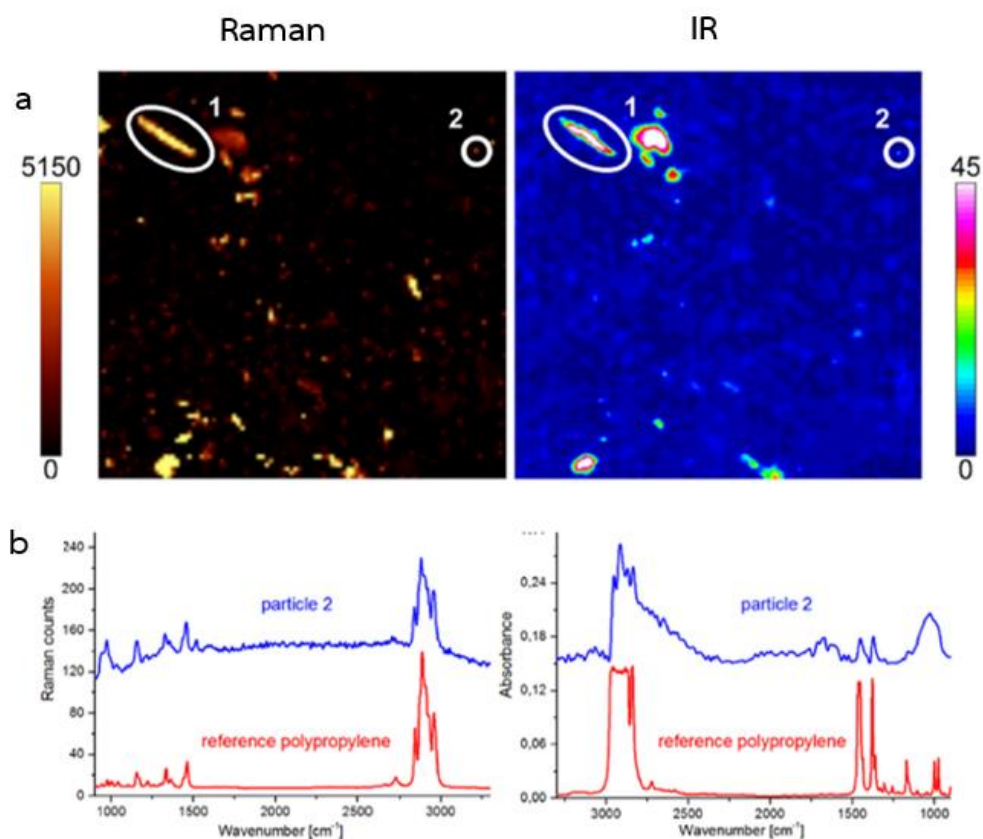
Figure 1.4 Raman image and IR image (a) false coloring denoting the spectral intensity in the 2780-2980 cm^{-1} range and (b) of particle 2 in comparison with a reference of polypropylene.[17]

1.4.   PET plastic degrading enzyme

In 2016, Yoshida and coworkers began searching for microbial PET degraders in the natural environment.[18] Using PET wastes, they screened for microorganisms that could use PET film as the major carbon source for growth. After a few weeks, one sediment sample contained a different microbial consortium formed on the PET film. The film showed clear signs of degradation (induced morphological change in the PET film) (Figure 1.5).
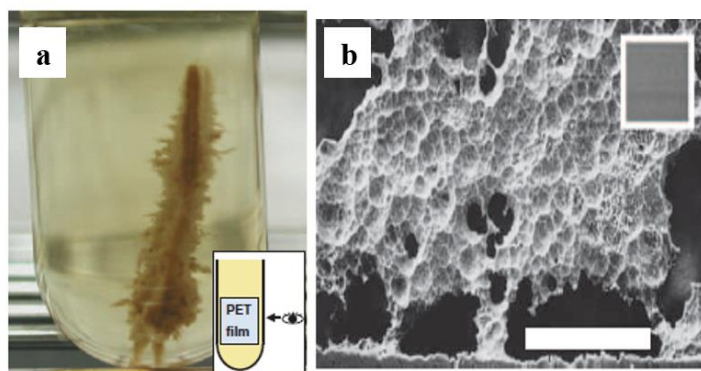
Figure 1.5 Microbial growth on PET (a) Growth of sample on PET film after 20 days. (b) SEM image of degraded PET film after 70 days. The inset shows entire PET film. Scale bar, 0.5 mm.[18]

From the microbial consortium, then Yoshida *et al*. successfully isolated the bacterium capable of degrading PET. As the bacterium was discovered from environmental samples taken in Sakai, Osaka Prefecture, it was given the name *Ideonella sakaiensis* 201-F6.

Additionally, the degradation mechanism and a genome analysis were studied to acquire more information on the enzymes that can break down PET. Completed functional analysis of the protein gene product showed their ability to catalyze PET hydrolysis.

Compared to previously known PET-degrading enzymes, this newly identified enzyme had a higher preference for PET degradation and was more active. This particular enzyme was named PETase.[18] When grown on PET, PETase produces two enzymes capable of hydrolyzing PET. The reaction intermediate, mono(2-hydroxyethyl) terephthalic acid (MHET) was also hydrolyzed. Both enzymes are required to enzymatically convert PET efficiently into its two environmentally benign monomers, terephthalic acid, and ethylene glycol.

1.5.   Characterization of PETase

In 2018, Austin and coworkers.[19] had also employed this newly discovered bacterium *Ideonella sakaiensis* 201-F6 in their study to gain a deeper understanding of the adaptations that contribute to the substrate specificity of PETase. It was found that PETase exhibits a canonical α/β-hydrolase structure with an open active-site cleft. The high-resolution structure described in their study revealed the binding site architecture of the *I. sakaiensis* 201-F6 PETase. As predicted from the sequence homology to the lipase and cutinase families, PETase adopts a classical α/β-hydrolase fold, with a core consisting of eight β- strands and six α-helices.

Another striking difference between PETase and the closest cutinase homologs is the broader active-site cleft, which upon observation, they hypothesized might be necessary to accommodate crystalline semi-aromatic polyesters. A single amino acid substitution from phenylalanine (*T. fusca* cutinase) to serine (PETase) in the lining of the active site cavity appears sufficient to cause this change, with the remaining cleft formed between Trp159 and Trp185 (Figure 1.6a, 1.6b). In terms of the active site, the well-studied catalytic triad is conserved across the lipases and cutinase families. In PETase, the catalytic triad comprises Ser160, Asp206, and His237 (Figure 1.6c).
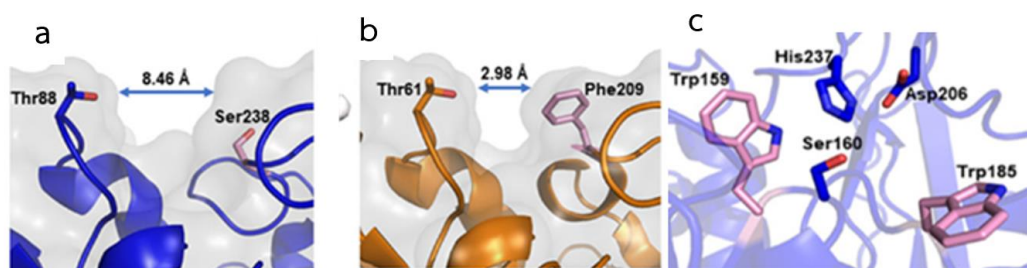
Figure 1.6 Active site structure of PETase [19]

Figure 1.6 (a) shows a view along the active-site cleft of PETase. The width of the cleft is shown between Thr88 and Ser238. Figure 1.6 (b) reveals the narrower cleft of the *T. fusca* cutinase active site which is shown with the width between Thr61 and

Phe209 in equivalent positions. A close-up view of the PETase active site is shown in Figure 1.6(c) with the catalytic triad residues His237, Ser160, and Asp206 colored blue. Residues Trp159 and Trp185 are colored pink.[19]

Prediction of PET-PETase binding modes by conducting induced-fit docking (IFD). The orientation shown in Figure 1.7 is one of several used to illustrate a productive PET-binding event in the wild-type enzyme: A PET carbonyl carbon is at a chemically relevant distance (5.1 Å) for nucleophilic attack from the Ser160 hydroxyl group. His237 is at an ideal distance (3.9 Å) to activate Ser160, and Asp206 provides hydrogen bonding support to His237 (2.8 Å).
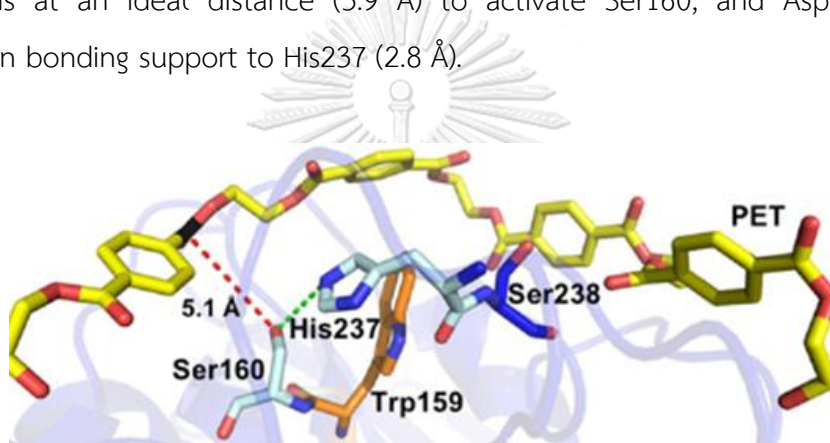
Figure 1.7 Predicted binding conformations of wild-type PETase from docking simulations. [19]

The illustration demonstrates that PET is accommodated in an optimum position for the carbon (black) interact with the nucleophilic hydroxyl group of Ser160, at a distance of 5.1 Å (red dash). His237 is positioned within 3.9 Å of the Ser160 hydroxyl (green dash). Residues Trp159 and Ser238 line the active-site channel (orange and blue, respectively).[19]

It is envisaged that a PET-degrading enzyme can be converted into a sensitive PET detector by using a genetic encode expansion technique.

1.6.   Genetic code expansion

Genetic code expansion is a technique used for the modification of genetic code. The genetic code for all life is based upon four nucleotides, 64 codons, and 20 amino acids. Yet, in the past two decades, biologists have expanded the genetic code by redirecting specific codons to encode amino acids beyond the 20 standard amino acids.[20]

Specific codons have been re-allocated to encode an unnatural amino acid. The key to expanding the genetic code is aminoacyl-tRNA synthetase/tRNA (aaRS/tRNA) pairs specifically with unnatural amino acids. This system must be orthogonal with the native translation system, including endogenous tRNA, natural amino acids, and endogenous aaRS.

Genetic code expansion has been commonly used to study protein structures and functions both in vitro and in vivo. The site-specific modification characteristic of the genetic code expansion technique makes it a powerful tool in improving the pharmacological properties of protein therapeutics and developing novel therapeutic methods.[21]

As for this work, a 2,3-diaminopropionic acid (DAP) derivative will be used as an unnatural amino acid due to the similarity of the structure of the DAP derivative with serine which is an active site of PETase that plays a vital role to bind to the carbonyl carbon by a hydroxyl group and break the ester bond of PET.

1.7.   Synthesis of 2,3-diaminopropionic acid (DAP) derivative

L-2,3-diaminopropionic acid (L-Dap) is a key precursor in the synthesis of many antibiotics such as viomycin and capreomycin, two structurally related antituberculosis drugs that belong to the tuberactinomycin family of nonribosomal peptide antibiotics.[22]

According to PETase, it can degrade PET film by Ser acting as a nucleophile attack to the carbonyl bond of PET. It is aimed to convert PET degrading enzyme to PET detecting agent. Thus, we have to change the function of an enzyme from hydrolysable to non-hydrolysable by trapping an intermediate of the degradation process.

In 2019, Huguenin-Dezot and coworker[23] reported a method for synthesizing DAP derivatives that would enable the trapping of acyl-enzyme intermediates linked through an amide bond (Figure 1.8a, b).

In Figure 1.8a, active-site serine or cysteine residues reacts with carbonyl groups to form tetrahedral intermediates that collapses to acyl-enzyme intermediates by losing R1–YH. Attack by nucleophilic R3 groups (commonly a hydroxyl, amine, or thiol) releases the bound substrate fragment and generates the enzyme. R1, R2, and Y represent the diverse chemical groups that may be found in distinct reactants. On the other hand, Figure 1.8b replacing cysteine or serine with DAP may result in a first acyl-enzyme intermediate resistant to cleavage.
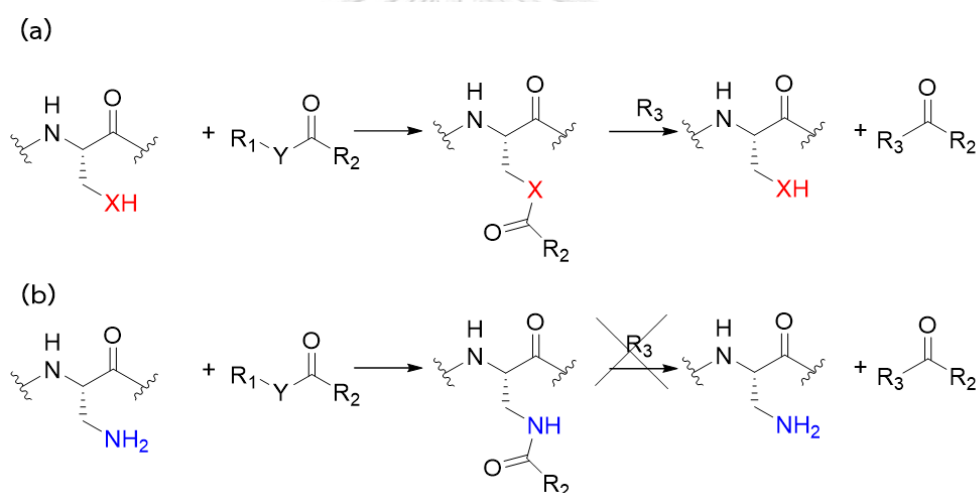
Figure 1.8 Capturing transient acyl-enzyme intermediates with DAP (a) Active-site Ser(O) or Cys(S) residues react with C=O that collapse to acyl-enzyme intermediates. (b) replacing Cys or Ser with DAP derivative may result in a first intermediate resistance to cleavage.[23]

The structural similarity of DAP to cysteine and serine makes it challenging to discover an aminoacyl-tRNA synthetase that is selective for DAP *in vivo*. Five protected versions of DAP (2–6) (Figure 1.9) were anticipated to be specific aminoacyl-tRNA synthetase/tRNA$_{CUA}$ pairs and enable site-specific incorporation into proteins. It was envisaged that derivatives 2-6 would allow the trapping of acyl-

enzyme intermediates linked through an amide bond (Figure 1.8b). These DAP derivatives can be prepared *via* a method developed by Huguenin-Dezot.[23] Due to the selection synthetase enzyme assay. It was found that derivatives 2–5 accumulated in *Escherichia coli* at low concentrations were unable to evolve a synthetase for these unnatural amino acids using several libraries of the orthogonal *Methanosarcina barkeri* (*Mb*) pyrrolysyl-tRNA synthetase (PylRS)/tRNA (Pyl/CUA) pair.

By contrast, compound **6** accumulated in *E. coli* at millimolar concentrations and is able to evolve a *Mb*PylRS variant for the site-specific incorporation of **6**. Therefore, compound **6** as the DAP derivative was selected to encode into the enzyme.
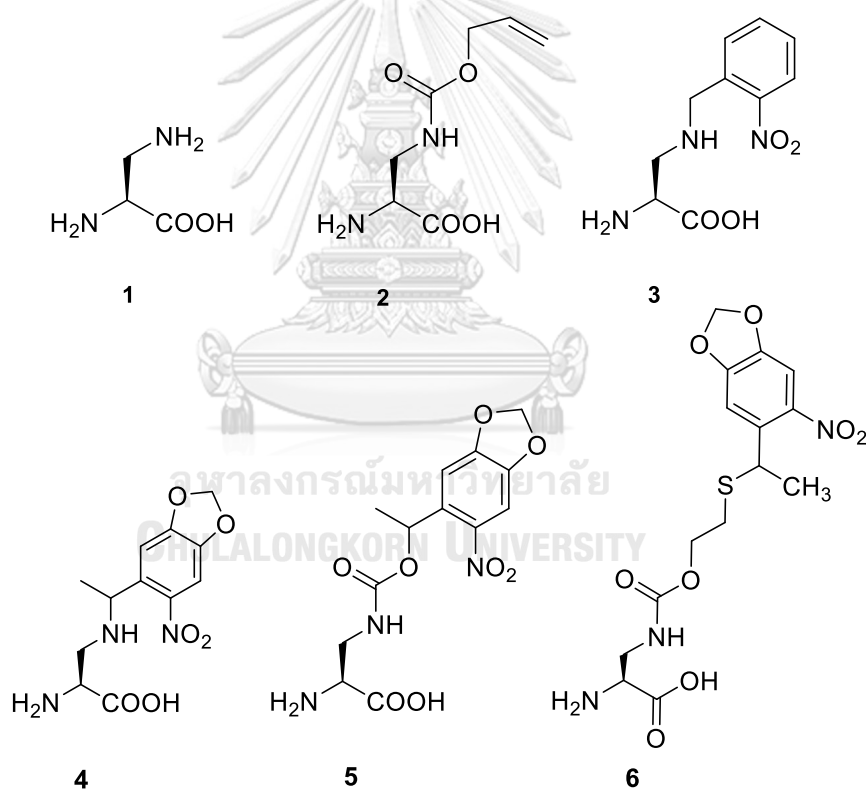
Figure 1.9 Structure of protected versions of DAP. [23]

While natural enzymes mentioned earlier already have the capacity to degrade PET, we hope to repurpose the enzymes from just degrading to detecting PET microplastics. To achieve sensitive microplastic detection, we aim to create enzyme variants that can

form covalent adducts with microplastic particles. The adduct is generated *via* the use of 2,3-diaminopropionic acid (DAP) derivative, which will substitute a catalytic serine in the enzyme of interest *via* genetic code expansion. This technique allows site-specific incorporation of a non-canonical amino acid (in this case, DAP derivative) into any desired site on a protein of interest. Unlike natural hydrolases which catalyze their reactions *via* an acyl enzyme intermediate, DAP-modified enzymes will form a stable, covalent substrate-enzyme adduct *via* an amide linkage. By either further conjugating fluorescent turn-on probes to DAP-modified enzymes or employing appropriate direct spectroscopic method, we hope to convert a PET-degrading enzyme into a sensitive PET detecting system.

1.8 Objectives

This research aimed to synthesize and optimize unnatural amino acid 2,3-diaminopropionic acid (DAP) derivative or compound 6 to find the appropriate conditions. However, remain up the highest yield of each step. Then use compound 6 to encode onto plastic degrading enzyme to change wild-type enzyme's function from hydrolysable to non-hydrolysable, which traps the PET plastic but does not degrade by genetic code expansion technique. As described earlier on different methods to detect microplastics, we have had interests in exploring an alternative detection method for PET microplastic. This may be done by either further conjugating fluorescent turn-on probes to DAP-modified enzymes or employing appropriate direct spectroscopic method. It is hoped to convert a PET-degrading enzyme into a sensitive PET detecting system.

CHAPTER II

EXPERIMENTAL

2.1 Materials and Chemicals

All reactions were performed in oven-dried glassware. All reagent grade chemicals for the synthesis in this work were purchased from Acros, Merck, Sigma-Aldrich, and TCI and were used without further purification. Laboratory grade organic solvents from RCI Labscan were used for column chromatography and thin-layer chromatography. Unless otherwise specified, analytical grade organic solvents from Burdick & Jackson and RCI Labscan were used for reaction set ups. The progress of the reactions was monitored by thin-layer chromatography (TLC) performed on Merck D.C. silica gel 60 F_{254} 0.2 mm precoated aluminium sheets and visualized using UV light (254 nm). Column chromatography was performed on Merck 70-230 mesh ASTM silica gel. Solvents for NMR experiments were purchased from Cambridge Isotope Laboratories or Euriso-top.

2.2 Instruments and Equipments

NMR spectra were obtained from Jeol NMR spectrometer and were recorded at 500 MHz for ^{1}H NMR experiments and 126 MHz for ^{13}C NMR experiments, using deuterated dimethylsulfoxide (DMSO-d_6), deuterated chloroform (CDCl$_3$), and deuterated methanol-d_4 as NMR solvents. The chemical shifts (δ) are reported in parts per million (ppm) relative to tetramethylsilane signal (δ_H = 0.00 ppm) employing residual protonated signal of deuterated solvent as a reference.

In each step of the genetic code expansion technique, the following were used. Cloning: T100TM Thermal Cycler (Bio-rad), Mupid-exU (Submarine electrophoresis system, Run agarose gel). Protein expression: Mini-PROTEAN Tetra system (SDS-PAGE and

2.3 Synthesis of 4',5' methylenedioxy-2'-nitroacetophenone (8)
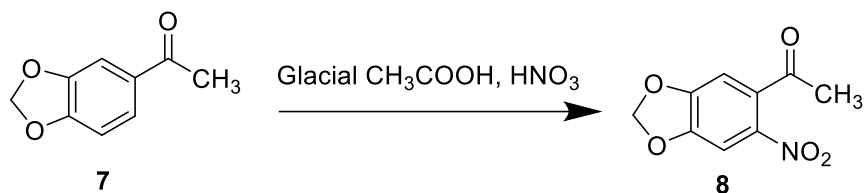
Figure 2.1 Synthesis of 4',5' methylenedioxy-2'-nitroaceto phenone (**8**).

3',4'-(methylenedioxy) acetophenone (**7**) (4 g, 0.02 mol, 1 eq) was stirred in glacial acetic acid (24 mL) for 30 min to achieve a clear solution. The solution was added dropwise to a 250 mL 3 necked-round bottom flask containing HNO_3 (44 mL) at 0 °C over a 30-minute addition. The reaction mixture was maintained at 0 °C during addition and for an additional 30 min while stirring under N_2 atmosphere. Then the mixture was warmed to 40 °C and stirred under N_2 atmosphere for an additional 30 minutes. The mixture was cooled to room temperature and poured slowly into ice in a beaker (500 mL). A yellow precipitate appeared. The mixture was then stirred for 15 min and filtered using a suction pump. The dark yellow gum was neutralized with Na_2CO_3, washed with water, and dried in an oven. The crude yellow solid was then purified by column chromatography on SiO_2 (eluent: 1:1 CH_2Cl_2:hexane to 100% CH_2Cl_2). The desired compound, 4',5'-Methylenedioxy-2'-nitroacetophenone (**8**) was obtained as the major product (1.8048 g, 35%): R_f= 0.66. ^{1}H NMR (500 MHz, CDCl$_3$) δ (ppm): δ 7.54 (s, 1H), 6.74 (s, 1H), 6.16 (s, 2H), 2.48 (s, 3H). ^{13}C NMR (126 MHz, CDCl$_3$) δ (ppm): 199.35, 152.82, 148.95, 140.24, 135.29, 106.32, 104.96, 103.72, 30.36.

2.4 Synthesis of 1-(4,5-Methylenedioxy-2-nitrophenyl) ethanol (9)
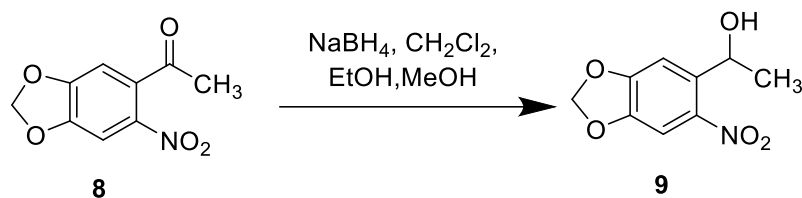
Figure 2.2 Synthesis of 1-(4,5-Methylenedioxy-2-nitrophenyl) ethanol (**9**).

4',5'-Methylenedioxy-2'-nitroacetophenone (**8**) (1.2528 g, 5.99 mmol, 1eq) was suspended in a solvent mixture of CH_2Cl_2 (12 mL), CH_3OH (19 mL), and absolute ethanol (13 mL) in 100 mL single-necked round-bottom flask. $NaBH_4$ granules (0.3408 g, 9 mmol, 1.5 eq.) were added in 4 portions to the yellow suspension every 5 min (total time = 20 min addition) at 15 °C. After the addition was complete, the reaction mixture was stirred at room temperature until the starting material was completely consumed as determined by TLC analysis (SiO_2, TLC eluent: 100% CH_2Cl_2). The reaction was quenched by the addition of acetone (3 mL), left stirring at room temperature for 10 min. The mixture was then evaporated to dryness under reduced pressure to obtain a yellow solid. The solid was re-dissolved in CH_2Cl_2 (10 mL×2) and washed with saturated aq. NH_4Cl solution (30 mL×2) and finally with saturated aq. NaCl solution (30 mL×2). The organic layer was separated, dried over anhydrous Na_2SO_4, filtered, and evaporated to dryness in an oven to obtain 1-(4,5-Methylenedioxy-2-nitrophenyl)ethanol (**9**) as a yellow solid (1.2569 g, 99%): R_f= 0.33. ^{1}H NMR (500 MHz, $CDCl_3$) δ (ppm): 7.45 (s, 1H), 7.26 (s, 1H), 6.12 – 6.08 (m, 2H), 5.45 (qd, J = 6.2, 3 Hz, 1H), 2.26 (d, J = 3.5 Hz, 1H), 1.53 (d, J = 6.3 Hz, 3H). ^{13}C NMR (126 MHz, $CDCl_3$) δ (ppm): 152.51, 147.02, 141.61, 139.05, 106.44, 105.23, 103.01, 65.78, 24.28.

2.5 Synthesis of 1-bromo-1-[4',5'-(methylenedioxy)-2'-nitro phenyl]ethane(10)

Figure 2.3 Synthesis of 1-bromo-1-[4',5'-(methylenedioxy)-2'-nitrophenyl]ethane (**10**).

A 250 mL, three-necked round-bottom flask was dried in an oven for 15 minutes then further with a heat gun and purged with N_2 gas. After that, the flask was charged with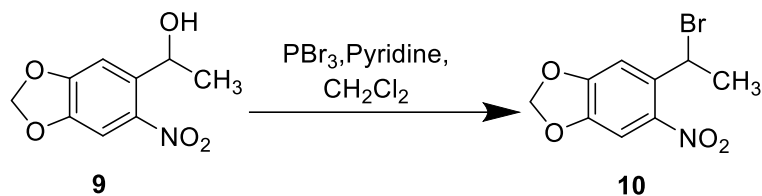 a solution of 1-(4,5-Methylenedioxy-2-nitrophenyl) ethanol (**9**) (1.9741 g, 9.34 mmol, 1 eq) in CH_2Cl_2 (30 mL). The flask was then wrapped with aluminum foil to shield the content from the light. The solution was stirred at 0 °C under N_2 atmosphere. After 20 min, PBr_3 (0.4 mL, 4.25 mmol, 0.45 eq) was added dropwise into the reaction mixture over 10 min using a syringe pump at 0 °C. Subsequently, pyridine (0.07 mL) was added, and the solution was stirred at 0°C for 15 min. Afterward, the reaction was warmed to room temperature and stirred continuously for 30 min. The reaction was judged to be complete by TLC analysis (SiO_2, TLC eluent: 100% CH_2Cl_2). It was then cooled to 0 °C and stirred for 5 min, then quenched by addition of MeOH (2 mL), brought to room temperature, and stirred for 10 min under N_2 atmosphere. After the quenching was complete, the reaction mixture was evaporated to dryness under reduced pressure. The resulting yellow gum was dissolved in CH_2Cl_2 (15 mL) and saturated aq. $NaHCO_3$ solution (15 mL). The organic phase was washed sequentially with a saturated aq. $NaHCO_3$ solution (2×30 mL) and saturated aq. NaCl solution (3×40 mL). The organic layer was separated, dried over anhydrous Na_2SO_4, filtered, and evaporated to dryness to obtain a yellow solid. The crude product was purified by column chromatography on SiO_2 (eluent: CH_2Cl_2: hexane (2:8 to 1:1)) to obtain 1-bromo-1-[4',5'-(methylenedioxy)-2'-nitrophenyl]ethane (**10**) in 77% yield (1.9832 g). ^1H NMR (500 MHz, $CDCl_3$) δ (ppm): 7.33 (s, 1H), 7.25 (s, 1H), 6.11 (d, J = 1.0 Hz, 1H), 5.88 (q, J = 6.8 Hz, 1H), 2.02 (d, J =

6.8 Hz, 3H). ^{13}C NMR (126 MHz, CDCl$_3$) δ (ppm): 152.06, 147.67, 141.60, 134.79, 108.75, 105.05, 103.27, 42.77, 27.59.

2.6 Synthesis of 2-{[1-(6-Nitrobenzo[d][1,3]dioxol-5-yl)ethyl]thio}ethan-1-ol(11)
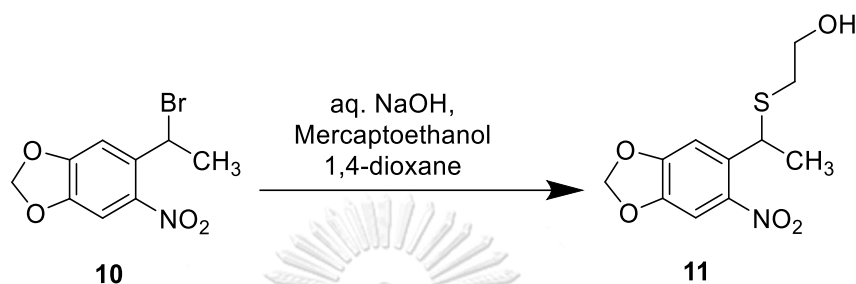
Figure 2.4 Synthesis of 2-{[1-(6-Nitrobenzo[d][1,3]dioxol-5-yl)ethyl] thio}ethan-1-ol (**11**).

A freshly prepared solution of NaOH (0.5 M, in 2 mL of deionized H$_2$O, 1 mmol, 1.2 eq) was loaded in a three-necked round-bottom flask and degassed. After 10 min, mercaptoethanol (0.08 mL, 1.13 mmol, 1.36 eq) was added to the flask, and degassing was continued for a further 10 min. Separately, the starting 1-bromo-1-[4',5'-(methylenedioxy)-2'-nitrophenyl]ethane (**10**) (0.2288 g, 0.83 mmol, 1 eq) was dissolved in 1,4-dioxane (2 mL) and degassed for 10 min. Both round bottom flasks were wrapped with aluminum foil to shield from the light. Compound **10** was transferred into the flask containing NaOH and mercaptoethanol using cannula over 10 min in the dark under a positive pressure of N$_2$ gas. A yellow precipitate formed, which was then dissolved with 1,4-dioxane (2 mL). The solution was subjected to sonication for 20 min in the dark until the reaction mixture became a clear yellow solution. The contents were left stirring for 6 h at room temperature in the dark under N$_2$ atmosphere. The reaction was judged to be complete by TLC (3:7EtOAc:hexane), and the solvent was evaporated. The yellow gum was then extracted with EtOAc (10mL×2), aq. NH$_4$Cl (10 mL×2) and saturated NaCl (10mL×3). The organic layer was

separated and dried over anhydrous Na$_2$SO$_4$, filtered, and the solvent was evaporated. The crude product was purified by column chromatography on SiO$_2$ (eluent: 15% EtOAc:hexane to 50% EtOAc/hexane) in the dark to obtain 2-{[1-(6-Nitrobenzo[d][1,3]dioxol-5-yl)ethyl]thio}ethan-1-ol (**11**) as a sticky yellow paste (0.2121 g, 94%). ^{1}H NMR (500 MHz, CDCl$_3$) δ (ppm): δ 7.27 (s, 1H), 7.26 (s, 1H), 6.09 (d, J = 3.6 Hz, 2H), 4.78 (q, J = 7.0 Hz, 1H), 3.68 – 3.57 (m, 2H), 2.62 – 2.48 (m, 2H), 1.55 (d, J = 7.0 Hz, 3H). ^{13}C NMR (126 MHz, CDCl$_3$) δ (ppm): 152.26, 146.88, 143.95, 136.02, 107.97, 104.76, 103.01, 60.85, 38.31, 34.88, 23.15.

2.7 Synthesis of 2-((1-(6-nitrobenzo[d][1,3]dioxol-5-yl)ethyl)thio)ethyl (4-nitrophenyl)carbonate (12)
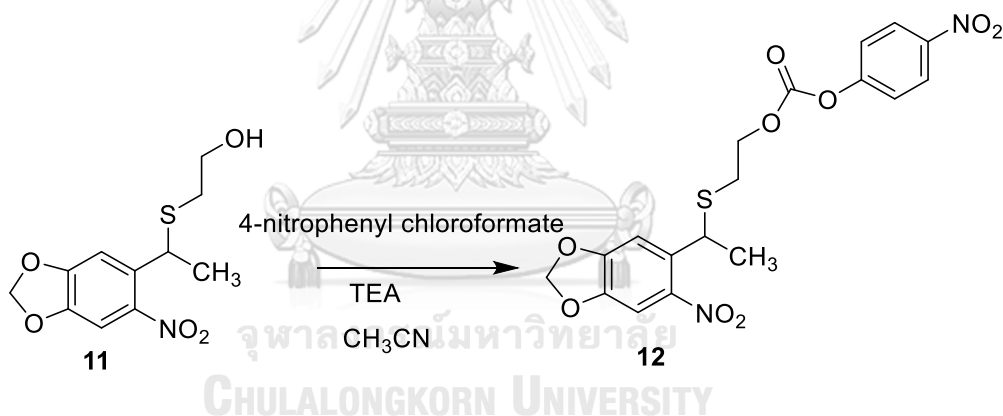
Figure 2.5 Synthesis of 2-((1-(6-nitrobenzo[d][1,3]dioxol-5-yl)ethyl) thio)ethyl(4-nitrophenyl)carbonate (**12**).

A three-necked round-bottomed flask was dried in an oven. The dry flask was charged with a solution of 2-{[1-(6-Nitrobenzo[d][1,3]dioxol-5-yl)ethyl]thio}ethan-1-ol (**11**) (0.2897 g, 1.06 mmol, 1 eq) in dry CH$_3$CN. Triethylamine (0.6 mL, 4.30 mmol, 4.05 eq) was added, followed by addition of 4-Nitrophenyl chloroformate (0.3598 g, 1.78 mmol, 1.68 eq). The reaction turned turbid and white precipitates were formed. The solution was then left stirring at rt for 6 hours. The reaction was judged to be

complete by TLC (3:7 EtOAC:hexane) and was evaporated to dryness under reduced pressure. The product was purified by column chromatography on SiO_2 (eluent: 5% to 30% EtOAc:hexane) in the dark to obtain 2-((1-(6-nitrobenzo[d][1,3]dioxol-5-yl)ethyl)thio)ethyl (4-nitrophenyl) carbonate (**12**) as a yellow gum (0.2853 g, 65%) with an R_f = 0.48 (SiO_2 plate, EtOAc/hexane = 3:7). ^{1}H NMR (500 MHz, $CDCl_3$) δ (ppm): 8.27 (d, *J* = 9.2 Hz, 2H), 7.38 (d, *J* = 9.1 Hz, 2H), 7.30 (s, 1H), 7.27 (s, 1H), 6.09 (s, 2H), 4.87 (q, *J* = 7.0 Hz, 1H), 4.32 (qt, *J* = 11.1, 6.6 Hz, 2H), 2.77 – 2.63 (m, 2H), 1.56 (s, 3H). ^{13}C NMR (126 MHz, $CDCl_3$) δ (ppm): 155.56, 152.32, 152.08, 146.75, 145.51, 143.37, 135.72, 125.39, 121.86, 107.97, 104.88, 103.05, 68.01, 38.98, 31.02, 23.14.

2.8 Synthesis of (2S)-2-[(tert-Butoxycarbonyl)amino]-3-{[(2-{[1-(6-nitrobenzo[d][1,3]dioxol-5-yl)ethyl] thio}ethoxy)carbonyl]amino} propanoic acid (13)

Figure 2.6 Synthesis of (2S)-2-[(tert-Butoxycarbonyl)amino]-3-{[(2-{[1-(6-nitrobenzo[d][1,3]dioxol-5-yl)ethyl] thio}ethoxy)carbonyl] amino}propanoic acid (**13**).
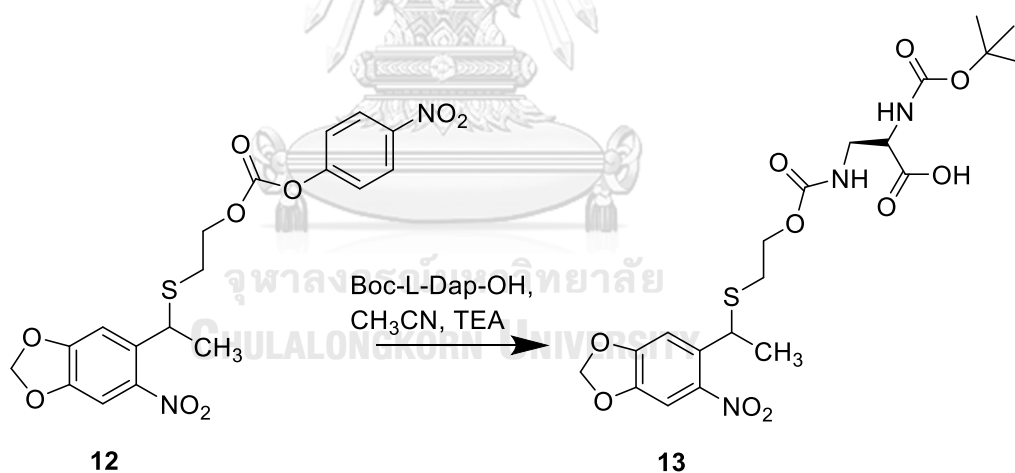
Compound **12** (0.2853 g, 0.65 mmol, 1 eq) was dissolved with dry CH_3CN (8 mL) and transferred into a three-necked round-bottom flask. Boc-Dap-OH (0.1460 g, 0.71 mmol, 1.09 eq) was added in one portion to the flask, followed by addition of

triethylamine (0.55 mL, 3.94 mmol, 6.06 eq). The reaction flask was wrapped with aluminium foil and stirred at rt for 6 h under N_2 atmosphere. After this time, the reaction was judged to be complete by TLC (98:2 EtOAc:CH_3COOH), then dried under reduced pressure. This was purified by column chromatography (eluent: 50:50 EtOAc: hexane to 100% EtOAc then 5%>40% MeOH:EtOAc) in the dark to obtain(2*S*)-2-[(*tert*-butoxycarbonyl)amino]-3-{[(2-{[1-(6-nitrobenzo[d][1,3]dioxol-5-yl)ethyl]thio}ethoxy) carbonyl]amino} propanoic acid (**13**) as a yellow gum (0.3098 g, 94 %). ^{1}H NMR (500 MHz, CDCl$_3$) δ (ppm): 7.28 (s, 1H), 7.25 (s, 1H), 6.09 (d, *J* = 15.1 Hz, 2H), 5.99 (s, 1H), 5.86 (s, 1H), 4.78 (q, *J* = 7.0 Hz, 1H), 4.17 (s, 1H), 4.07 – 4.01 (m, 2H), 3.51 (s, 2H), 2.51 (tq, *J* = 13.3, 6.7 Hz, 2H), 1.51 (d, *J* = 6.9 Hz, 3H), 1.38 (s, 9H). ^{13}C NMR (126 MHz, CDCl$_3$) δ (ppm): 173.74, 157.92, 156.49,152.06, 146.86, 143.25, 136.20, 108.11, 104.76, 103.07, 81.77, 64.63, 54.44, 43.24, 38.94, 32.02, 28.43.

2.9 Synthesis of (2S)-2-amino-3-{[(2-{[1-(6- nitrobenzo[d][1,3] dioxol-5-yl)ethyl] thio}ethoxy) carbonyl]amino}propanoic acid (6)
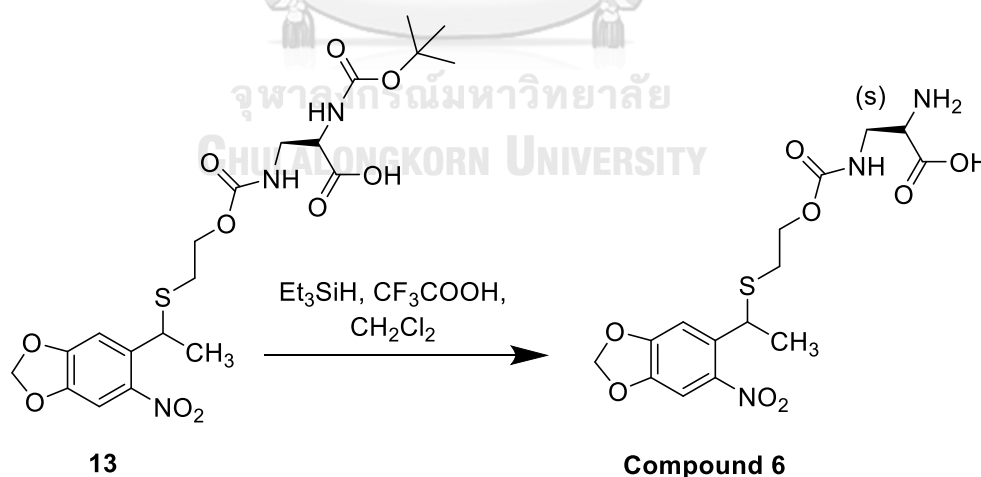

Figure 2.7 Synthesis of (2S)-2-amino-3-{[(2-{[1-(6- nitrobenzo[d][1,3] dioxol-5-yl)ethyl] thio}ethoxy)carbonyl]amino}propanoic acid (**6**)

Compound **13** (0.5044 g, 1.00 mmol, 1 eq) was dissolved with CH_2Cl_2 (12 mL) and loaded to a dry single necked round bottom flask. The flask was wrapped with aluminum foil to shield from the light and stirred at rt for 5 min. After that, triethylsilane (1.6 mL, 10.01 mmol, 10.01 eq) was added to the solution and stirred for 5 min. Subsequently, trifluoroacetic acid (1.6 mL, 20.89 mmol, 20.89 eq) was added drop-wise *via* syringe over 5 min at room temperature. The reaction mixture turned from light yellow to dark yellow color and was left stirring at room temperature for 2 h. The reaction was judged to be complete by TLC (98:2 EtOAc: CH_3COOH), then the solution was concentrated to dryness under reduced pressure to obtain a yellow-brown gum. This was dissolved with CH_3OH (10 mL) and evaporated to dryness under reduced pressure; repeated five-time to remove any CF_3COOH, Et_3SiH, H_2O. The yellow gum was dissolved with CH_3OH (10 mL) and transferred to a dry three-necked round-bottomed flask. The solution was stirred at 0 °C under N_2 atmosphere for 10 min. Et_2O was then transferred into the flask *via* cannula under a positive pressure of N_2 gas while the contents were vigorously stirred. A white yellow precipitate formed, and the contents stirred vigorously at 0 °C for 30 min, then r.t. for an additional 2 h. The precipitate was then filtered and washed with cool Et_2O (3×10 mL), followed by cool n-hexane (10 mL×2). The product was left dried at room temperature overnight in the dark to obtain (2S)-2-amino-3-{[(2-{[1-(6-nitrobenzo[d][1,3]dioxol-5-yl)ethyl]thio}ethoxy)carbonyl]amino}propanoic acid (**6**) as a pale-yellow powder (0.1942 g, 48%). ^{1}H NMR (500 MHz, CDCl$_3$) δ (ppm): 7.31 (s, 1H), 7.27 (s, 1H), 6.11 (d, J = 4.5 Hz, 2H), 4.96 (dt, J = 11.8, 6.4 Hz, 56H), 4.73 (q, J = 6.9 Hz, 1H), 4.15 – 3.98 (m, 3H), 3.69 (ddd, J = 14.9, 5.1, 3.9 Hz, 1H), 3.54 (dd, J = 15.1, 6.2 Hz, 2H), 2.66 – 2.47 (m, 2H), 1.52 (d, J = 6.9 Hz, 3H). ^{13}C NMR (126 MHz, Methanol-d$_4$) δ (ppm): 168.48, 161.37, 160.02, 152.08, 147.12, 141.04, 135.37, 115.84, 107.4, 104.03, 103.33, 64.34, 53.61, 40.47, 38.44, 29.86, 21.69.

2.10   Genetic code expansion: Cloning of an expression construct for His6-SUMO-
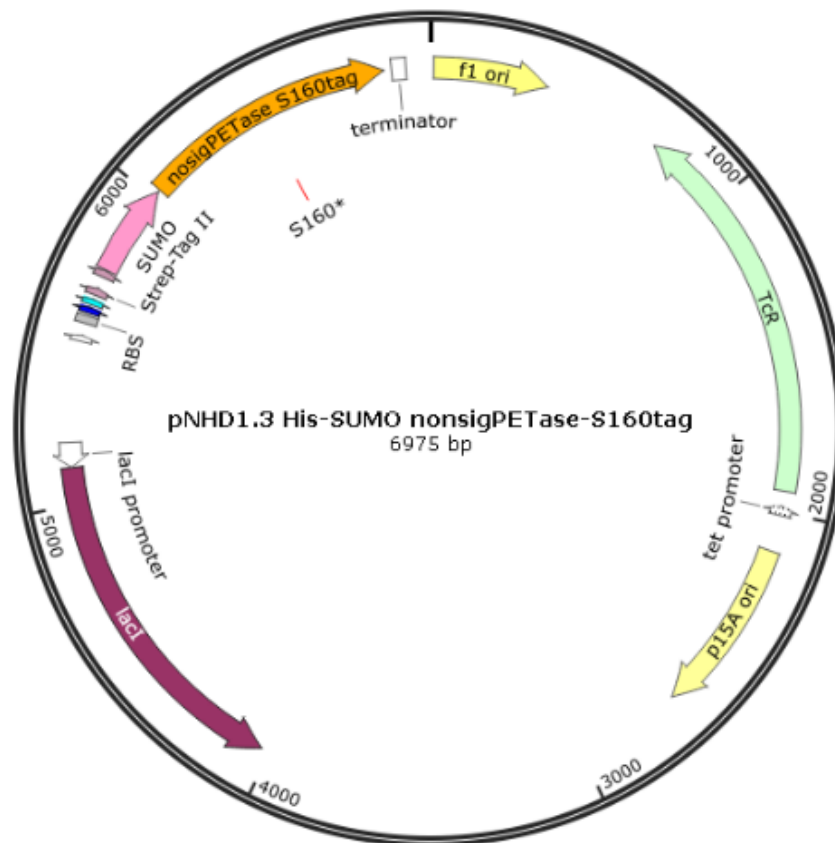
PETase (S160TAG)

The coding sequence for *Ideonella sakeiensis* PETase gene with its signal peptide removed was PCR-amplified using Q5® High-Fidelity DNA Polymerase from pET21b-Is-PETase plasmid (Addgene # 112202) with primers PETase_S160*_F (23-mer, GATGGGCTGGtagATGGGGGGCG) and PETase_S160*_R (20-mer, ACACCCATGCGGGCAGTATC). During the amplification, the catalytic residue S160 in the PETase gene was replaced by an amber stop codon (TAG). The PETase gene was circularized by a KLD reaction in a thermal cycler.

The putatively mutated PETase gene was amplified by primers nonsigPETase_OVL_SUMO_F (cagagaacagattggtggatcccagaccaatccgtatgcgcg) and PETase_TGA_OVL_XhoI_R (AGCAGCCTAGGTTAATTA AGCCTCGAGTCAggaacagttcgcggtgcg) to generate overhangs for Gibson assembly. The solubility tag SUMO gene was amplified from pC013 - Twinstrep-SUMO-huLwCas13a using primers His-SuMO pHND-OVL F (TTTGTTTAACTTTAAGAAGGAGATGTACATATGcatcatcatcatcatcacagcagc) and His-SUMO R (ggatccaccaatctgttctctgtgag). An acceptor plasmid p-His-Lipoyl_TEV-Strep plasmid (a kind gift from Jason Chin, MRC LMB, United Kingdom) was digested with NdeI and XhoI and assembled with the PETase, and SUMO inserts *via* Gibson assembly before transformation into *E. coli*. Plasmids were isolated from single colonies and sequence-analyzed for confirmation.

2.11   Genetic code expansion: Expression of His6-SUMO-PETase (S160BocK) *E. coli* BL21

Two expression plasmids for His6-SUMO-PETase(S160TAG) (Figure 2.8) and *Methanosarcina Mazei pyrrolysyl* tRNA synthetase and its cognate amber-suppressor tRNAPyl were transformed into *E. coli* BL21. Upon reaching the OD_{600} of 0.5-0.6, the culture was supplemented with 1 mM tert-butyloxycarbonyl lysine (BocK) and 1 mM

isopropyl-β-D thiogalactopyranoside (IPTG), and protein expression was carried out at 37 °C for 4 h. Whole-cell lysates were electrophoretically separated in SDS-PAGE and analyzed *via* Coomassie blue staining and anti-His$_6$ western blotting.

Figure 2.8 An expression construct for His6-SUMO-PETase (S160TAG).

CHAPTER III

RESULTS AND DISCUSSION

The objective of this work is to synthesize and optimize compound **6** which can be prepared from 3',4'-(methylenedioxy) acetophenone in 7 steps from a method of Nicolas Huguenin-Dezot's[23] with various modifications as shown in Figure 3.1. Then use compound 6 to encode onto plastic degrading enzyme to change enzyme's function from hydrolysable to non-hydrolysable, which traps the PET plastic but does not degrade, to develop the PET detecting method combined staining method and fluorescent spectroscopy. The synthesis of each step can be laid out as follows.
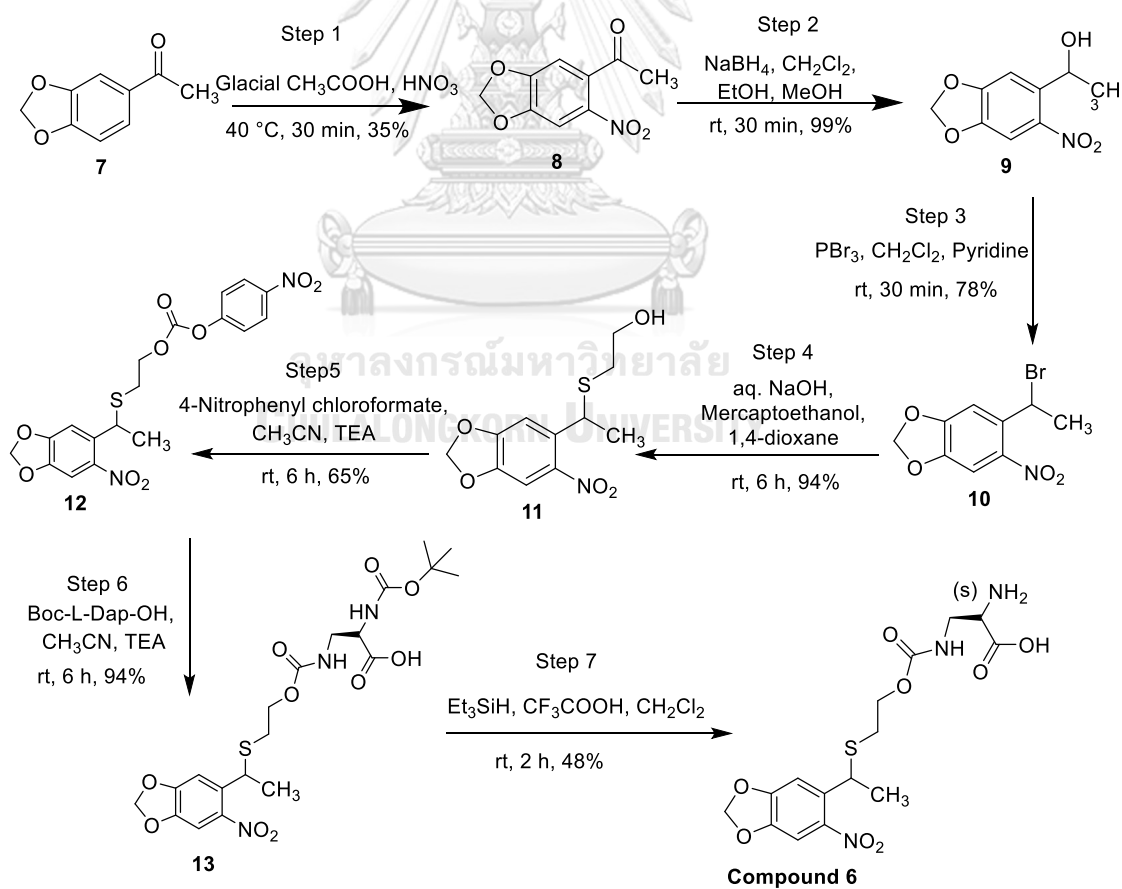

Figure 3.1 The synthetic scheme of compound **6**.

3.1 Synthesis and optimization of DAP derivative

The desired Compound **6** which is a derivative of 2,3-diaminopropionic acid (DAP) was successfully synthesized from 3',4'-(methylenedioxy) acetophenone in seven steps as shown in Figure 3.1. Optimization of reaction conditions had also been accomplished for most of the steps.

3.1.1. Synthesis of 4',5'methylenedioxy-2'-nitroacetophenone (8)
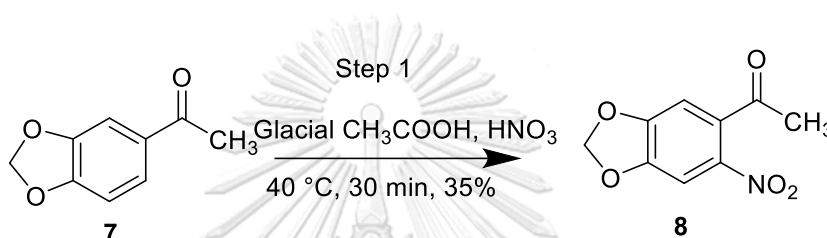
Reaction step 1

This is achieved by a nitration reaction by an addition of a nitro group to an aromatic ring of 3',4' (methylenedioxy)acetophenone (**7**). The product resulted from the electrophilic attack of the nitronium ion to the 2' position of **7**. In the experiment, the solution of **7** in glacial acetic acid was added dropwise to nitric acid. After warming the mixture up to 40 °C, the reaction got started. The optimization of reaction conditions includes the decrease in heating time from 2.5 hours to 30 minutes. The desired nitration product was obtained as a major product among three other by-products. Attempts to recrystallize the desired product with various solvent system failed to give the product. Therefore, the crude yellow solid product mixture was subjected to purification by column chromatography which yielded compound **8** in 35%. Overall, the desired product was obtained in a much shorter reaction period. ^{1}H NMR spectrum of compound **8** is shown in Figure 3.2 while the ^{13}C NMR spectrum is included in the Appendix.
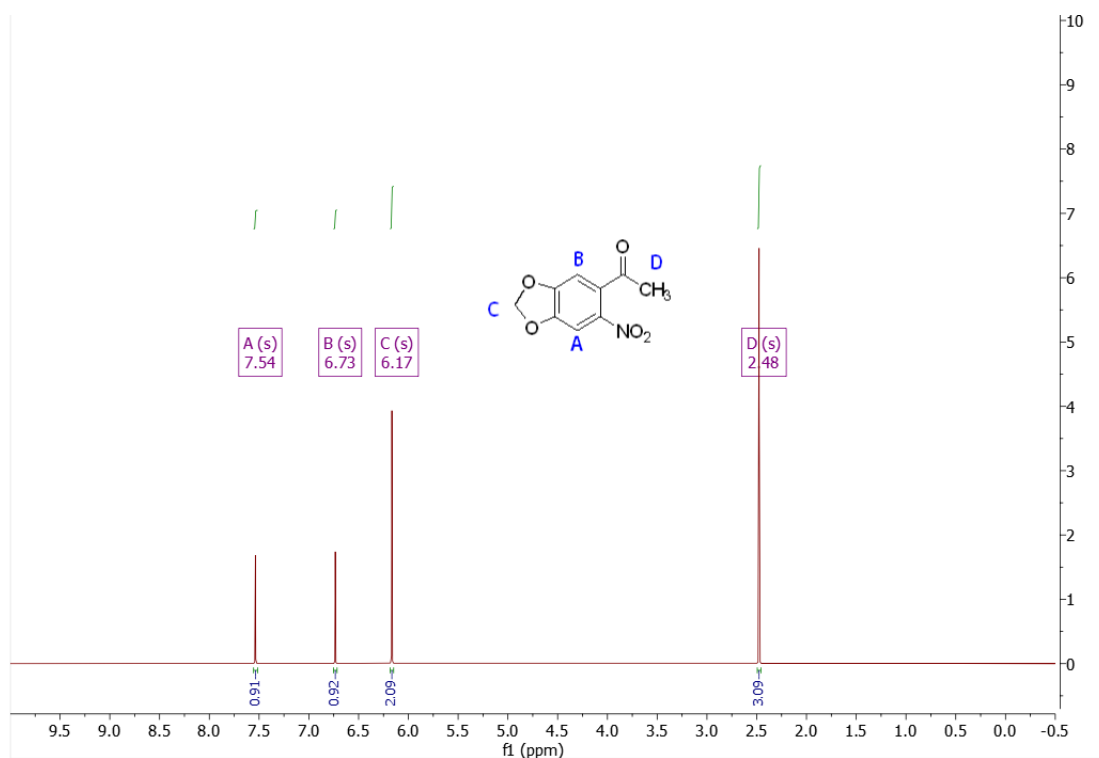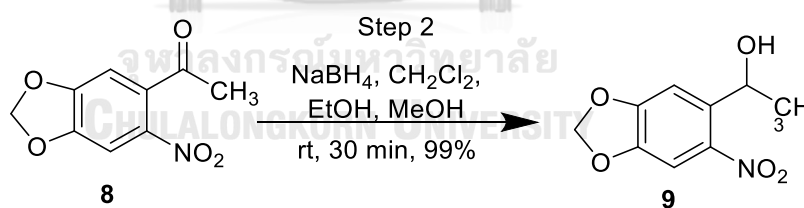
Figure 3.2 ^{1}H NMR spectrum of compound **8**.

3.1.2. Synthesis of 1-(4,5-Methylenedioxy-2-nitrophenyl) ethanol (9)

Reaction step 2

The next step involved a reduction reaction of the carbonyl group of compound **8** using granules NaBH$_4$. The reaction time was optimized from 4 hours to 30 minutes. Alcohol **9** was obtained in a quantitative yield similar to those reported in the literature. The identity of compound **9** was confirmed by ^{1}H NMR spectroscopic analysis. The spectrum of compound **9** in CDCl$_3$ is shown in Figure 3.3. ^{1}H NMR analysis of a solution of **9** in CDCl$_3$ confirmed the identity of the desired

product as the signal of the methine proton on the carbon with the hydroxyl group clearly appeared at 5.45 ppm (qd, 1H). The ^{13}C NMR spectrum is included in the Appendix.
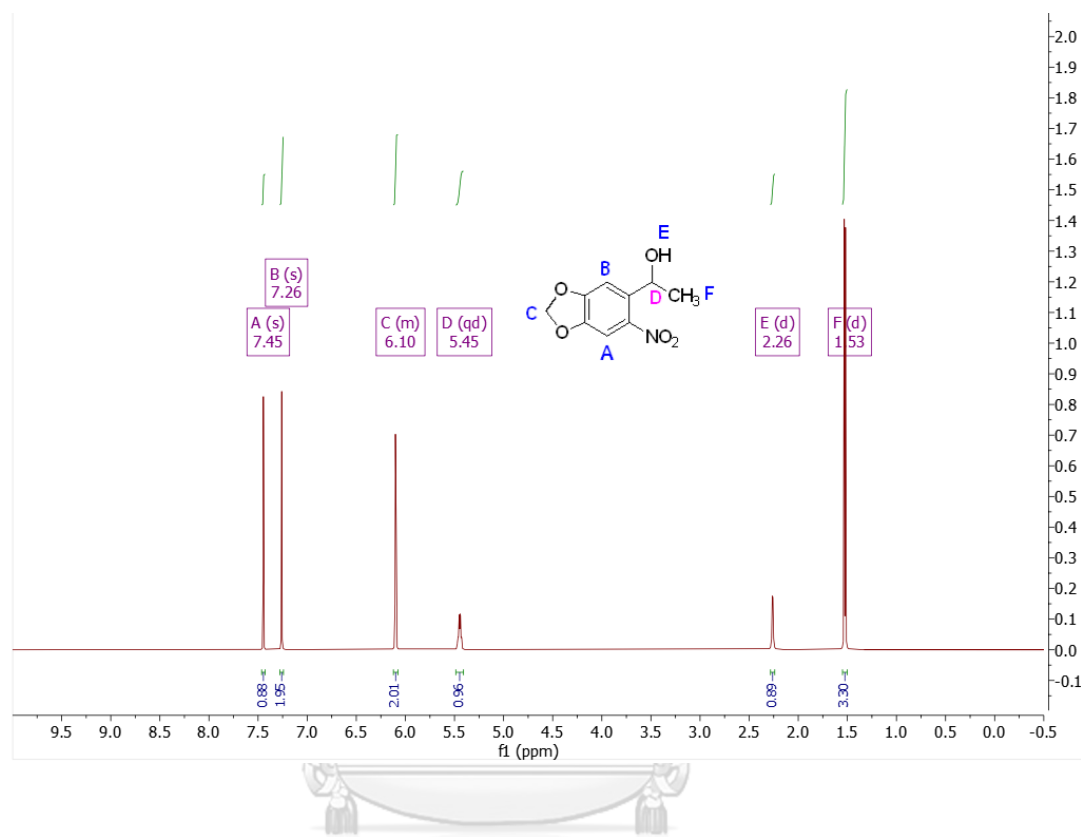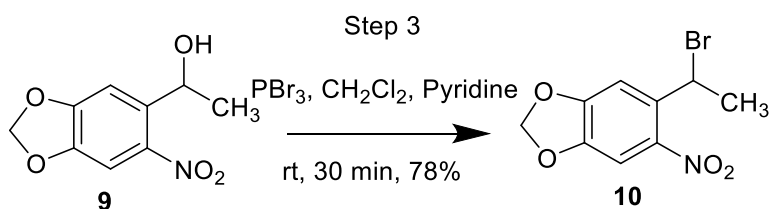

Figure 3.3 ^{1}H NMR spectrum of compound **9**.

3.1.3. Synthesis of 1-bromo-1-[4',5'-(methylenedioxy)-2'nitrophenyl]ethane(10)

Reaction step 3

In step 3, the hydroxyl group in **9** was displaced with bromine using PBr$_3$. The reaction was first carried out on a small scale and could be successfully reproduced at a larger scale to give a relatively good yield of about 70%. In addition, optimization by decreasing the reaction time from 1.5 hours to 30 minutes showed no effect on the reaction and resulted in even a higher percent yield of **10** than those reported in the reference.[23] The product of this step is relatively sensitive to light. Therefore, the reaction had to be carried out with minimum light. The compound **10** was dissolved with CDCl$_3$ to confirm the identity of the desired product by NMR (Figure 3.4). The slightly shifted signal of 5.88 ppm (q, 1H) from that of the precursor at 5.45 ppm (qd, 1H) represents the proton on the carbon after the hydroxyl was replaced with bromine. The desired product was protected from light and stored in a refrigerator.
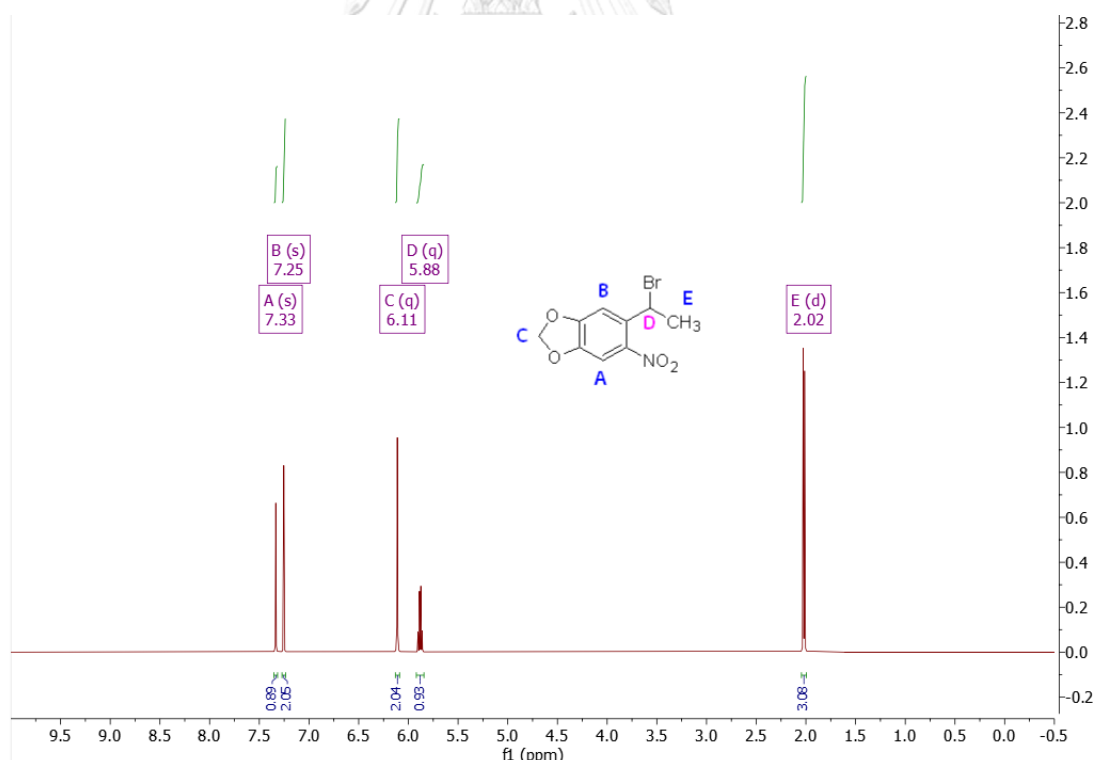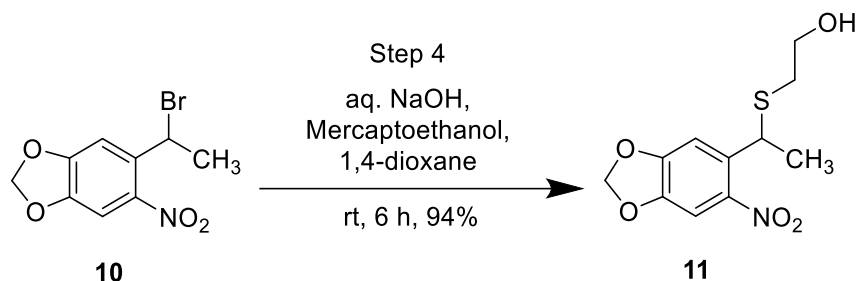

Figure 3.4 ^{1}H NMR spectrum of compound **10**.

3.1.4. Synthesis of 2-{[1-(6-Nitrobenzo[d][1,3]dioxol-5-yl)ethyl]thio}ethan-1-ol (11)

Reaction step 4

It is essential that the reaction in step 4 was carried out with minimum light. Mercaptoethanol in aqueous sodium hydroxide solution was used to replace the bromine atom in compound **10**. Under a basic condition both the sulfur atom of the thiol and the oxygen atom of the hydroxyl group would be deprotonated and can act as strong nucleophiles. In principle, sulfur is a stronger nucleophile since it is a larger atom than oxygen making its electrons more polarizable. When sulfur and oxygen atoms are both present in the same molecule such as in mercaptoethanol, it was envisaged that the sulfur atom, and not the oxygen counterpart, would undergo an S_N2 reaction to displace the bromine.

In the experiment, the degassed solution of starting compound **10** in 1,4-dioxane was transferred *via* cannula into the flask containing a mixture of mercaptoethanol solution and aq. NaOH under positive pressure of N_2 gas. The reaction was performed in a freshly distilled THF and a new bottle of 1,4-dioxane for comparison. The reactions in either polar aprotic solvent turned out to be successful. However, several by products were observed in THF while those in fresh 1,4-dioxane proceeded very cleanly without any by-products.

Moreover, the reaction stirring time had been optimized. It was found that the reaction went to completion in about 6 h. It was not necessary to perform the

reaction overnight, as reported previously, without any compromise in the yield of the desired product **11**. ^{1}H NMR analysis was done in CDCl$_3$ to confirm the identity of the desired product (Figure 3.5).   The signals at 3.65 ppm (m, 2H), 2.55 ppm (m, 2H), and 1.57 ppm (broad s, 1H) corresponded to methylene protons of the mercaptoethanol part.
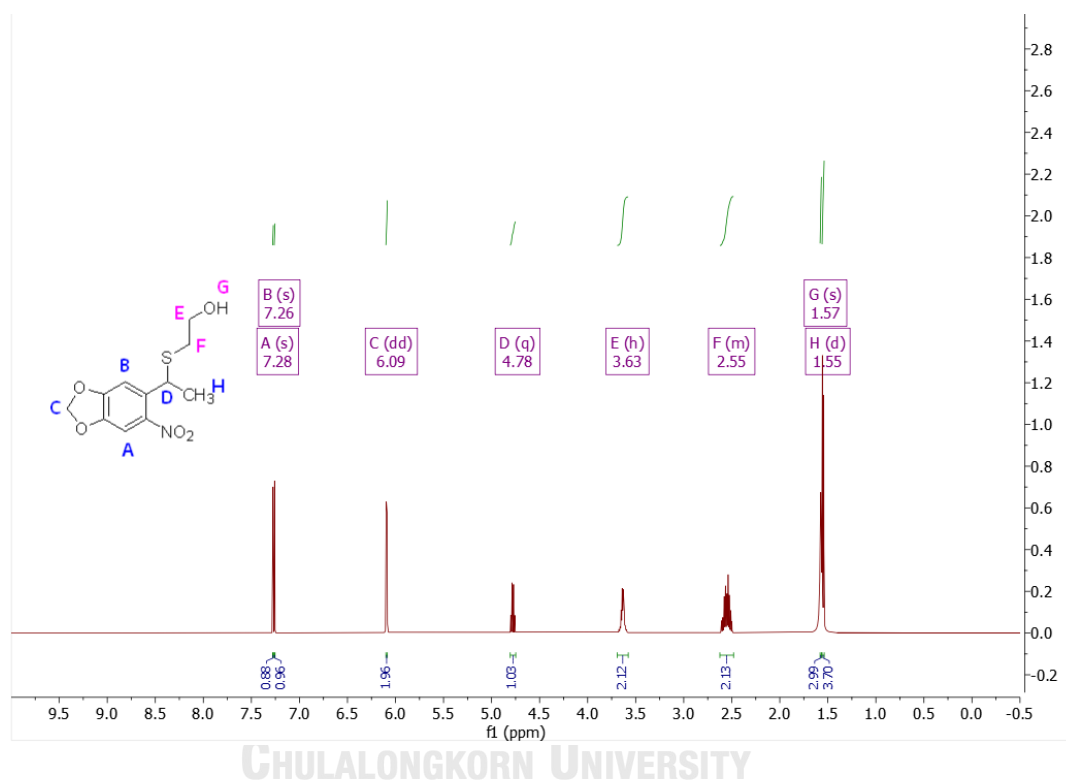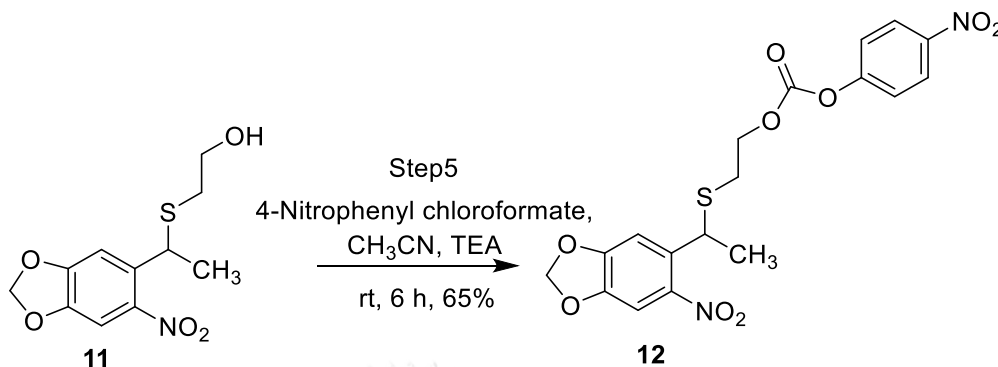

Figure 3.5 ^{1}H NMR spectrum of compound **11**.

3.1.5. Synthesis of 2-((1-(6-nitrobenzo[d][1,3]dioxol-5-yl)ethyl)thio) ethyl (4-nitrophenyl) carbonate (12)

Reaction step5

In order to synthesize the desired product, *N,N'*-disuccinimidyl carbonate (DSC) was added to a solution of compound **11** in acetonitrile followed by an addition of trimethylamine. It was anticipated that a nucleophilic acyl substitution reaction would occur to afford product **12**. However, the reaction following the literature reported procedure resulted in no reaction as only unreacted starting materials were recovered. Several other attempts in changing the solvent system from CH$_3$CN to THF or 1,4-dioxane also failed to get the reaction going. Changing the base from DIPEA to TEA have also been carried out. Again, the starting material did not react.

Alternatively, 4-nitrophenyl chloroformate had been used as a substitute for DSC. To a solution of compound **11** in acetonitrile was added 4-Nitrophenyl chloroformate in one portion followed by an addition of triethylamine. The reaction had proceeded very nicely, yielding the crude product compound **12**.

An additional optimization was to successfully decrease the reaction time from overnight to 6 h. The crude product using 4-nitrophenyl chloroformate as a reagent was thermally stable yet light sensitive. Storage in the dark is required. Exposure of the crude to light had to be kept minimum. Subsequent purification of the crude product with column chromatography resulted in pure compound **12** in 65%.

Compound **12** in CDCl$_3$ was analyzed by ^{1}H NMR spectroscopy to confirm the identity (Figure 3.6).
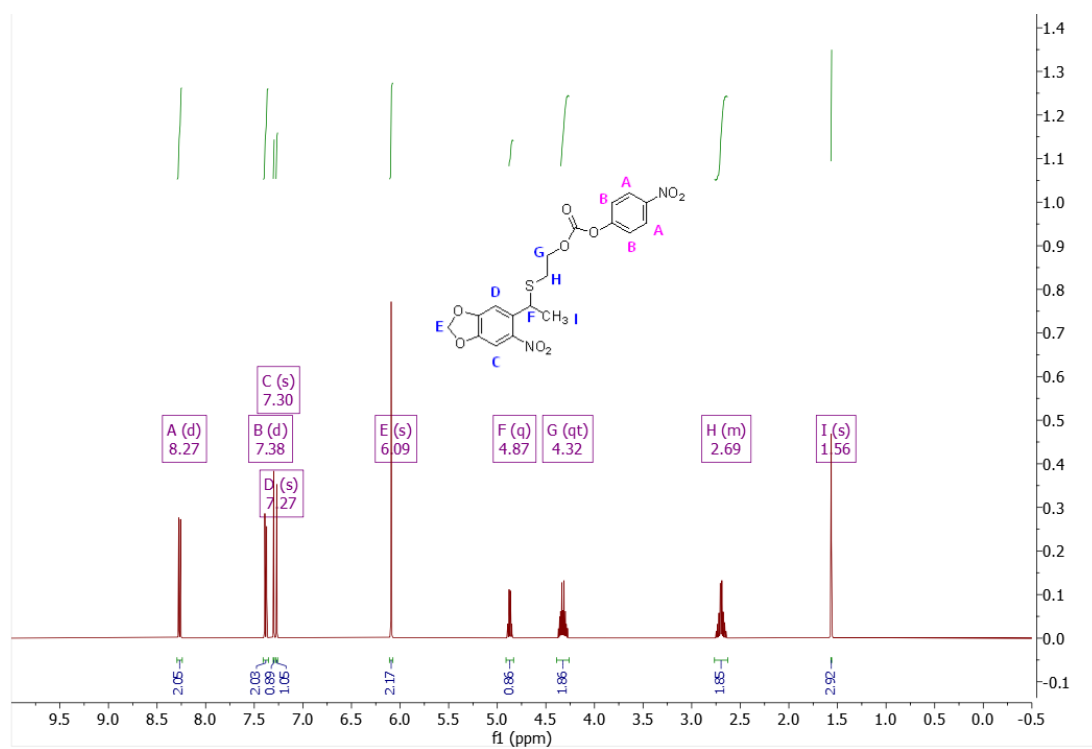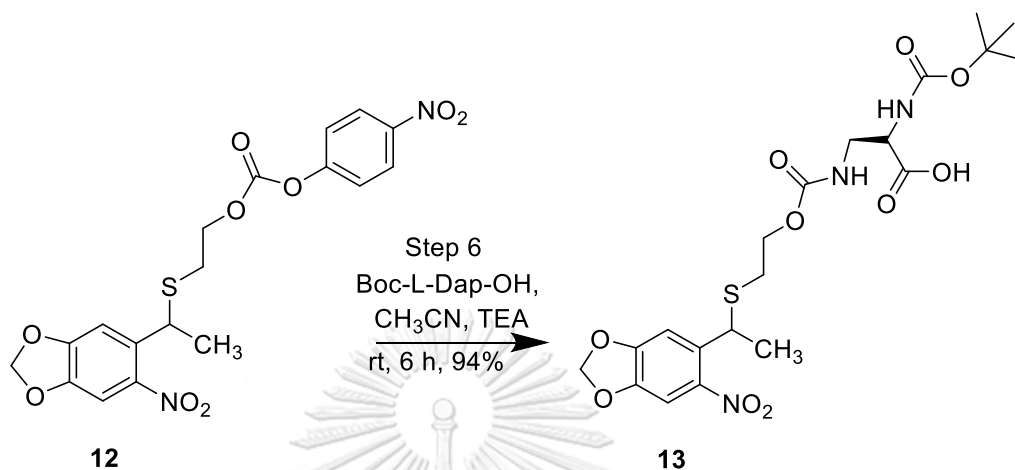

Figure 3.6 ^{1}H NMR spectrum of compound **12**.

3.1.6. Synthesis of (2*S*)-2-[(tert-Butoxycarbonyl)amino]-3-{[(2-{1-(6-nitro benzo[d][1,3]dioxol-5-yl)ethyl]zzthio}ethoxy)carbonyl] amino} propanoic acid (13)

Reaction step 6

In step 6, at first attempts to treat a solution of **12** with Boc-Dap-OH failed to give the product. Boc-Dap-OH is an amino acid molecule that is a zwitterion. Therefore, the addition of a base is required to prepare a nucleophilic amino acid. DIPEA and TEA have been used as a base for comparison. It was observed that this procedure was successful when TEA was used. With DIPEA, the reaction was incomplete, and by-products were also obtained. On the other hand, as TEA is a slightly stronger base, the reaction proceeded to completion.

The reaction occurred through a nucleophilic acyl substitution reaction where Boc-Dap-OH acts as a nucleophile to attack the acyl carbon of **12** by using NH_2 group. Then TEA draws a proton of $^+NH_2$ to generate **13** (Figure 3.7).
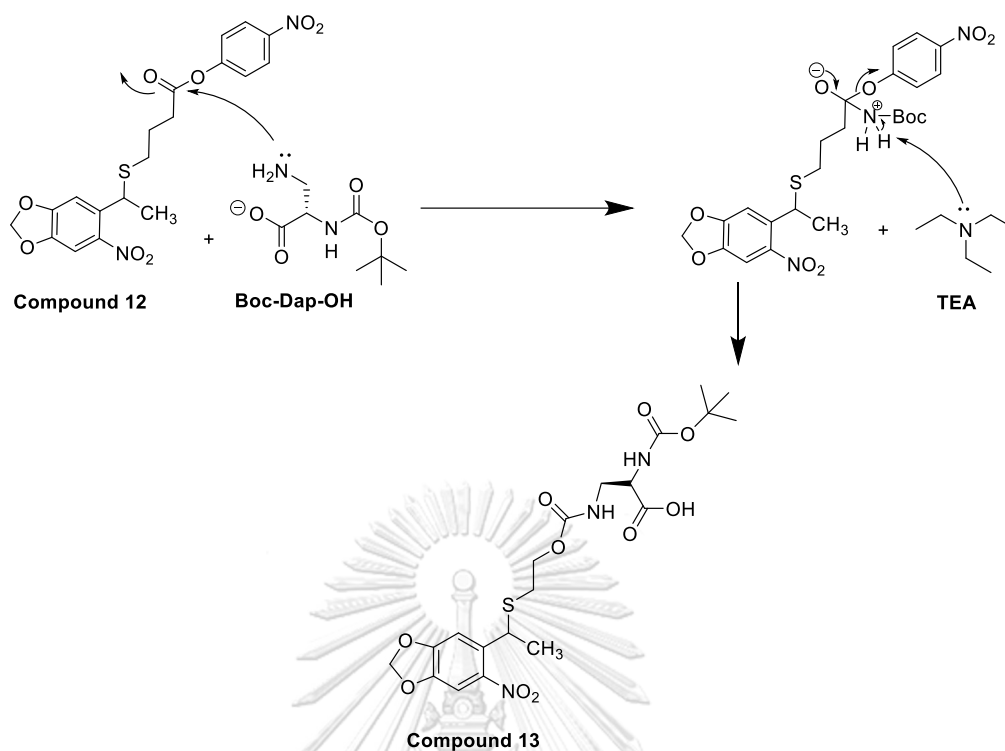
Figure 3.7 The reaction mechanism of compound **13.**

Apart from that, the reaction time was decreased from overnight to 6 h to give compound **13** in comparable amount. Although the literature recommended that the crude material be subjected to pre-purification using the Biotage Isolute HM-N® sorbent, it was found that this is not necessary. Compound **13** was obtained through column chromatographic purification in 94% yield. Figure 3.8 shows ^{1}H NMR spectrum of **13**. The chemical shifts at 5.99 ppm (s, 1H), 5.86 pp, (s, 1H), 4.17 ppm(s, 1H), 3.51 ppm (s, 2H), 1.38 ppm (s, 9H) are characteristics of the Boc-DAP-OH part.
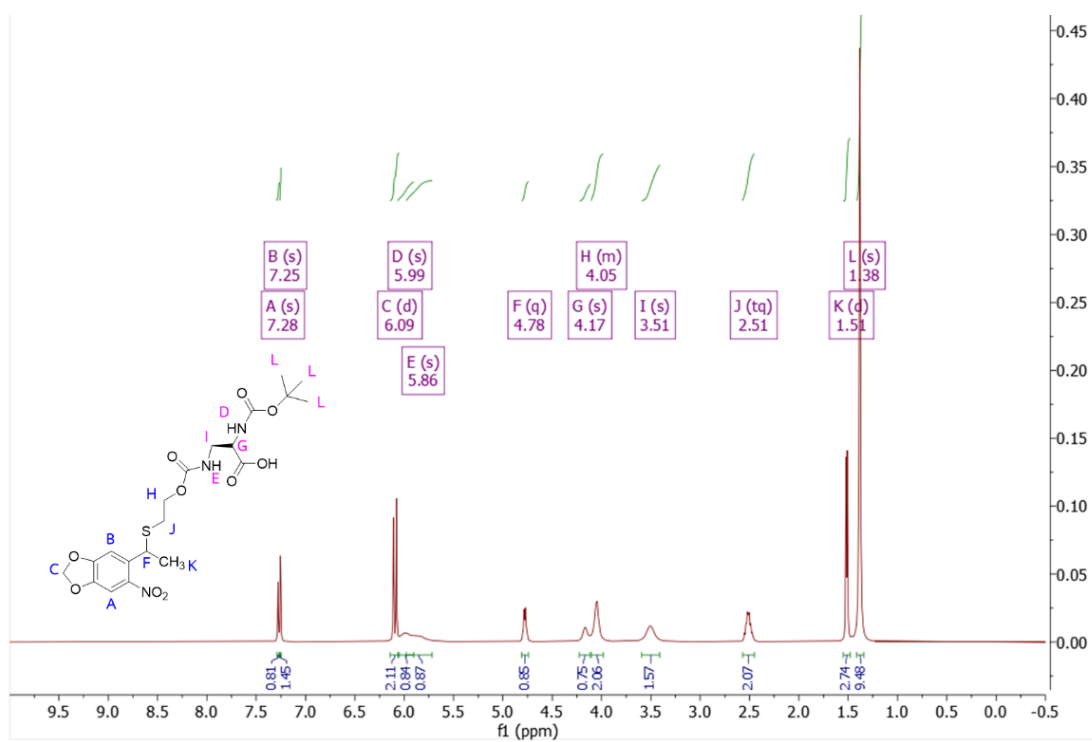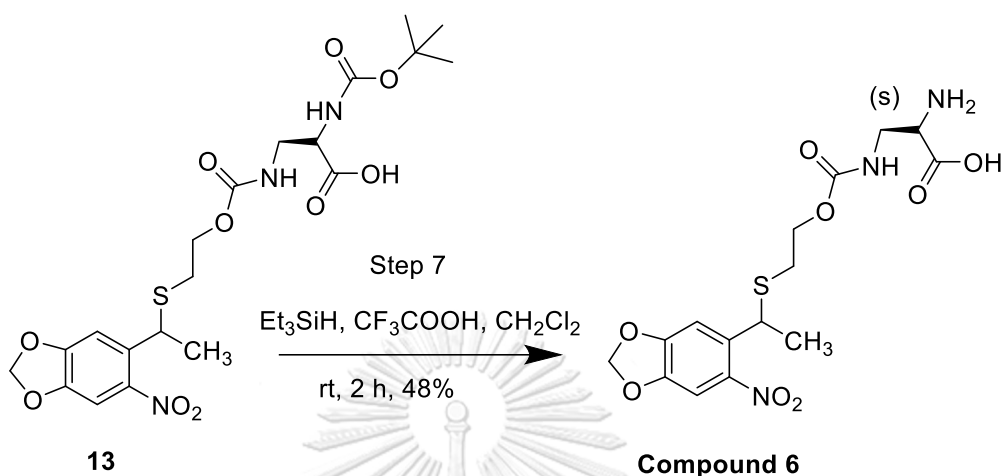
Figure 3.8 ^{1}H NMR spectrum of compound **13**.

3.1.7. Synthesis of (2*S*)-2-amino-3-{[(2-{[1-(6-nitrobenzo[d][1,3]dioxol-5-yl) ethyl]thio}ethoxy) carbonyl]amino}propanoic acid (6)

Reaction step 7

In the last step, triethylsilane and trifluoroacetic acid were used to dispose of the Boc-group. For the reaction mechanism, the proton of TFA was pulled by carbonyl of the tert-butyl acetate group in **13**, then loss of *tert*-butyl, which Et$_3$SiH was using to stabilize a carbocation. The main structure converts to a stable form *via* decarboxylation and generates a $^-$NH, then protonation by TFA to obtain compound **6**. It was found that to get a good yield of the desired DAP derivative (compound **6**), the precipitate should not be allowed to dry at room temperature more than 1 night to avoid decomposition. Figure 3.9 shows a reaction mechanism of compound **6**.
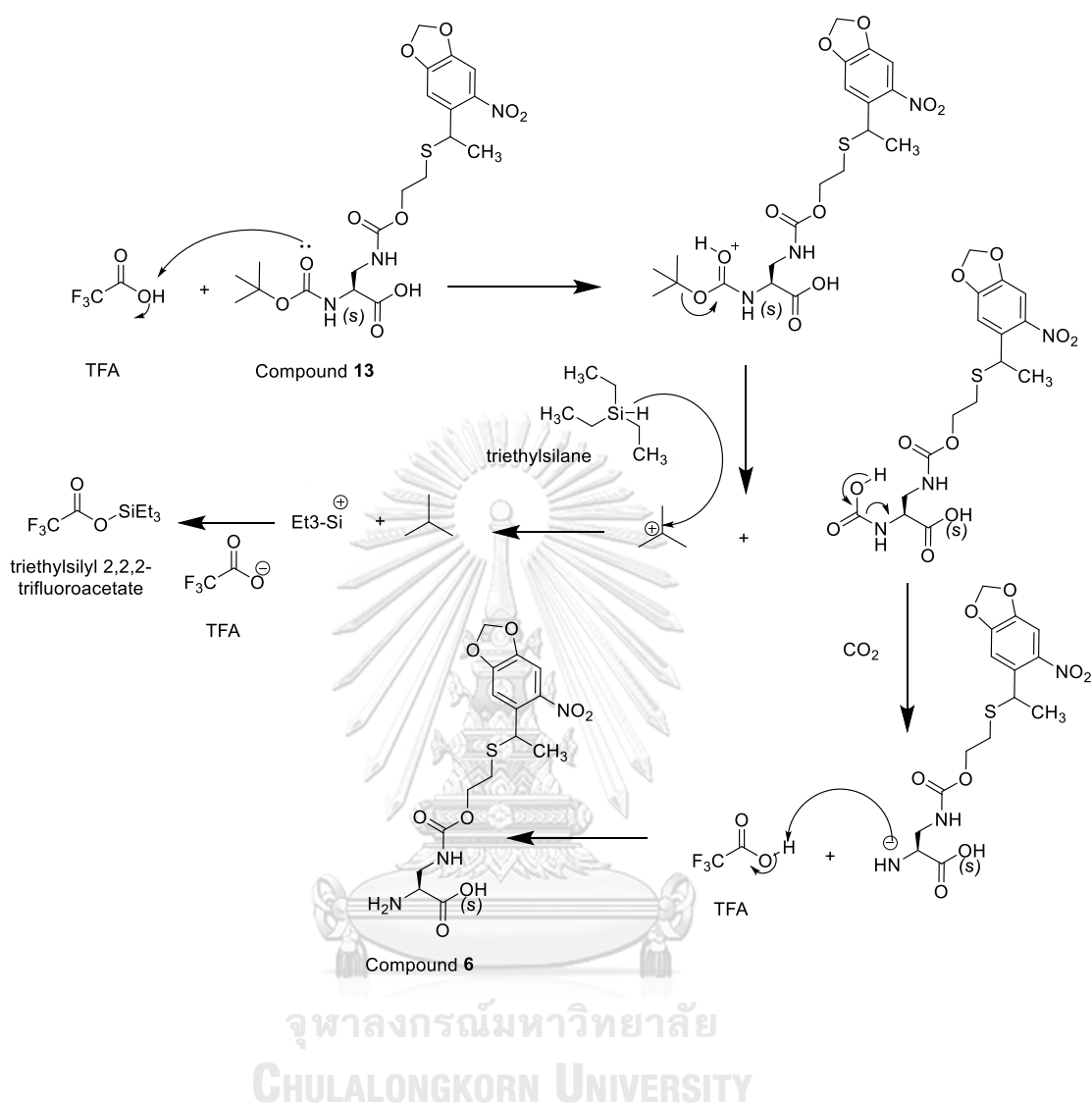
Figure 3.9 The reaction mechanism of compound **6**.

The structure of compound **6** was confirmed by ^{1}H and ^{13}C NMR spectroscopy. Ideally, the sample should be dissolved in deuterated methanol (methanol-d_4) in the presence of deuterated trifluoroacetic acid. The latter would help increase compound solubility in methanol-d_4. Instead, a small amount of non-deuterated trifluoroacetic acid was added to increase the solubility of the sample. No interference of the proton in TFA was observed in the range of chemical shifts of

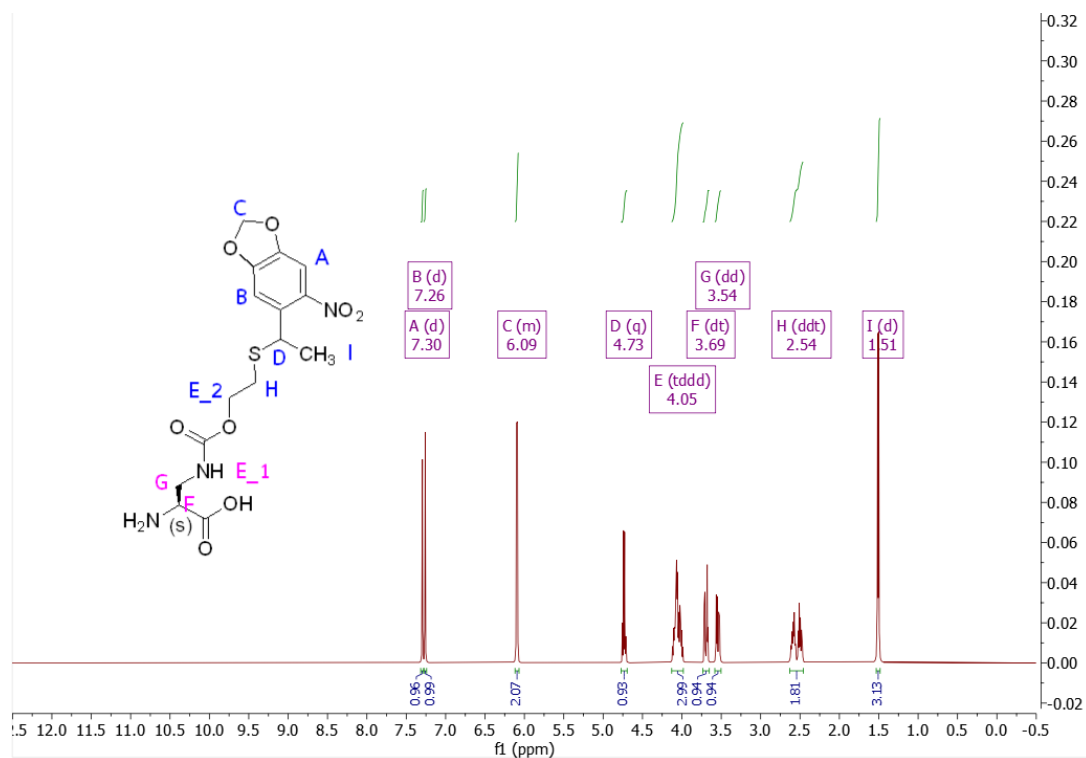interest. The ^{1}H NMR spectrum is shown in Figure 3.10 to confirm the identity of the desired product.

Figure 3.10 ^{1}H NMR spectrum of compound **6**.

^{13}C DEPT 135 experiment (Figure 3.11) was used to confirm existing carbons. The CH$_3$ and CH groups correspond positive signals, and the CH$_2$ groups represent negative signals. On the spectrum, the chemical shifts at 107.40 ppm, 104.04 ppm, 53.63 ppm, 38.44 ppm, and 21.69 ppm are positive signals of the CH and CH$_3$ carbons. The chemical shifts at 103.34 ppm, 64.16 ppm, 40.47 ppm, and 29.87 ppm represent negative signals of CH$_2$ carbon.
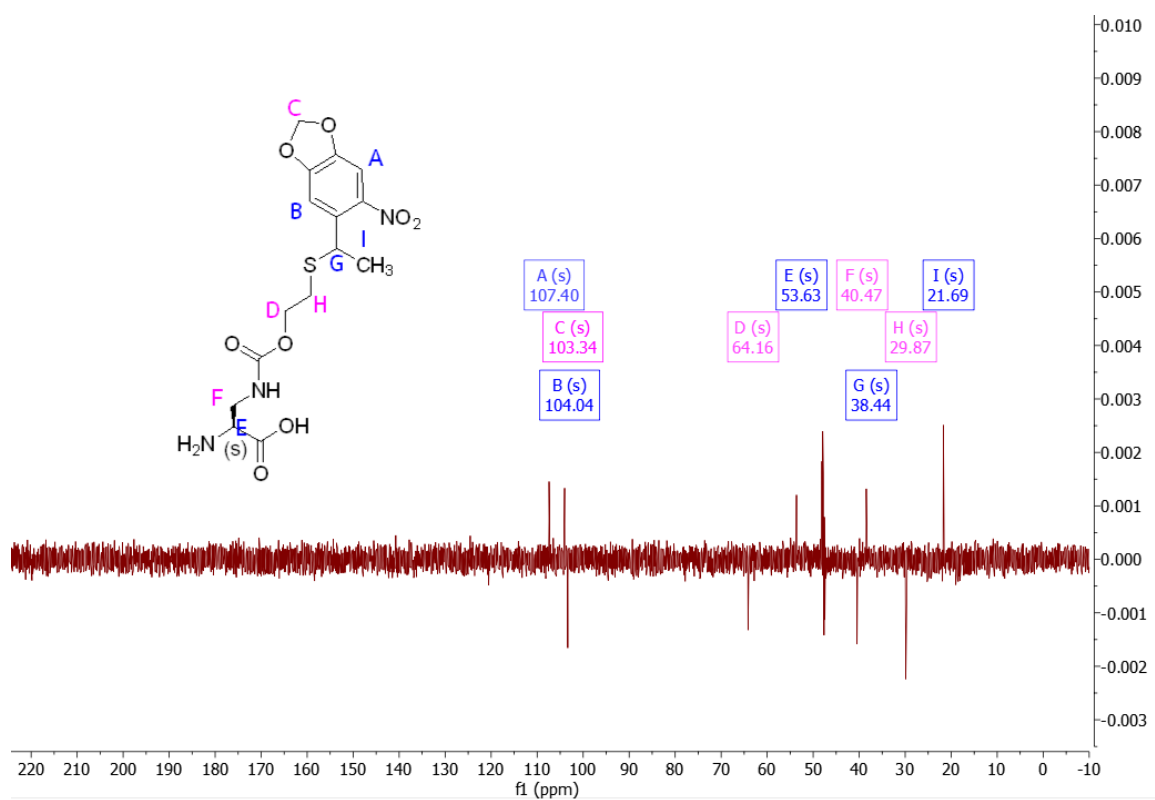
Figure 3.11 ^{13}C NMR DEPT 135 spectrum of compound **6**.

3.2. Genetic code expansion

The experiments in this section were performed in collaboration with Mr. Bhumrapee Eiamthong and Ms. Piyachat Meesawat from Vidyasirimedhi Institute of Science and Technology.

3.2.1. Genetic code expansion model system using BocK

We first established a genetic code expansion system for a PET-degrading enzyme, *Ideonella sakaiensis* PETase (IsPETase), with an unnatural amino acid known to be efficiently incorporated into proteins. We chose Boc-protected lysine (BocK), as the initial unnatural amino acid to test, as BocK is incorporated efficiently in response to an amber codon (TAG) placed within a gene of interest by wild-type amber-suppressor pyrrolysyl-tRNA synthetase/pyrrolysyl tRNA pair from *Methanosarcina mazei* [23]. We selected the catalytic serine residue of PETase, Ser160, to be replaced with BocK; in the eventual system, Ser160 will be replaced with its amino analog DAP.

An *E. coli* expression plasmid for IsPETase(Ser160TAG) was cloned on a pNHD1.3 backbone (a gift from Jason Chin, MRC LMB, UK). We previously observed limited solubility of wild-type IsPETase upon expression in *E. coli*; therefore, we included a protein solubility tag, a small ubiquitin-like modifier (SUMO) protein, with a cleavable TEV protease linker at the N-terminus of PETase (Ser160TAG), as well as a hexahistidine (His$_6$) tag for affinity purification. We first cloned pNHD1.3-His$_6$-SUMO-IsPETase *via* PCR amplification of SUMO and PETase genes, followed by Gibson assembly of the PCR amplicons with the digested backbone. We then introduced the Ser160TAG mutation *via* site-directed mutagenesis. Construct sequences were confirmed by Sanger sequencing.

We proceeded to test the expression of BocK-incorporated His$_6$-SUMO-IsPETase. We co-transformed *E. coli* BL21 with pNHD1.3-His$_6$-SUMO-IsPETase

(Ser160TAG) and pKW-pylRS/pylT, the latter containing expression cassettes for *Methanosarcina mazei* pyrrolysyl-tRNA synthetase/pyrrolysyl tRNA$_{CUA}$. We supplied 1 mM BocK with the cell growth media, and once the cells reached OD$_{600}$ of 0.5-0.6, added 1mM IPTG for 4 hours at 37 °C. Cells were then lysed, and their protein contents analyzed with Coomassie Blue staining and anti-His$_6$ western blotting. The expression analysis is as shown in Figure 3.12. We only observed under Coomassie and anti-His$_6$ blot the production of full-length His6-SUMO-IsPETase(Ser160TAG), ~44 kD in size, in the presence of the pKW plasmid, BocK amino acid, and IPTG inducer. A lot of truncated His6-SUMO-IsPETase(Ser160TAG) was also observed upon addition of IPTG in the absence of BocK; the size of the truncated protein (~30 kD) is consistent with translation termination, a natural process which competes with genetic code expansion, at the TAG160 position. While further optimizations are needed to maximize the yield of full-length SUMO-PETase, this initial genetic code expansion experiment confirmed that we can produce a PET-degrading enzyme IsPETase with an introduced unnatural amino acid at the catalytic serine position.
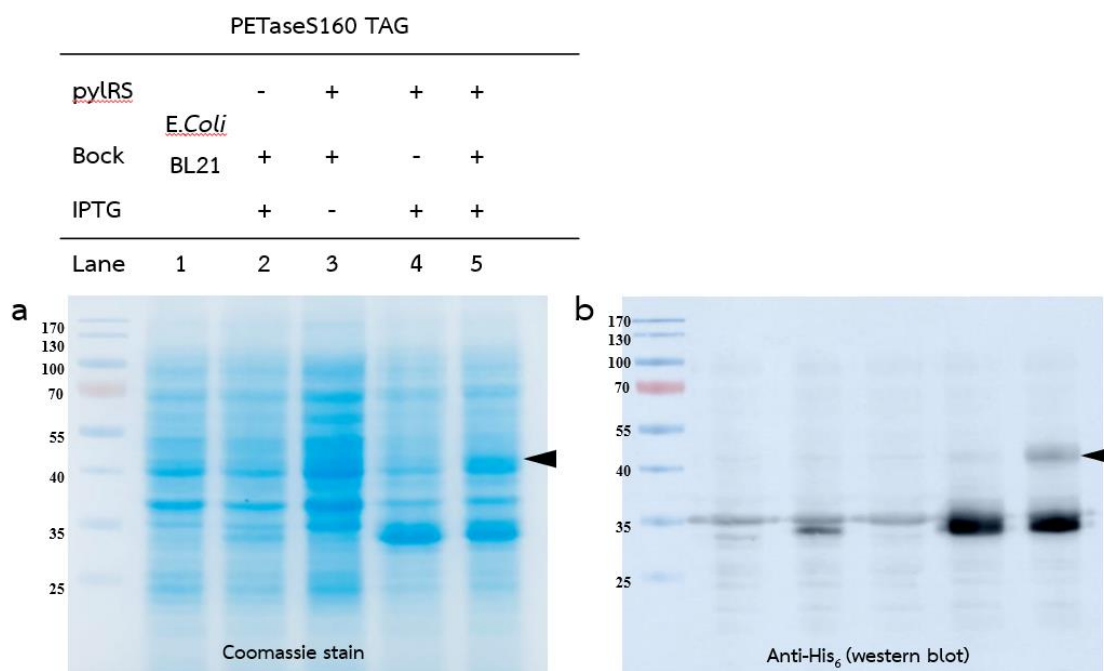

Figure 3.12 SDS-PAGE and Western blot analysis of genetic code expansion of *Ideonella sakeiensis* PETase (Ser160TAG).

(a) SDS-PAGE analysis of His6-SUMO-IsPETase(S160TAG) expression. (b) anti-His6 western blotting.

3.2.2. Genetic code expansion of a PET degrading enzyme encoded with DAP

During our investigations of BocK-dependent expression of IsPETase, we discovered a new PET-degrading enzyme from human saliva microbiome, which showed higher efficiency than IsPETase in PET degradation under a variety of conditions. We envisioned that the higher degradation activity of the new enzyme would also be beneficial for PET detection applications of a DAP-incorporated PET-degrading enzyme. We therefore switched our PET-degrading enzyme platform from IsPETase to this new enzyme, tentatively called MG8. We found that MG8 has higher solubility than IsPETase, obviating the need to use the solubility tag such as SUMO upon protein expression. The DNA sequence encoding the putative PET-degrading enzyme MG8 was custom-synthesized, then cloned into pNHD1.3 *via* restriction digestion with NdeI and XhoI. The catalytic serine of MG8, Ser185, was then mutated to TAG using site-directed mutagenesis. All constructs were verified by Sanger sequencing.

To express DAP-incorporated His_6-MG8, we co-transformed *E. coli* BL21 with pNHD1.3-His_6-MG8(Ser185TAG) and pMB1-DapRS/pylT, the latter containing expression cassettes for *Methanosarcina mazei* pyrrolysyl-tRNA synthetase mutant specific for DAP and an amber-suppressor pyrrolysyl $tRNA_{CUA}$. We supplied 100 µM DAP derivative (compound **6**) to the cell growth media, and grew cells in the dark once compound **6** was added. Once the cells reached OD_{600} of 0.5-0.6, we added 1mM IPTG for 20 hours at 37 °C. Cells were then lyzed, and the extracted proteins purified by affinity chromatography (nickel-nitrilotriacetic acid resin) under urea-induced denaturing condition to maximize the amount of soluble proteins. After elution with imidazole-containing buffer and confirmation of the presence of the desired protein within

collected fractions by SDS-PAGE, we dialyzed desired protein fractions into a buffer containing 25 mM Tris-HCl, pH 7.5, and 150 mM NaCl for refolding. We obtained putative high-purity MG8(Ser185-DAP derivative) as shown on SDS-PAGE analysis (Figure 3.13).
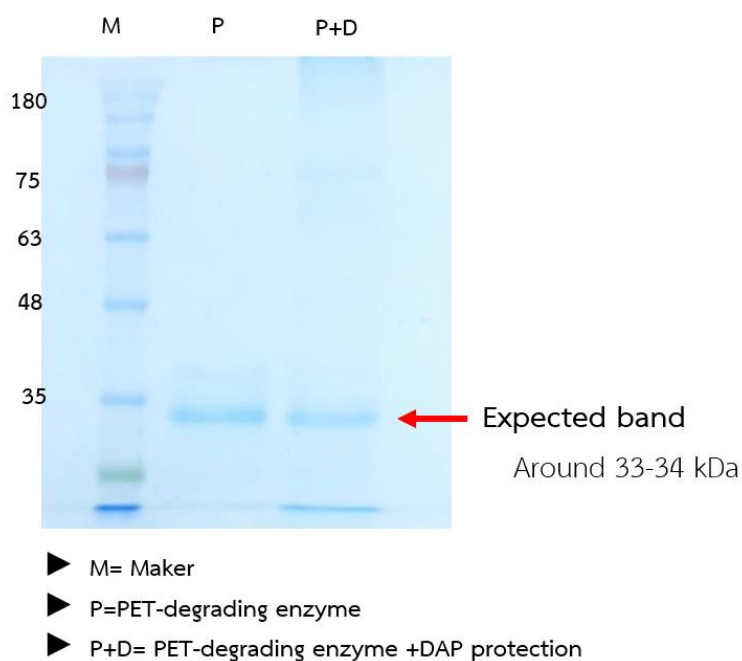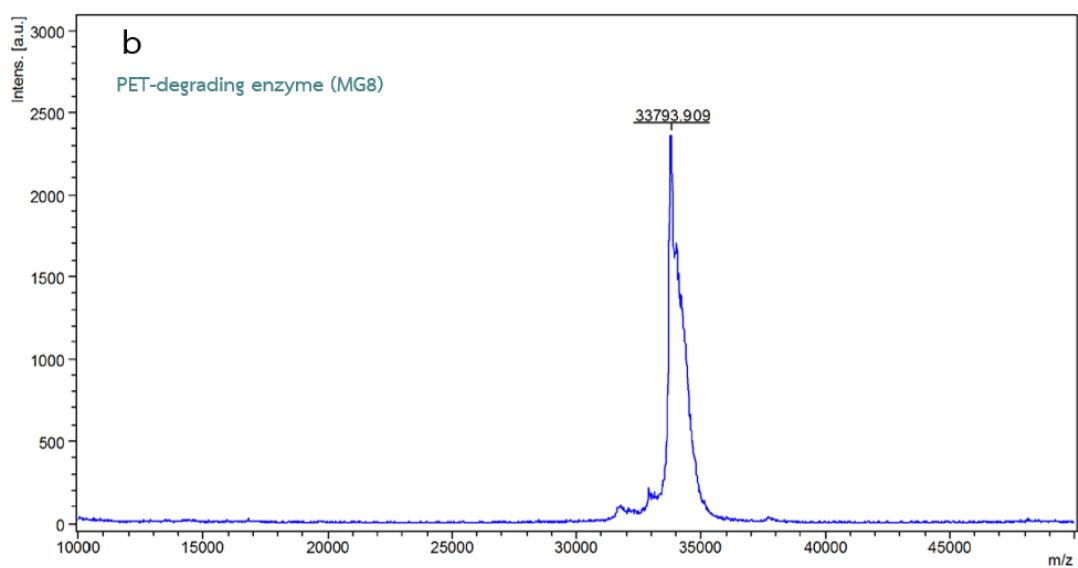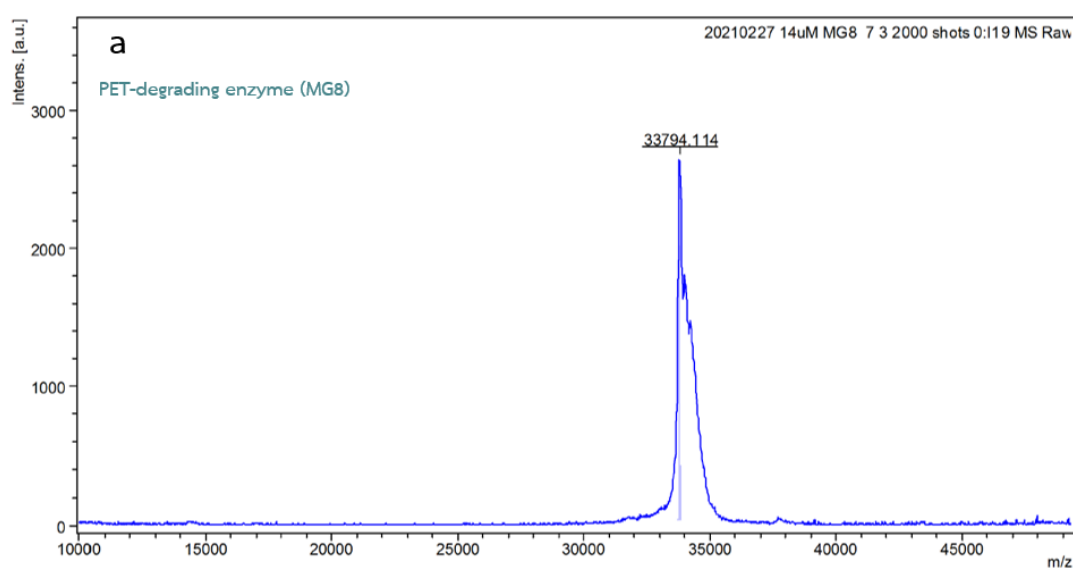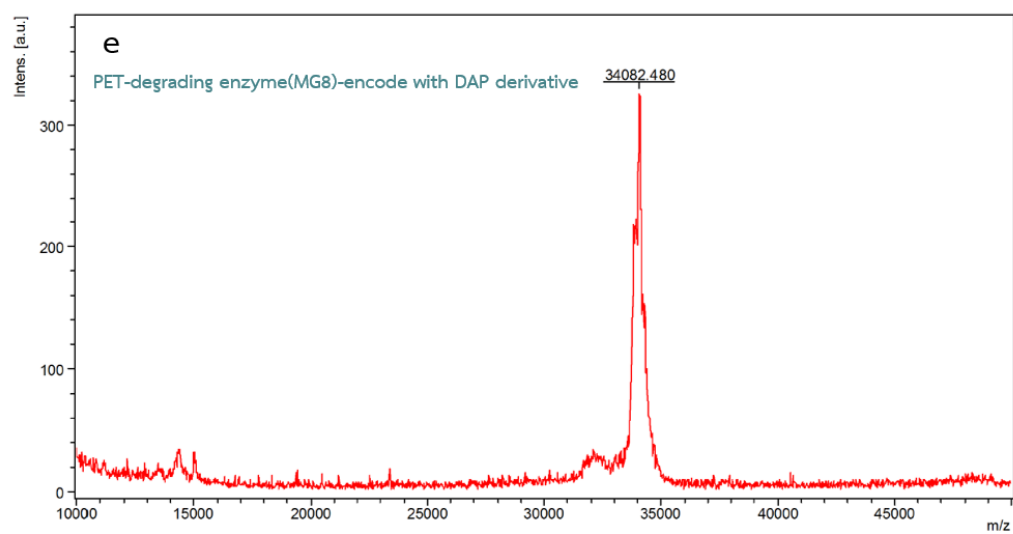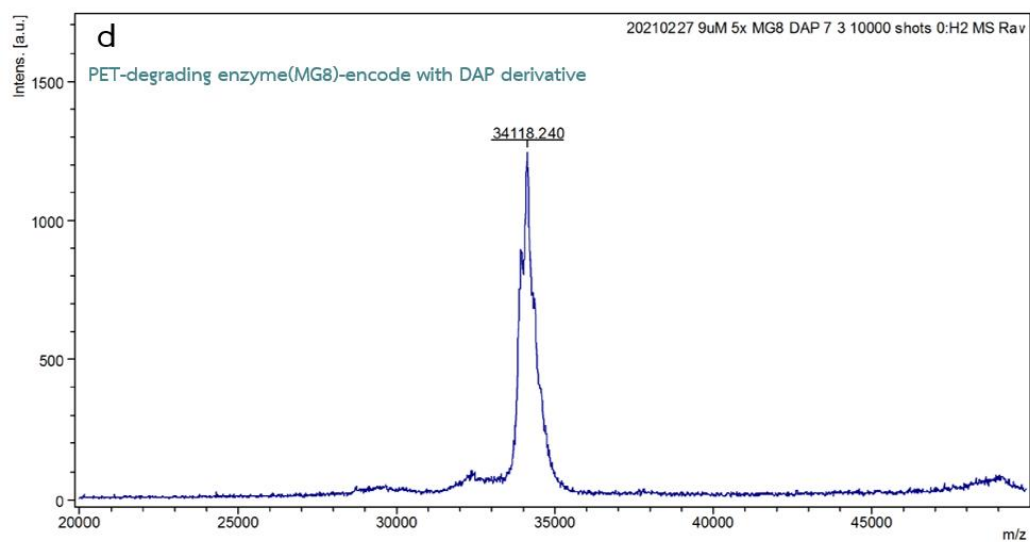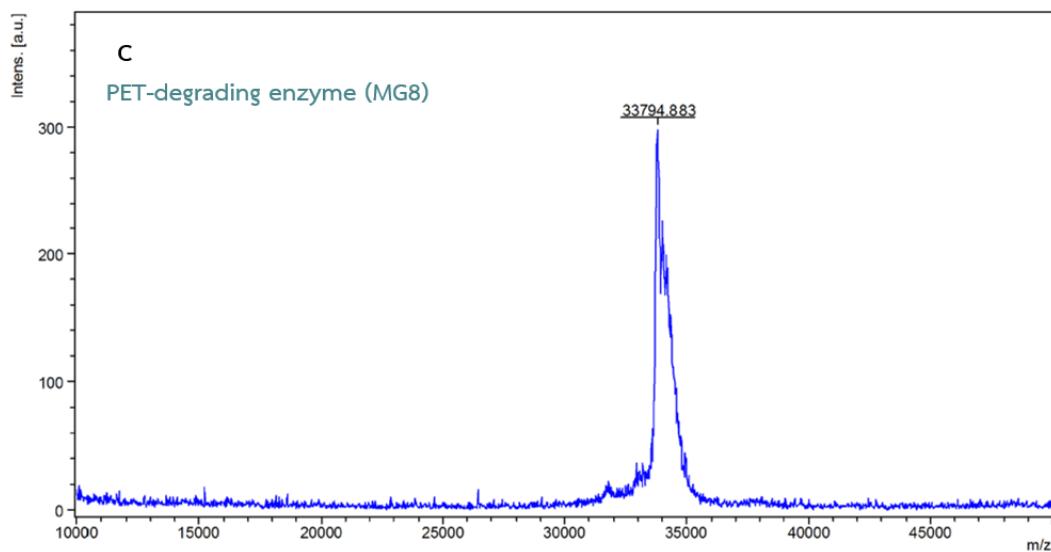

Figure 3.13 SDS-PAGE analysis of PET degrading enzyme (MG8)-DAP derivative (compound 6) was expressed into E. coli BL21 (Coomassie stain)
Lane 1(M): A Maker. Lane 2 (P): A pure PET degrading enzyme (MG8). Lane 3 (P+D): All combination of required components for genetic code expansion of PET degrading enzyme and DAP derivative resulting in a preferred protein was observed (around 33-34 kDa).

We further confirmed successful DAP derivative incorporation on MG8 by MALDI-TOF Mass Spectrometer (Figure 3.14). MG8 with incorporated DAP derivative (compound **6**) showed consistent increase in molecular weight as a result of the

large DAP derivative amino acid (observed 34,093.95 ± 21.04; predicted 34,089.4) compared to wild-type MG8 (observed 33,794.3 ± 0.5; predicted 33,791.4). This mass spectrometric experiment also confirmed that the DAP derivative, compound **6**, which was synthesized using modified protocols from an establish procedure, remains fully functional for genetic code expansion.
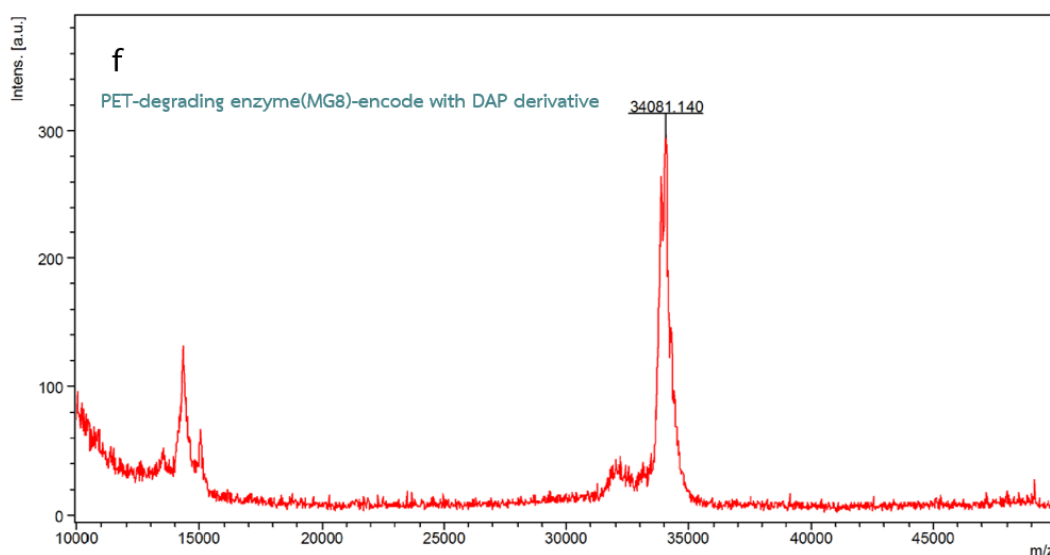
c PET-degrading enzyme (MG8)

33794.883

d PET-degrading enzyme(MG8)-encode with DAP derivative

20210227 9uM 5x MG8 DAP 7 3 10000 shots 0:H2 MS Rav

34118.240

e PET-degrading enzyme(MG8)-encode with DAP derivative

34082.480

Figure 3.14 DAP derivative (compound 6) in PET-degrading modified enzyme followed by MALDI.

(a-c), pure PET-degrading enzyme: expected molecular mass 33,791.36; observed 33,794.3 ± 0.51. (d-f), PET-degrading modified enzyme encoded with DAP derivative: expected 34,089.40; observed 34,093.95 ± 21.04. The experiment was performed in three biological replicates with similar results.

We still need to verify that the DAP derivative on MG8 can be efficiently deprotected by UV light to generate the desired MG8-DAP. The light-mediated deprotection mechanism is illustrated in Figure 3.15. First, the 6-nitropiperonulmethyl group of the protecting moiety is cleaved by UV light irradiation at 365 nm. Intramolecular cyclization to evict episulfide and carbon dioxide molecules is then promoted by incubating the light-treated protein with 5 mM dithiothreitol (DTT) at pH 8.5. We will confirm the successful deprotection of the DAP derivative to generate MG8-DAP with MALDI-TOF.
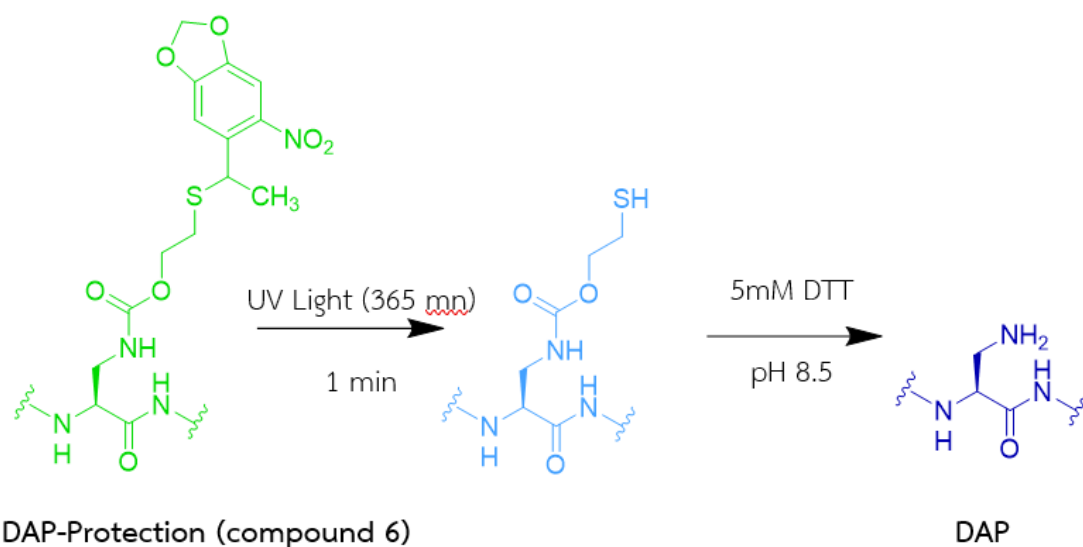
Figure 3.15 Encoded compound **6** was photo-deprotected leading to an intermediate, which spontaneously fragments under nucleophilic conditions to reveal DAP.

We further confirmed that compound **6** incorporated into the MG8 enzyme can be deprotected by light to generate DAP. Upon UV irradiation for 1 min followed by incubation in the presence of DTT at pH 8.5 overnight, the molecular weight of MG8 containing DAP could be observed by MALDI-TOF Mass Spectrometer (Figure 3.16). MG8 with incorporated DAP showed a consistent decrease in molecular weight because of the removal of the protecting group.
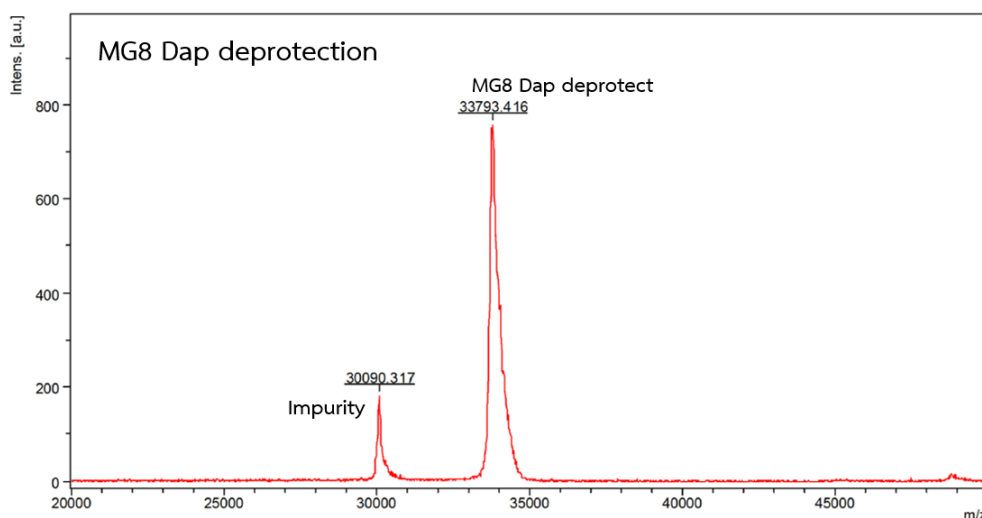
Figure 3.16 Deprotection of DAP derivative (compound 6)
in PET-degrading modified enzyme(MG8) followed by MALDI, observed 33,786.67±
7.07; predicted 33,790.36.

3.3 Detection of PET microplastic by using a new PET degrading enzyme (MG8) encoded with DAP

We configured an assay utilizing DAP-incorporated MG8 to detect PET primary microplastic, *via* fusion of DAP-incorporated MG8 to a split green fluorescent protein (GFP) system. Here, MG8-DAP was expressed as a fusion to GFP11, a smaller fragment of the split GFP system. Addition of the large fragment of split GFP, called GFP1-10, allows reconstitution of the beta-barrel structure of GFP and fluorophore maturation. We proceeded to test the detection with PET powder (~2 mm) incubated with 7.59 µM of DAP-incorporated MG8-GFP11 in 50 mM Tris-HCl, pH 9.0, 5M NaCl at 50 °C, which we replenished three times over for 5h. Addition of GFP1-10 to allow GFP to reconstitute was performed at 37 °C for 24 h, with 5 mg/mL BSA added as a blocking reagent. GFP fluorescence from MG8-DAP-labeled PET primary microplastic can be

visualized by naked eye upon excitation with a blue LED illuminator (Figure 3.17). In contrast, MG8-DAP inactivated with a pan-serine hydrolase inhibitor, PMSF, showed minimal fluorescence at background levels, comparable to a blank (omit enzyme) control. Figure 3.18 shows fluorescence intensity quantification of PET primary microplastic labeled with GFP through MG8-DAP, which exhibited ~35-fold increase in fluorescence intensity compared to control reactions.
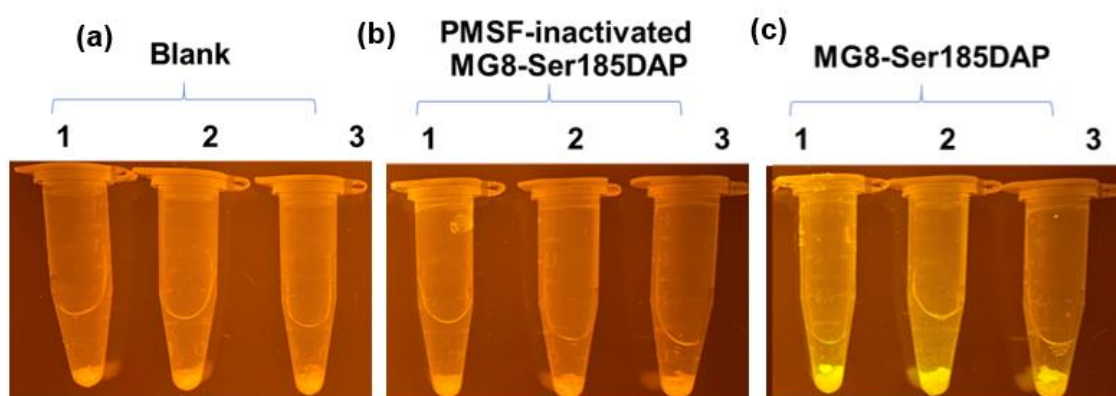

Figure 3.17 PET primary microplastic detection with MG8-Ser185DAP.

(a) and (b) control reactions with no enzyme added, and PMSF-inactivated MG8-Ser185DAP, respectively. (c) GFP fluorescence from GFP-labeled microplastic *via* MG8-DAP.
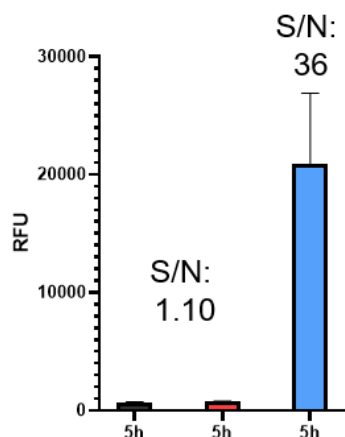
Figure 3.18 Quantification of fluorescence intensity from the three conditions from Figure 3.18. Reactions for each condition were performed in triplicate. Error bars, +/- SD. Black bar, no enzyme control; orange bar, PMSF-inactivated MG8-DAP control; blue bar, MG8-DAP.

3.4. Summary

The synthesis and optimization of 2,3-diaminopropionic acid derivative (Compound **6**) was carried out using a method of Nicolas Huguenin-Dezot's[23] with a major modification in some steps and slight modification in others. The desired compound was successfully synthesized in seven steps. We then used compound **6** successfully in genetic code expansion experiments in *E. coli* to produce a PET-degrading enzyme modified with a DAP derivative at its catalytic site.

CHAPTER IV

CONCLUSION

The synthesis and optimization of (2*S*)-2-amino-3-{[(2-{[1-(6-nitrobenzo[d]
[1,3]dioxol-5-yl)ethyl] thio}ethoxy)carbonyl] amino}propanoic acid (compound **6**) was
successfully carried out. The methods of Huguenin-Dezot's[23] was utilized with some
major modifications to give the target compound in seven steps and 7 % overall
yield and a much shorter time. The compounds from step 3 onwards are sensitive to
light. Therefore, they were carefully handled and exposure to light was minimized.

The target compound **6** is a derivative of DAP, which has been reported to be
able to trap acyl-enzyme intermediates through a stable amide linkage upon
incorporation into proteins to place their catalytic residues such as serine and
cysteine, *via* genetic code expansion. Therefore, once the PET degrading enzyme is
encoded with DAP derivative or compound **6**, then the degradation process is
blocked. We were using this trapping acyl-enzyme intermediate to detect PET plastic
combined staining method and fluorescence spectroscopy. We set up genetic code
expansion systems for two PET-degrading enzymes—*Ideonella sakeiensis* PETase and
a newly discovered MG8 enzyme—and demonstrated BocK unnatural amino acid
incorporation in the former, and DAP derivative incorporation in the latter. Once
light-mediated deprotection of the 6-nitropiperonulmethyl group on the DAP
derivative on the PET-degrading enzyme is confirmed, the system will be poised for
use for PET microplastic detection. To detect PET plastics, we envision an assay akin
to enzyme-linked immunosorbent assay (ELISA) where the DAP-modified PET-
degrading enzyme, which can now covalently capture PET plastics, would replace
the conventional antibodies and other antigen-binding molecules used in these
assays.

Beyond PET microplastic detection, DAP-modified PET-degrading enzymes
have several other utilities which we plan to explore. The ability to capture the acyl-

enzyme intermediate of a PET-degrading enzyme would provide a unique PET plastic-PET degrading enzyme complex for structural characterizations; currently, no enzyme-substrate complex of PET-degrading enzymes has been reported. DAP-modified PET-degrading enzymes also have the ability to directly functionalize PET plastics, *via* genetic fusion of desired cargoes onto the enzyme gene. We envision appending diverse cargoes—including fluorescent reporters, metabolite or metal sensors, and genetic material sensors, directly onto PET, and convert such plastics into versatile sensors for diverse applications.

REFERENCES

1. Eriksen, M.; Lebreton, L.C.M.; Carson, H.S.; Thiel, M.; Moore, C.J.; Borerro, J.C.; Galgani, F.; Ryan, P.G.; Reisser, J. "Plastic Pollution in the World's Oceans: More than 5 Trillion Plastic Pieces Weighing over 250,000 Tons Afloat at Sea" *PLoS One*, **2014**, *9*, 1-15.

2. Farrel, P.; Nelson, K. "Trophic level transfer of microplastic: *Mytilus edulis* (L.) to *Carcinus maenas* (L.)" *ENVIRON POLLUT,* **2013**, *177*, 1-3.

3. Kühn, S.; Van Franeker, J.A. "Quantitative overview of marine debris ingested by marine megafauna" *Mar. Pollut. Bull,* **2020**, *151*, 110858.

4. Kara Rogers "Microplastics" https://www.britannica.com (accessed October 5, 2019)

5. Rochman, M.C. "The Story of Plastic Pollution: From the Distant Ocean Gyres to the Global Policy Stage" *Oceanography,* **2020**, *33*, 60 – 70.

6. "Polyethylene Terephthalate (PET): A Comprehensive Review" https://omnexus.specialchem.com (accessed October 14, 2019)

7. Zarfl, C. "Promising techniques and open challenges for microplastic identification and quantification in environmental matrices" *Anal. Bioanal. Chem,* **2019**, *411*, 3743–3756.

8. McDermid, J.K.; McMullen, L.T. "Quantitative analysis of small-plastic debris on beaches in the Hawaiian archipelago" *Mar. Pollut. Bull,* **2004**, *48*, 790-794.

9. Mariano, S.; Tacconi, S.; Fidaleo, M.; Rossi, M.; Dini, L. "Micro and Nanoplastics Identification: Classic Methods and Innovative Detection Techniques" *Front. Toxicol*, **2021**, *3*, 636640.

10. "Guide to Infrared Spectroscopy" https://www.bruker.com/en/products-and-solutions/infrared-and-raman/ft-ir-routine-spectrometer/what-is-ft-ir-spectroscopy.html (accessed October 14, 2021)

11. Löder, G. J. M.; Gerdts, G. "Methodology Used for the Detection and Identification of Microplastics—A Critical Appraisal" In: Bergmann M.; Gutow L.; Klages M. (Eds) *Marine Anthropogenic Litter*, Springer, Cham. 2015

12. "Raman Imaging and Spectroscopy" https://www.horiba.com/en_en/raman-imaging-and-spectroscopy/ (accessed October 14, 2021)

13. "Advantages and disadvantages of Raman Spectroscopy" http://www.rdrs.ro/blog/articles/advantages-disadvantages-raman-spectroscopy/ (accessed October 14, 2021)

14. Erni-Cassola, G.; Gibson, M.I.; Thompson, R.C.; Christie-Oleza, J.A. "Lost, but Found with Nile Red: A Novel Method for Detecting and Quantifying Small Microplastics (1 mm to 20 µm) in Environmental Samples" *Environ. Sci. Technol,* **2017***, 51,* 13641–13648.

15. Song, Y.K.; Hong, S.H.; Jang, M.; Han, G.M.; Rani, M.; Lee, J.; Shim, W.J. "A comparison of microscopic and spectroscopic identification methods for analysis of microplastics in environmental samples" *Mar. Pollut. Bull*, **2015**, *93*, 202–209.

16. Gniadek, M.; Dabrowska, A. "The marine nano- and microplastics characterisation by SEM-EDX: The potential of the method in comparison with various physical and chemical approaches" *Mar. Pollut. Bull*, **2019**, *148*, 210–216.

17. Araujo, C.F.; Nolasco, M.M.; Ribeiro, M.P.A.; Ribeiro-Claro, J.A.P. "Identification of microplastics using Raman spectroscopy: Latest developments and future prospects" *Water Res*, **2018**, *142*, 426-440.

18. Yoshida, S.; Hiraga, K.; Takehana, T.; Taniguchi, I.; Yamaji, H.; Maeda, Y.; Toyohara, K.; Miyamoto, Kenji.; Kimura, Y.; Oda, K. "A bacterium that degrades and assimilates poly (ethylene terephthalate)" *Science*, **2016**, *351*, 1196-1199.

19. Austin, H. P.; Allen, M.D.; Donohoe, B.S.; Rorrer, N. A.; Kearns, F.L.; Silveira, R.L.; Pollard, B.C.; Dominick, G.; Duman, R., Omari, K.E.; Mykhaylyk, V.; Wagner, A.; Michener, W.E.; Amore, A.; Skaf, M.S.; Crowley, M.F.; Thorne, A.W.; Johnson, C.W.; Woodcock, H. L.; McGeehan, J.E.; Beckham, G.T. "Characterization and engineering of a plastic-degrading aromatic polyesterase" *PNAS*, **2018**, *115*, E4350-E4357.

20. "Genetic Code Expansion" https://www.addgene.org (accessed October 20, 2019)

21. Huang, Y.; Liu, T. "Therapeutic applications of genetic code expansion" *Synth Syst Biotechnol*, **2018**, *3*, 150–158.

22. Kobylarz, J.K.; Grigg, C.J.; Takayama, J.S.; Rai, K.D.; Heinrichs, E.D.;

Murphy, E.P.M. "Synthesis of L-2,3-Diaminopropionic Acid, a Siderophore and Antibiotic Precursor" *Chem. Biol*, **2014**, *21*, 379-388.

23. Huguenin-Dezot, N.; Alonzo, D.A.; Heberlig, G.W.; Mahesh, M.; Nguyen, D.P.; Dornan, M.H.; Boddy, C.N.; Schmeing, T. M.; Chin, J.W. "Trapping biosynthetic acyl-enzyme intermediates with encoded 2,3-diaminopropionic acid" *Nature*, **2019**, *565*, 112–117.
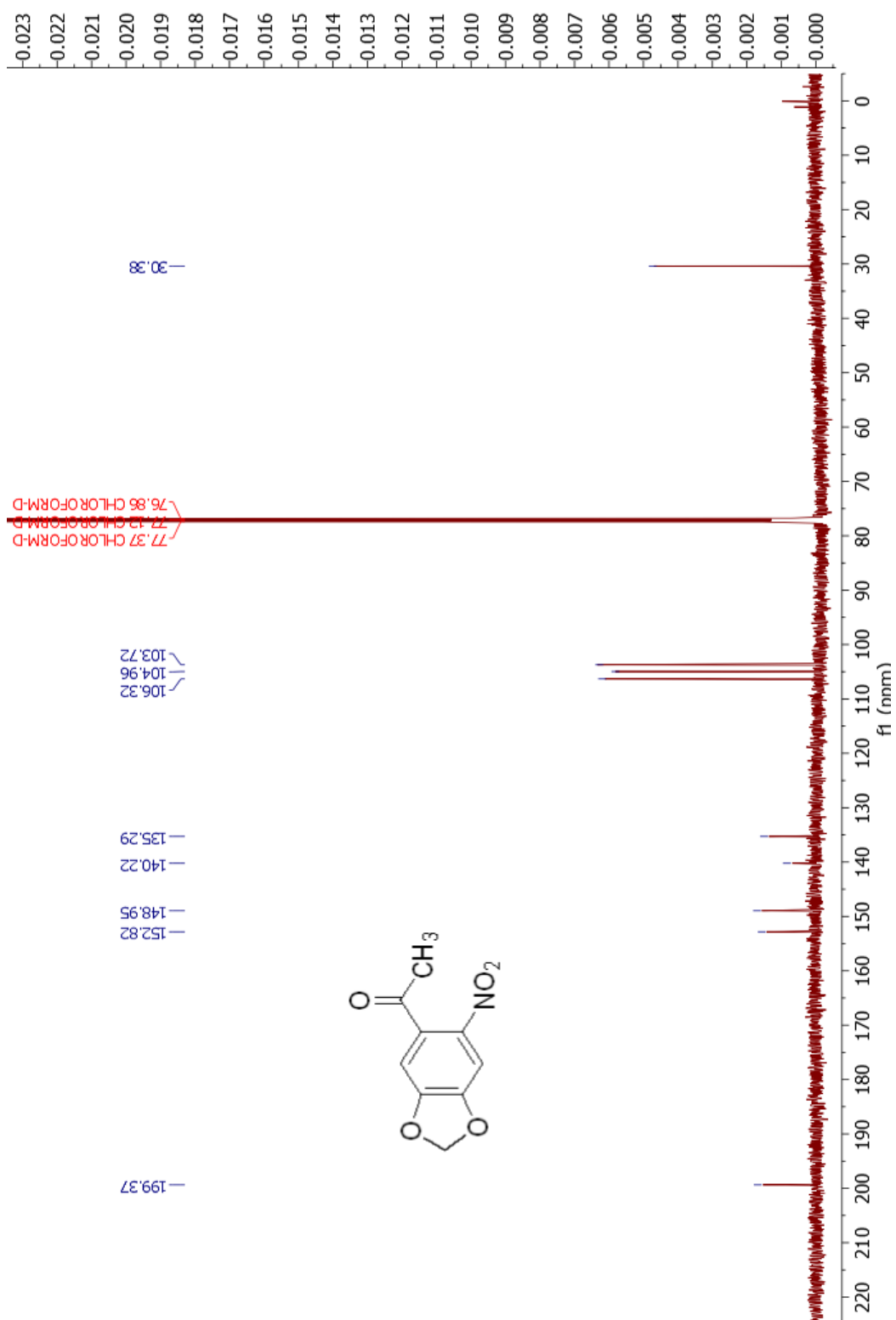
APPENDIX

Figure A-1 ^{13}C NMR spectrum of 4',5'-methylenedioxy-2'-nitroacetophenone (**8**)
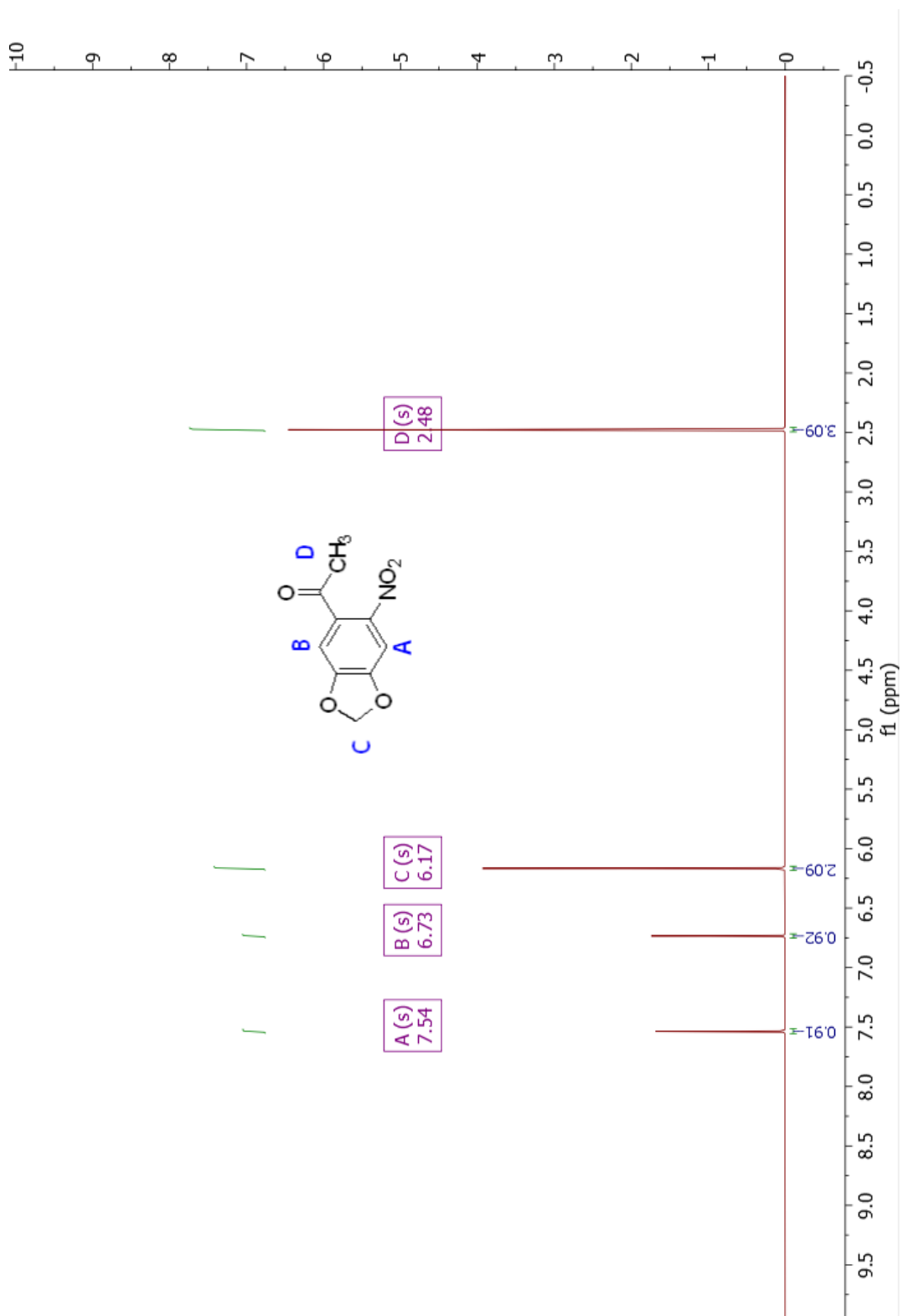
Figure A-2 ^{1}H NMR spectrum of 4',5'-methylenedioxy-2'-nitroacetophenone (**8**)
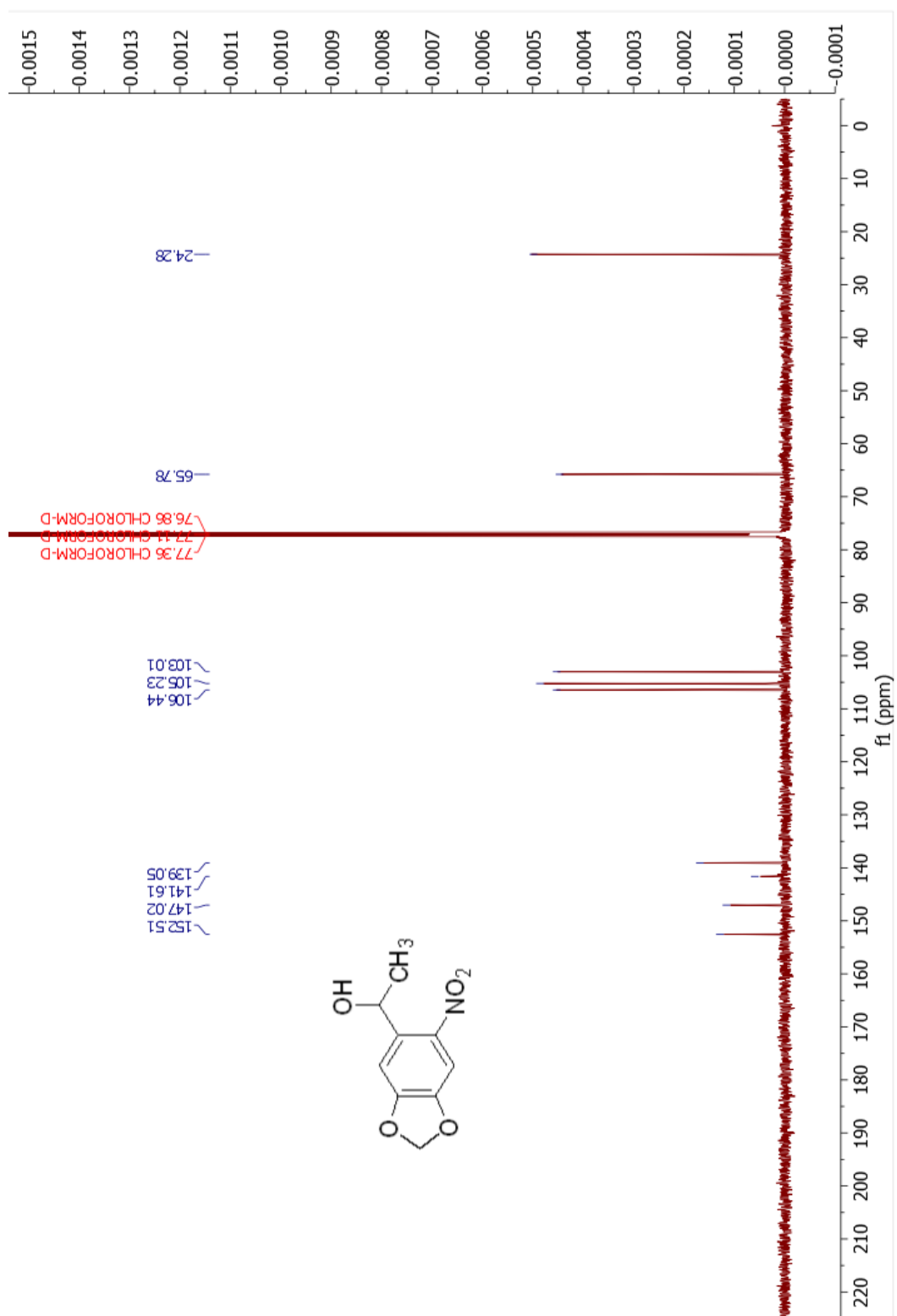
Figure A-3 ^{13}C NMR spectrum of 1-[4',5'-(Methylenedioxy)-2'-nitrophenyl]ethanol (**9**)
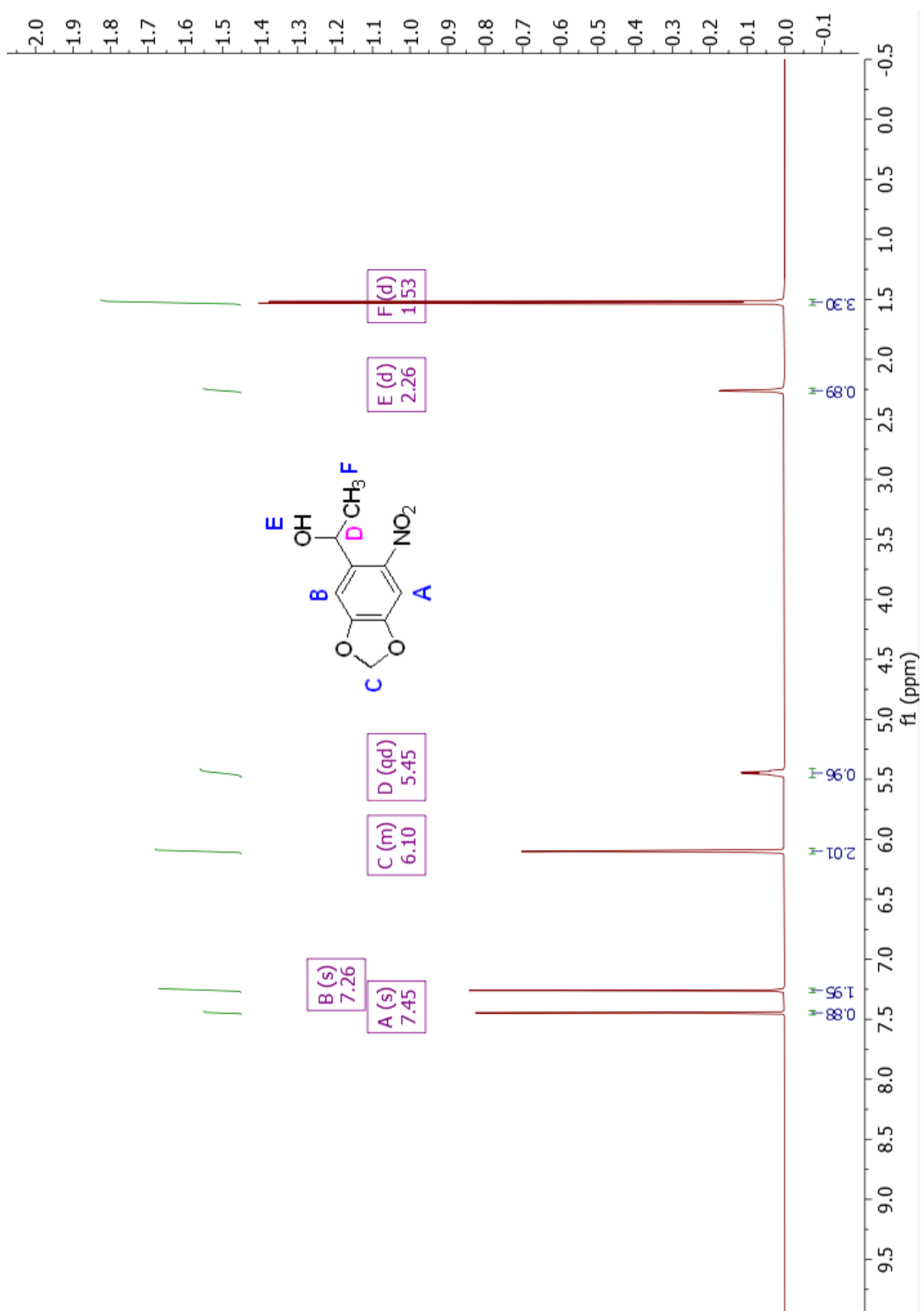
Figure A-4 ^{1}H NMR spectrum of 1-[4',5'-(Methylenedioxy)-2'-nitrophenyl]ethanol (**9**)
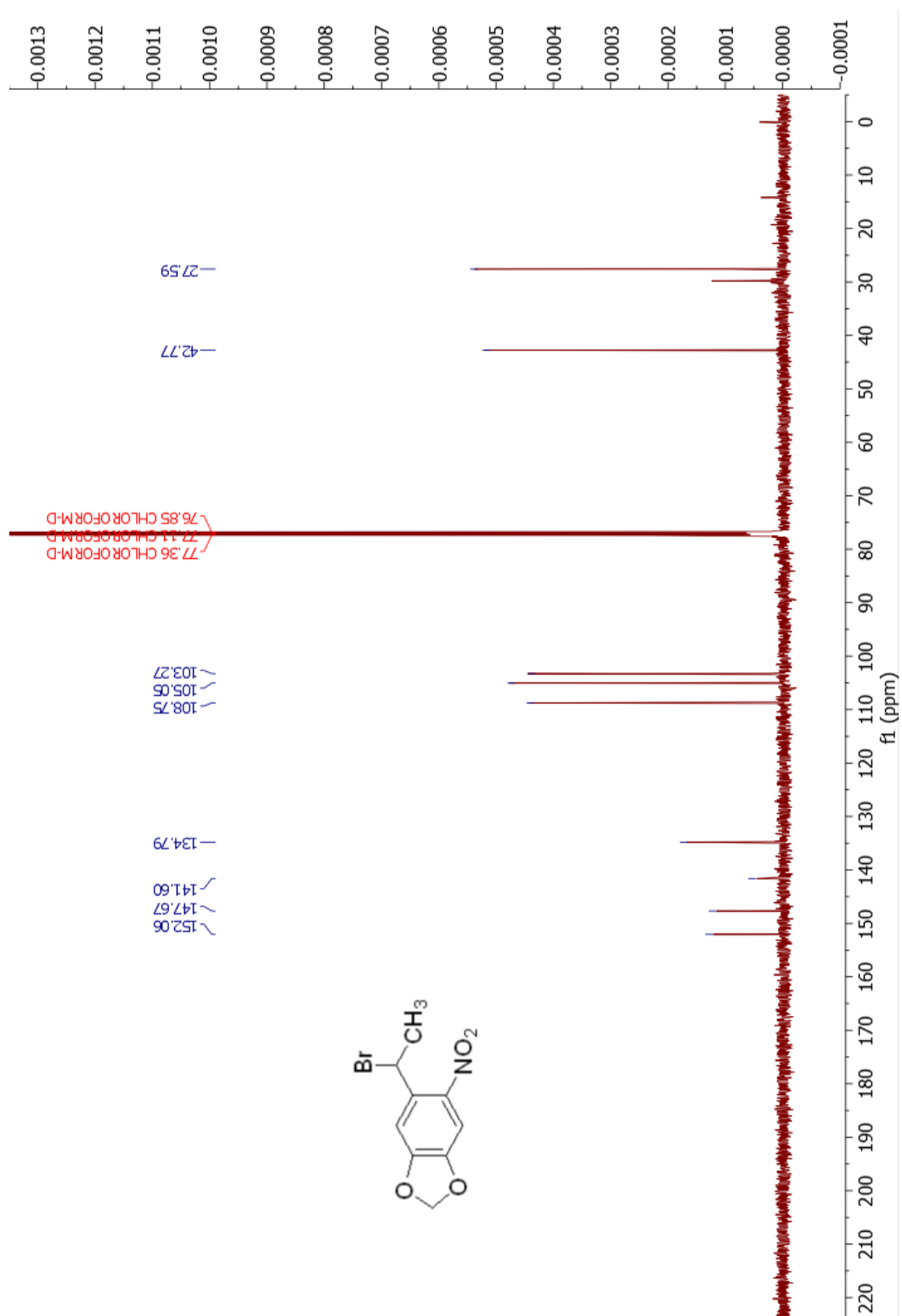
Figure A-5 ^{13}C NMR spectrum of 1- bromo-1-[4',5'-(methylenedioxy)-2'-nitrophenyl] ethane (**10**)
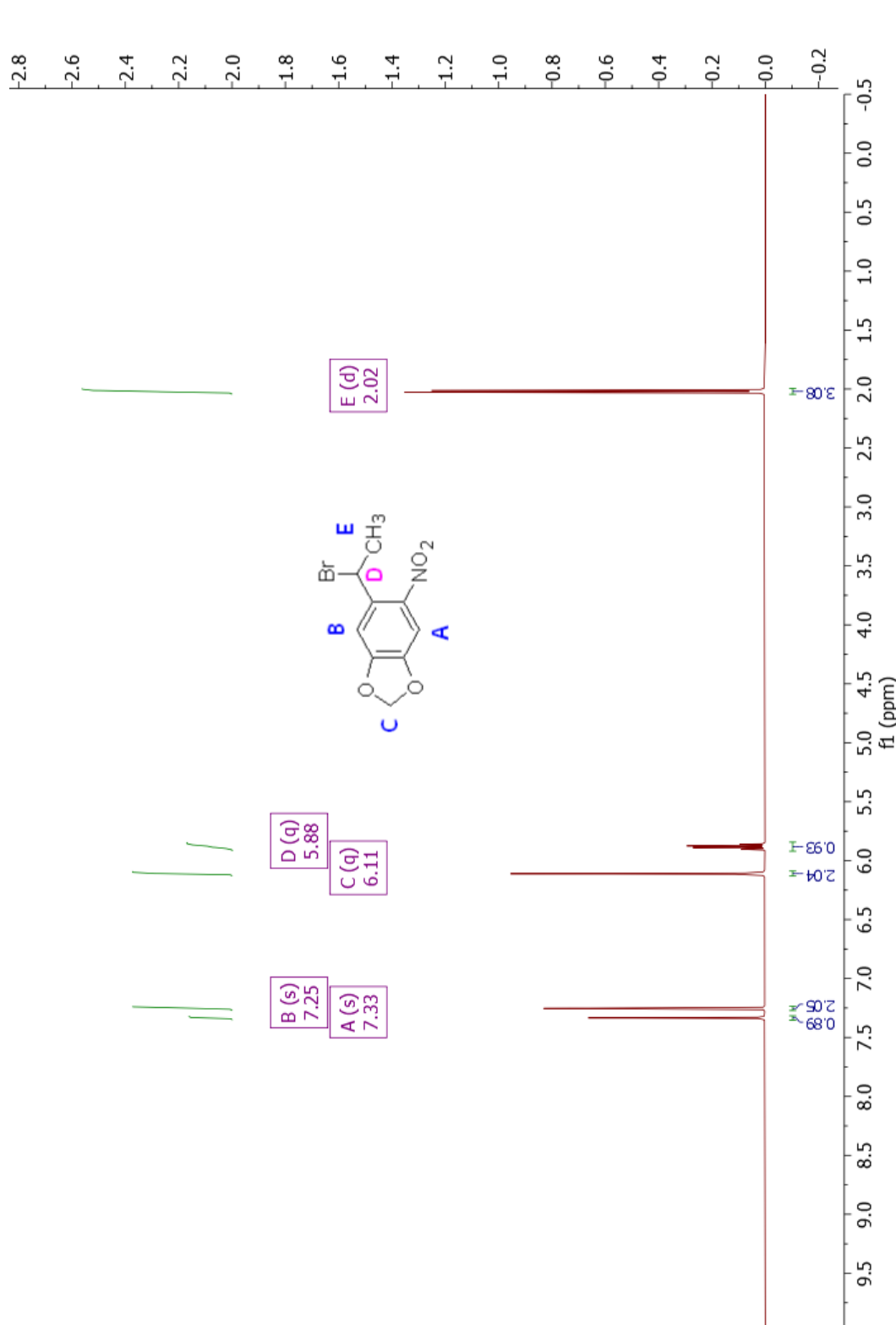
Figure A-6 ^{1}H NMR spectrum of 1- bromo-1-[4',5'-(methylenedioxy)-2'-nitrophenyl]
ethane (**10**)
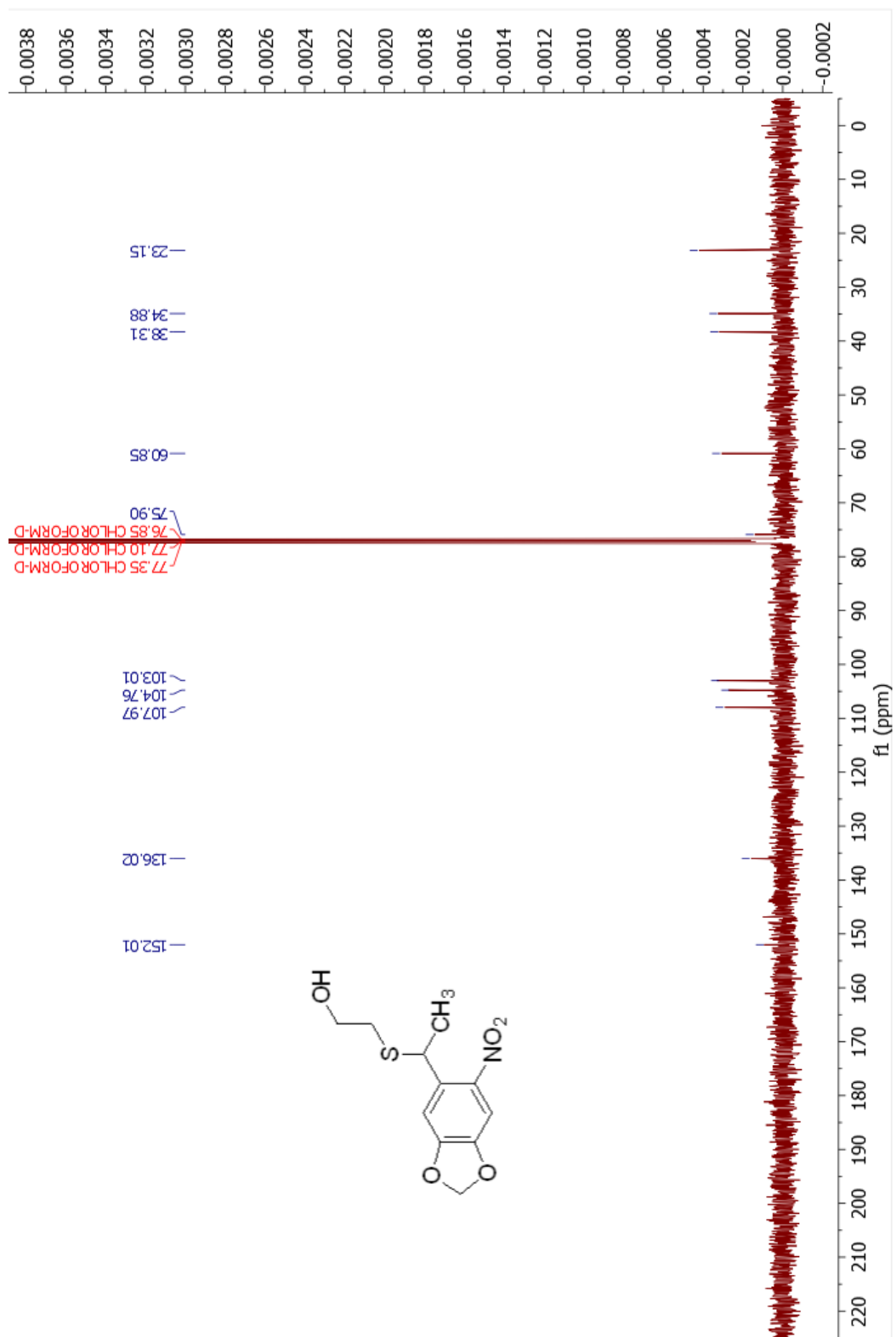
Figure A-7 ^{13}C NMR spectrum of 2-{[1-(6-Nitrobenzo[d][1,3]dioxol-5-yl)ethyl]thio} ethan-1-ol (**11**)
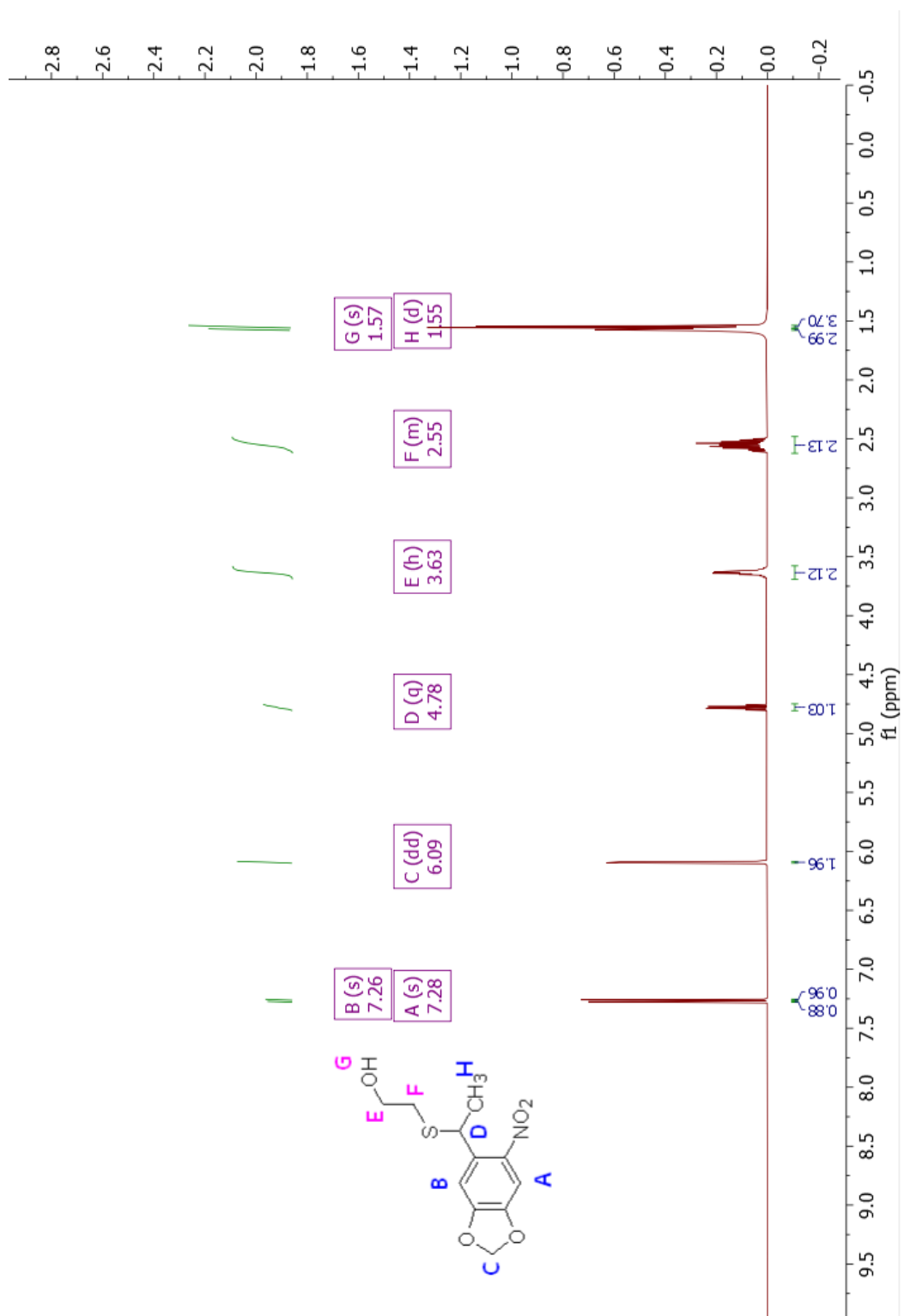
Figure A-8 ¹H NMR spectrum of 2-{[1-(6-Nitrobenzo[d][1,3]dioxol-5-yl)ethyl]thio} ethan-1-ol (**11**)
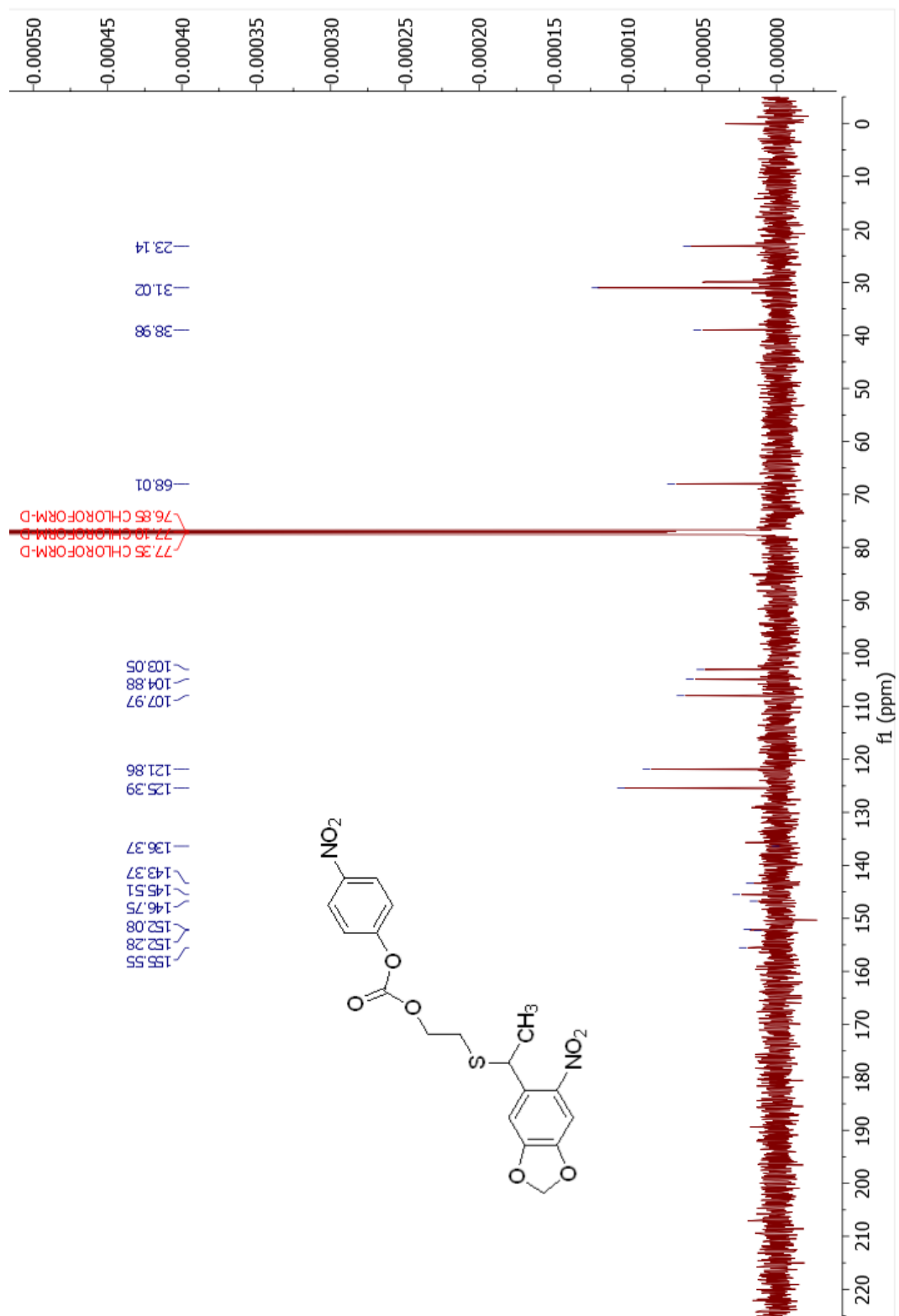
Figure A-9 ^{13}C NMR spectrum of 2-((1-(6-nitrobenzo[d][1,3]dioxol-5-yl)ethyl)thio)ethyl (4-nitrophenyl) carbonate (**12**)
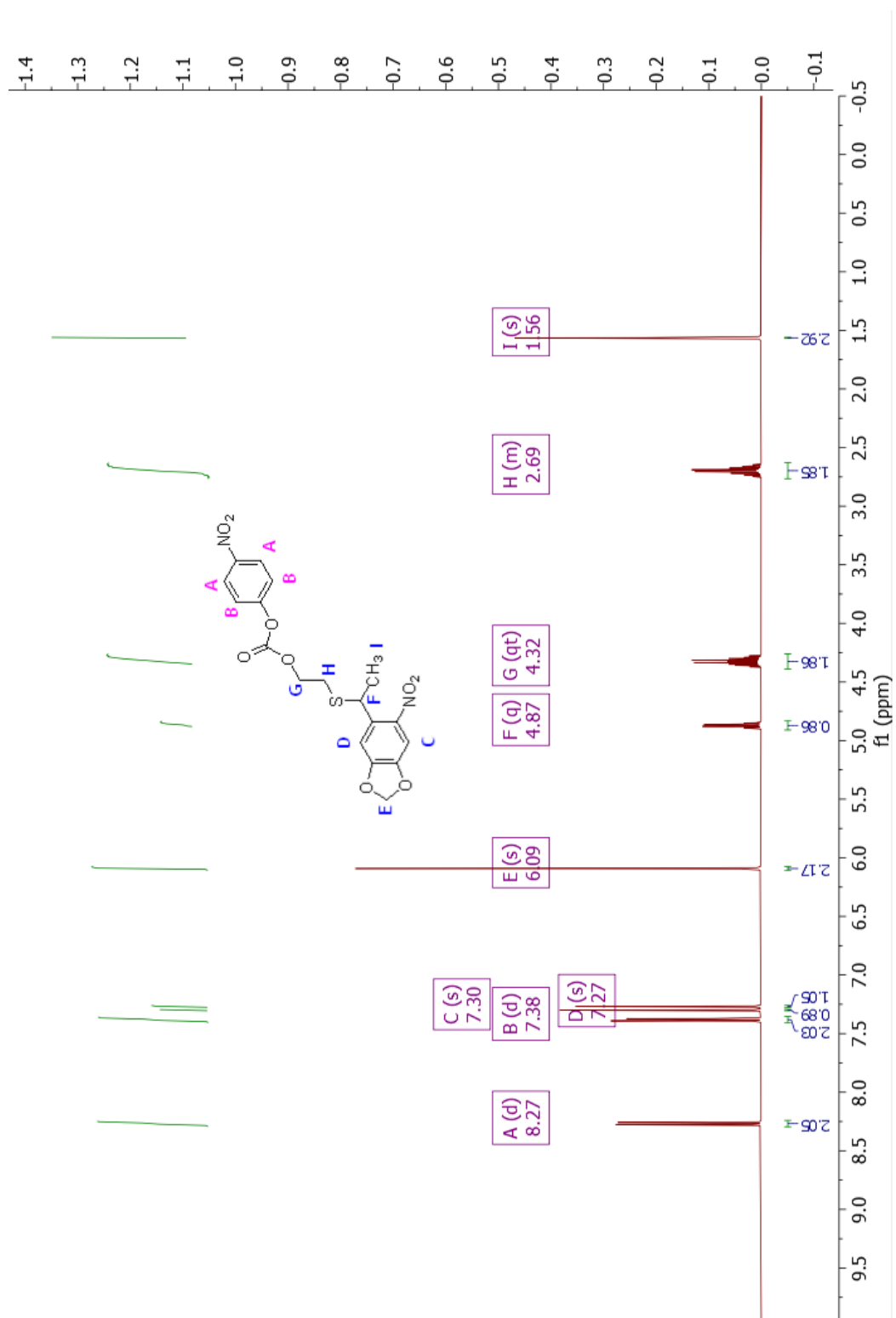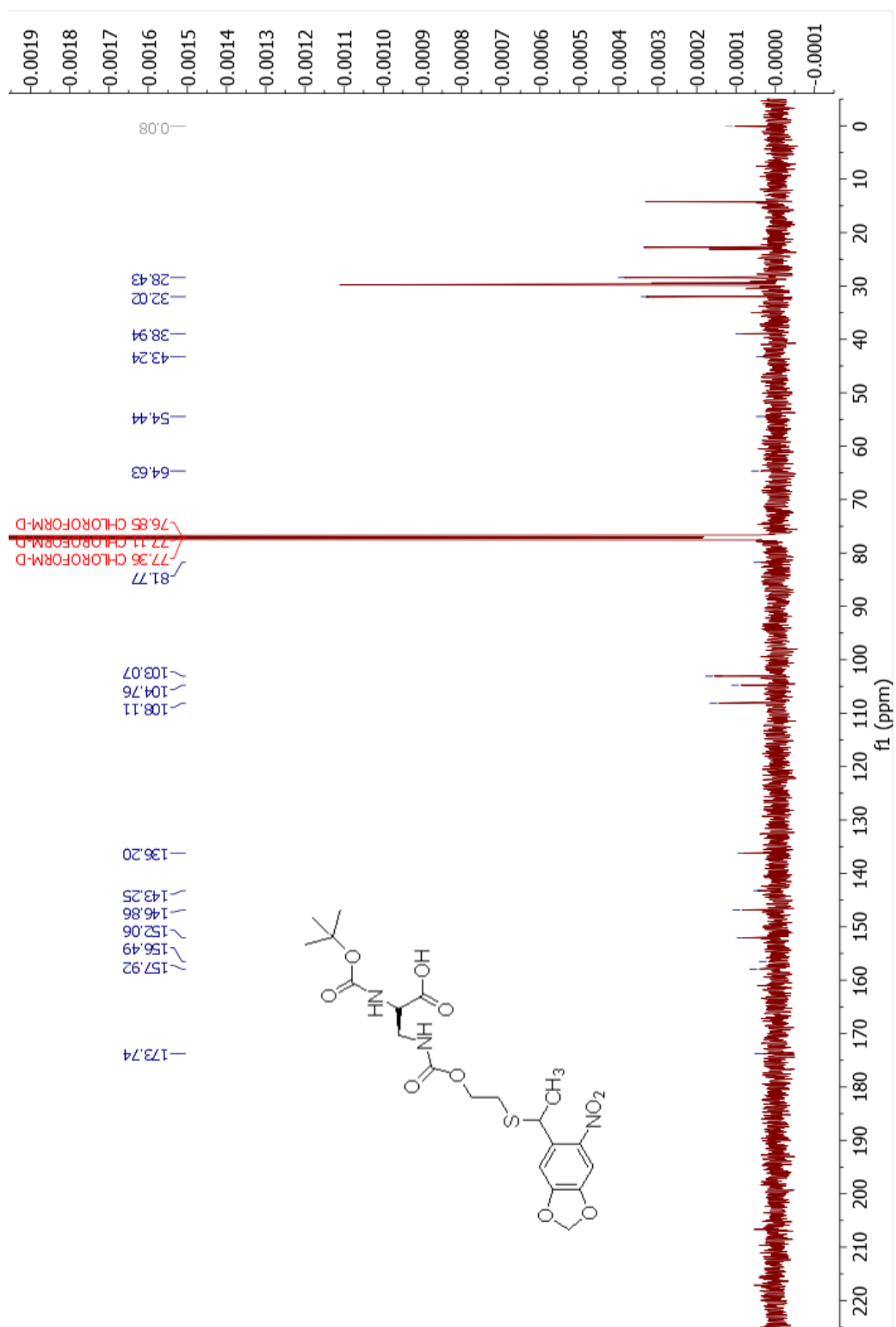
Figure A-10 ¹H NMR spectrum of 2-((1-(6-nitrobenzo[d][1,3]dioxol-5-yl)ethyl)thio) ethyl (4-nitrophenyl) carbonate (**12**)

Figure A-11 ^{13}C NMR spectrum of (2S)-2-[(tert-Butoxycarbonyl)amino]-3-{[(2-{[1-(6-nitrobenzo [d][1,3]dioxol-5-yl)ethyl] thio}ethoxy)carbonyl]amino}propanoic acid (**13**)
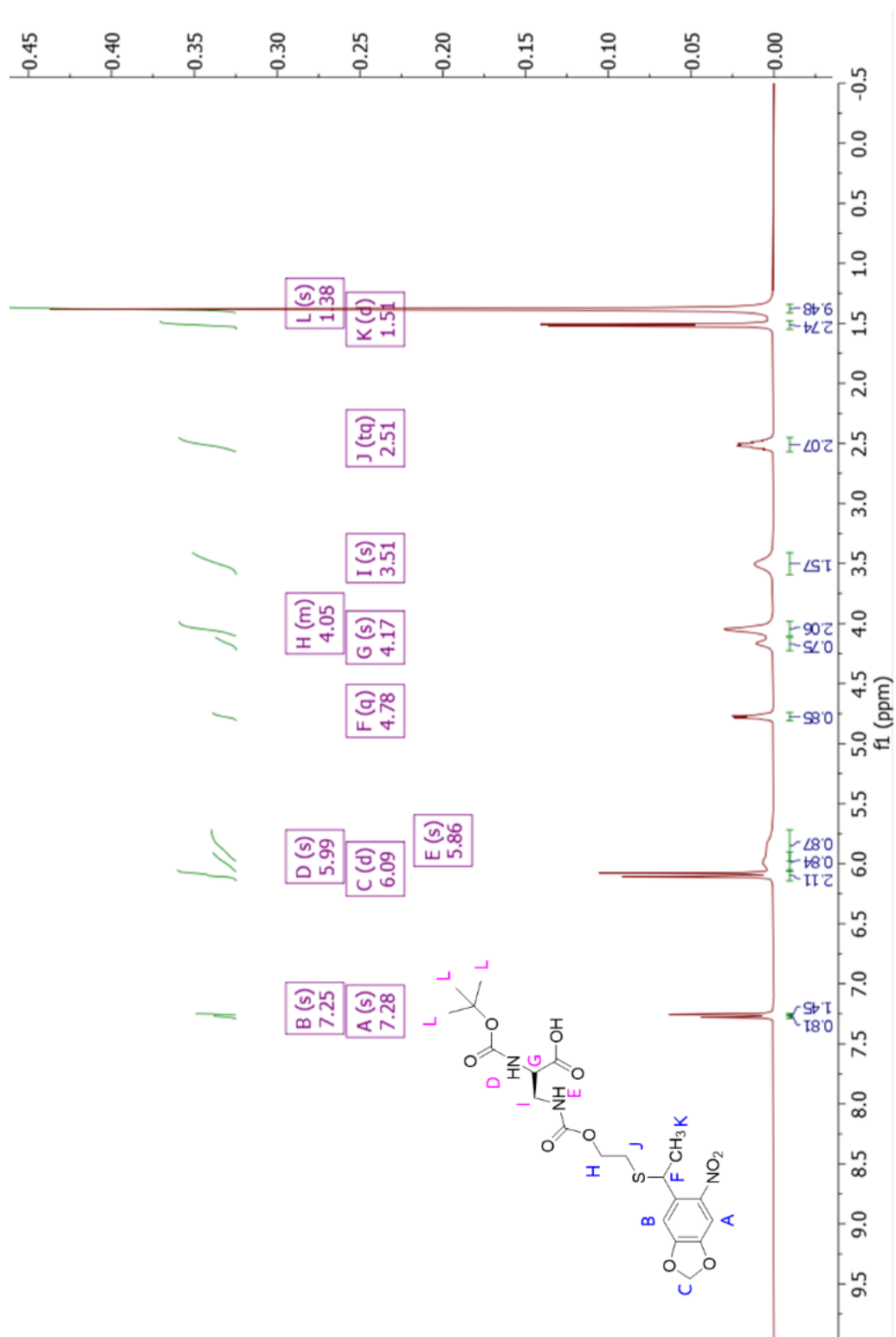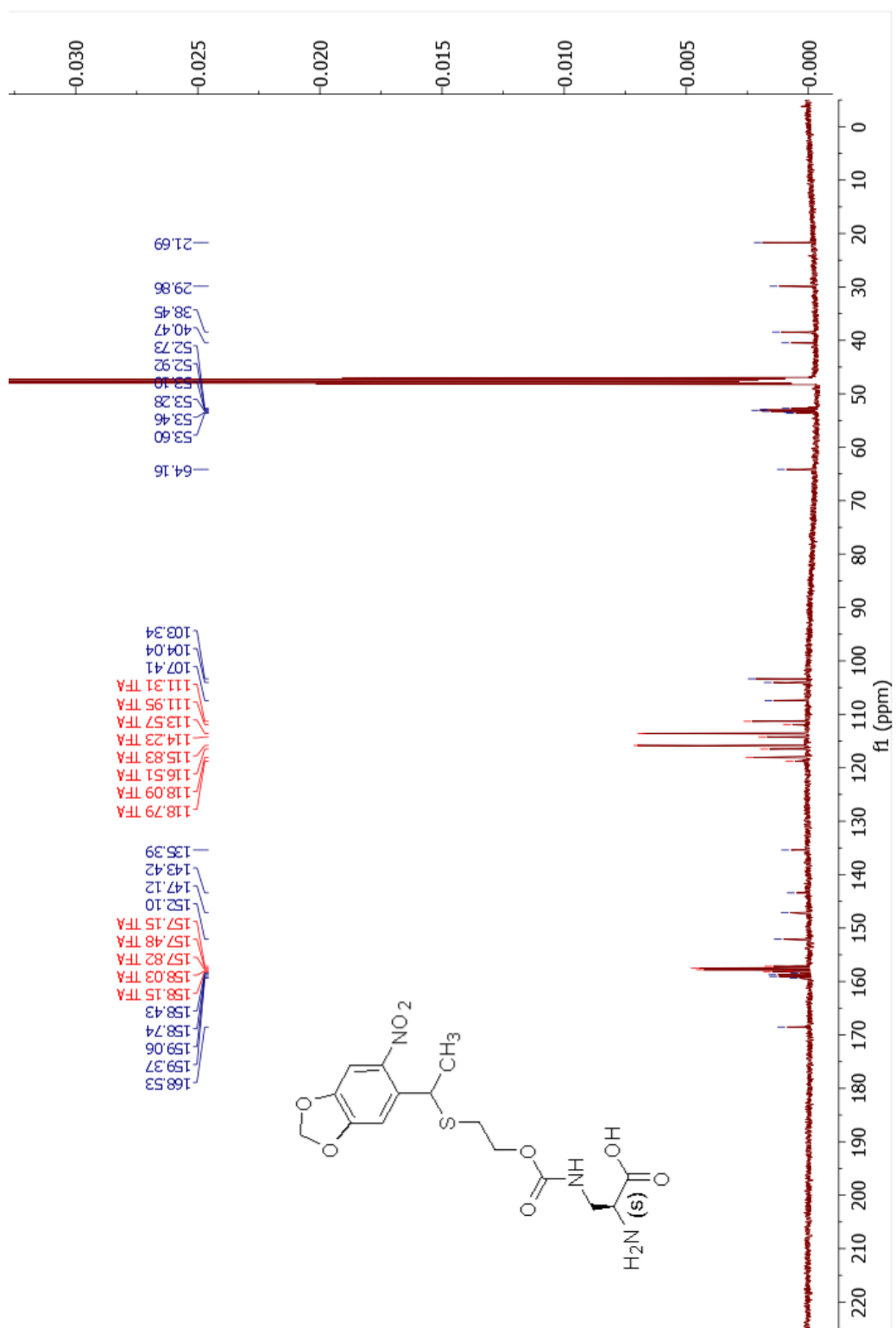
Figure A-12 ^{1}H NMR spectrum of (2S)-2-[(tert-Butoxycarbonyl)amino]-3-{[(2-{[1-(6-nitrobenzo [d][1,3]dioxol-5-yl)ethyl] thio}ethoxy)carbonyl]amino}propanoic acid (**13**)

Figure A-13 ^{13}C NMR spectrum of (2S)-2-amino-3-{[(2-{[1-(6- nitrobenzo[d][1,3]dioxol-5 yl)ethyl]thio}ethoxy) carbonyl]amino}propanoic acid (**6**)
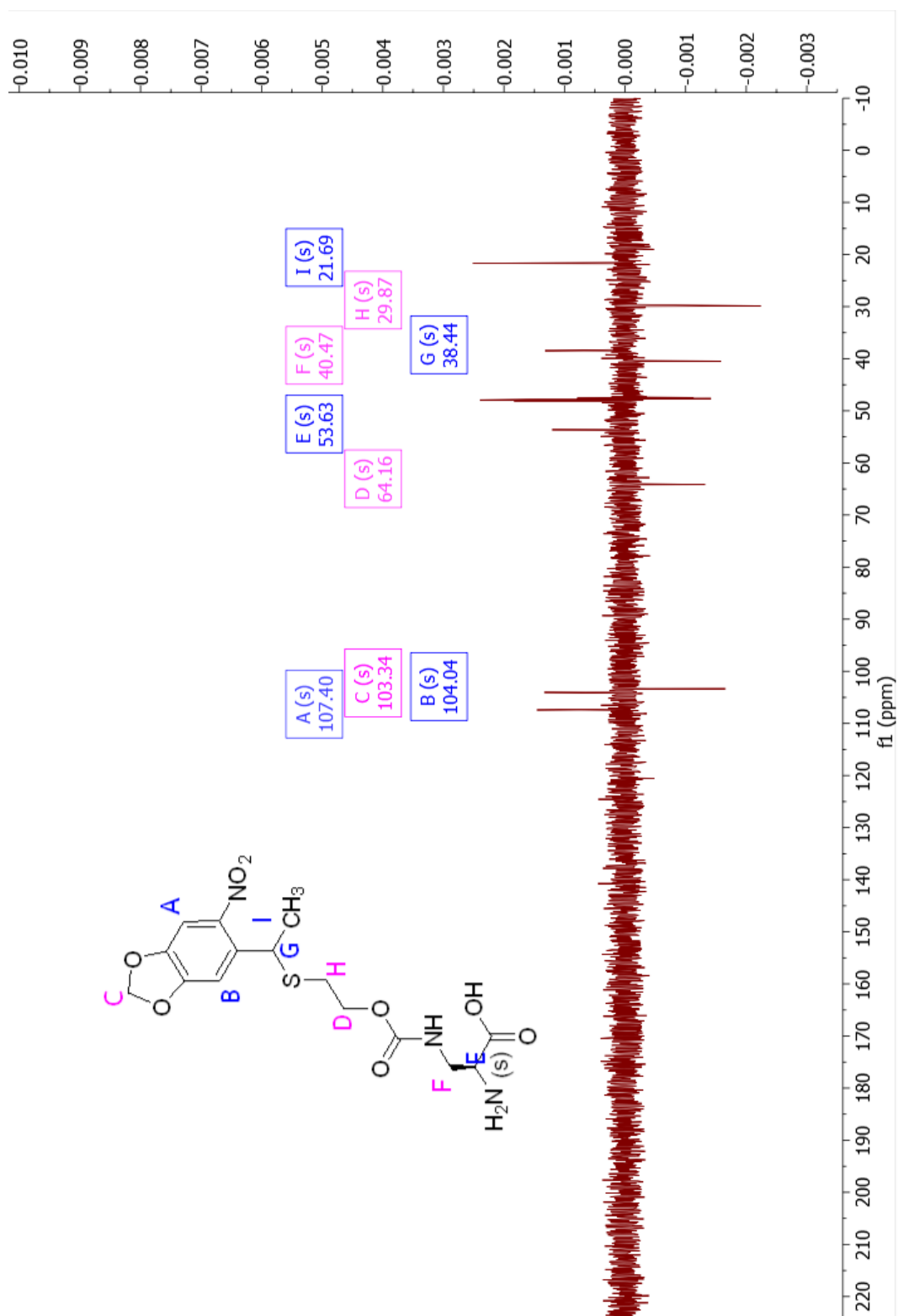
Figure A-14 ^{13}C NMR DEPT 135 spectrum of (2S)-2-amino-3-{[(2-{[1-(6- nitrobenzo [d][1,3]dioxol-5 yl)ethyl]thio}ethoxy) carbonyl]amino}propanoic acid (**6**)
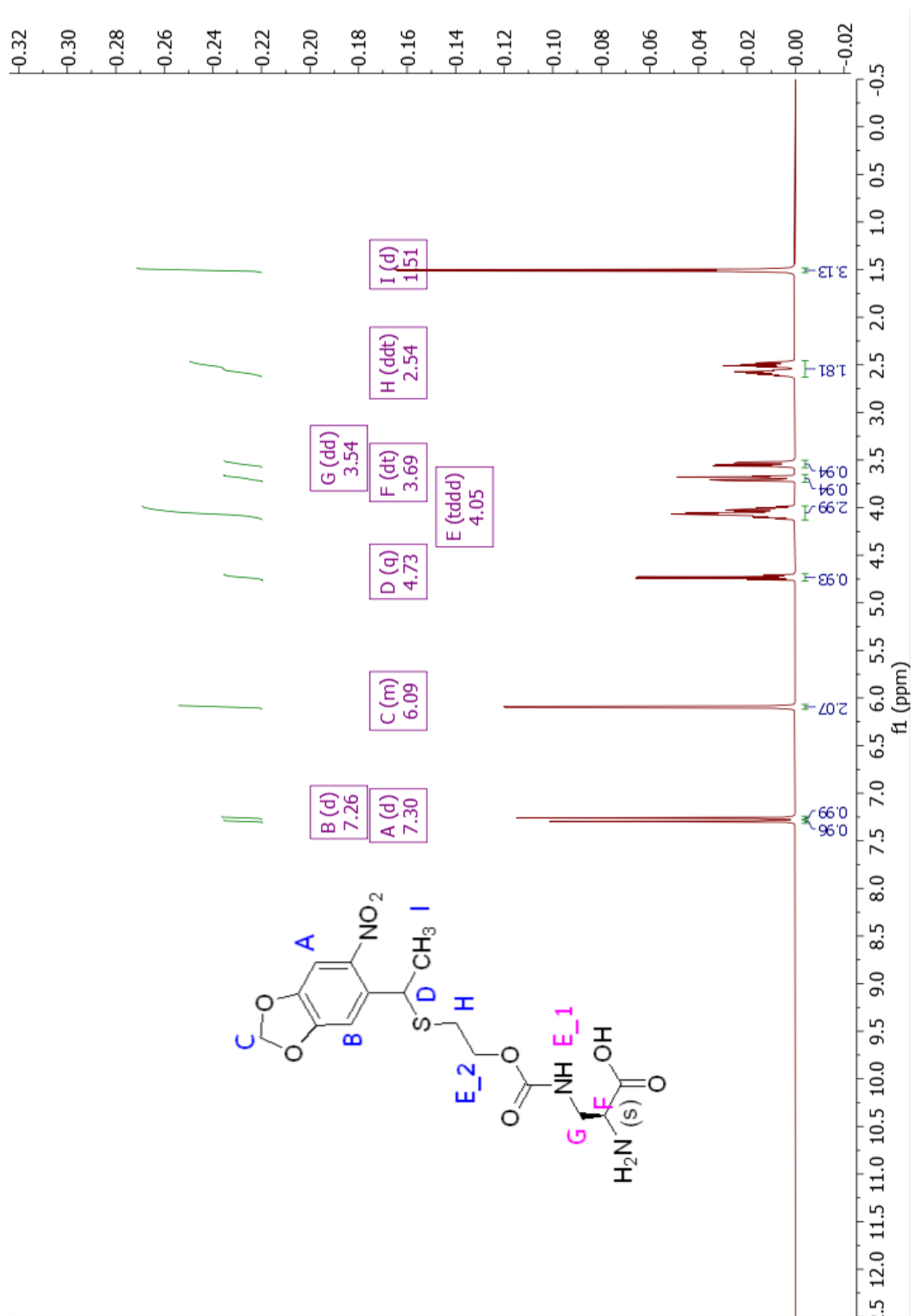
Figure A-15 ^{1}H NMR spectrum of (2S)-2-amino-3-{[(2-{[1-(6- nitrobenzo[d][1,3]dioxol-5 yl)ethyl]thio}ethoxy) carbonyl]amino}propanoic acid (**6**)
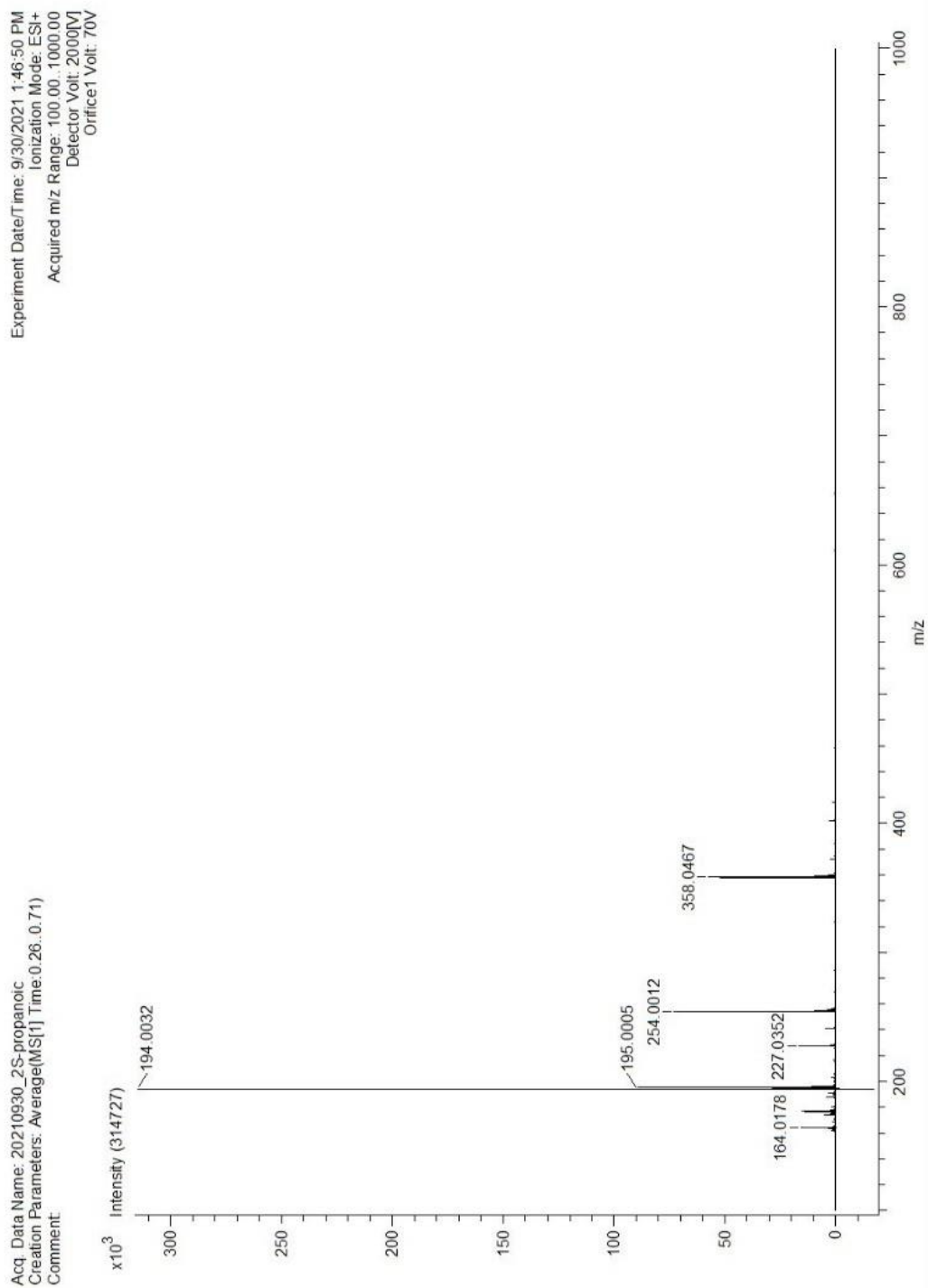
Figure A-16 Solid sample DART-MS of (2S)-2-amino-3-{[(2-{[1-(6- nitrobenzo[d]
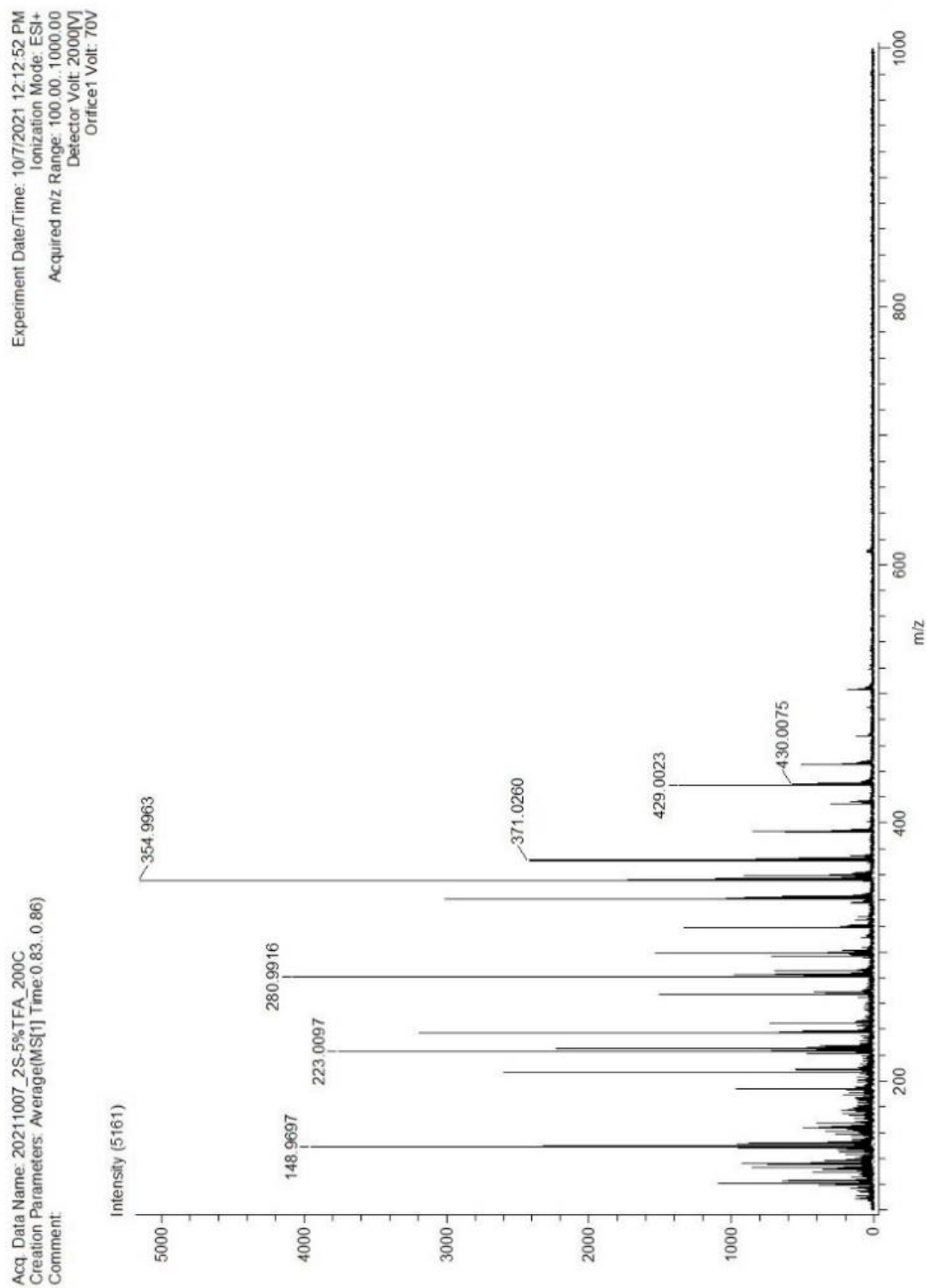[1,3]dioxol-5 yl)ethyl]thio}ethoxy) carbonyl]amino}propanoic acid (**6**) at 300 °C

Figure A-17 Liquid sample (15 mg in MeOD (5%TFA)) DART-MS of (2S)-2-amino-3-{[(2-{[1-(6- nitrobenzo[d] [1,3]dioxol-5 yl)ethyl]thio}ethoxy) carbonyl]amino} propanoic acid (**6**) at 200 °C
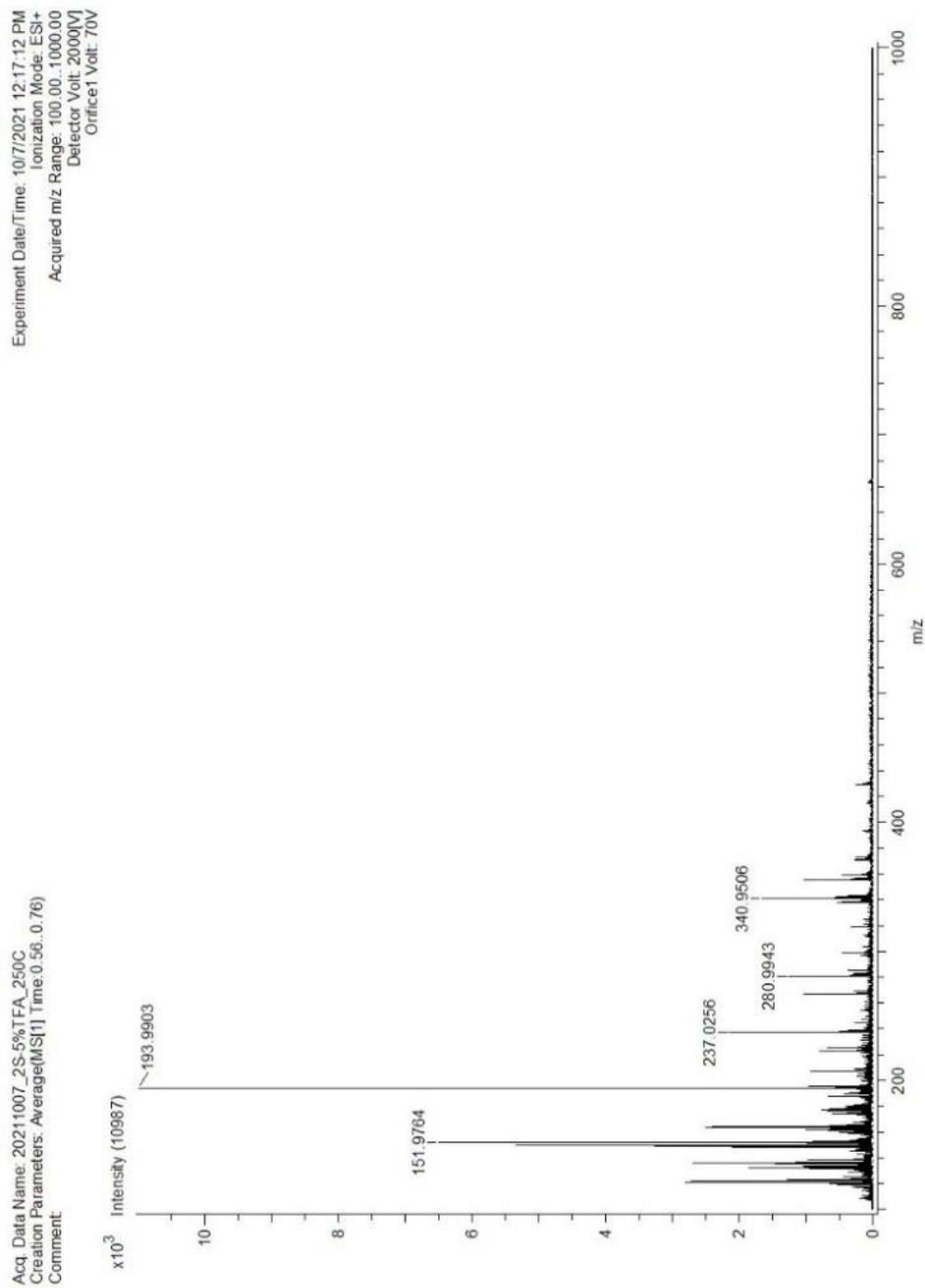
Figure A-18 Liquid sample (15 mg in MeOD (5%TFA)) DART-MS of (2S)-2-amino-3-{[(2-{[1-(6- nitrobenzo[d][1,3]dioxol-5yl)ethyl]thio}ethoxy)carbonyl]amino}propanoicacid (**6**) at 250 ℃
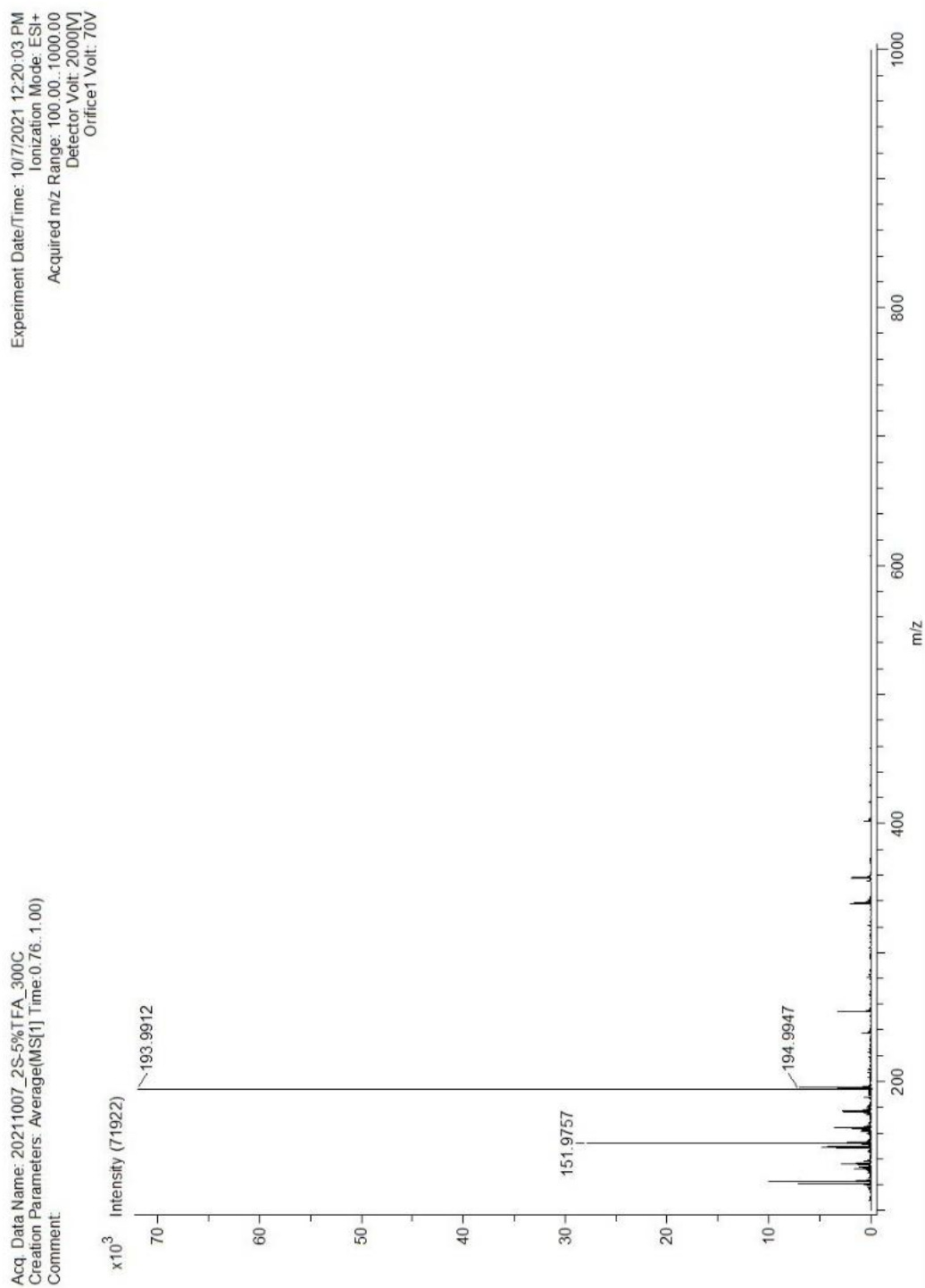
Figure A-19 Liquid sample (15 mg in MeOD (5%TFA)) DART-MS of (2S)-2-amino-3-{[(2-{[1-(6- nitrobenzo[d] [1,3]dioxol-5 yl)ethyl]thio}ethoxy) carbonyl]amino} propanoic acid **(6)** at 300 °C
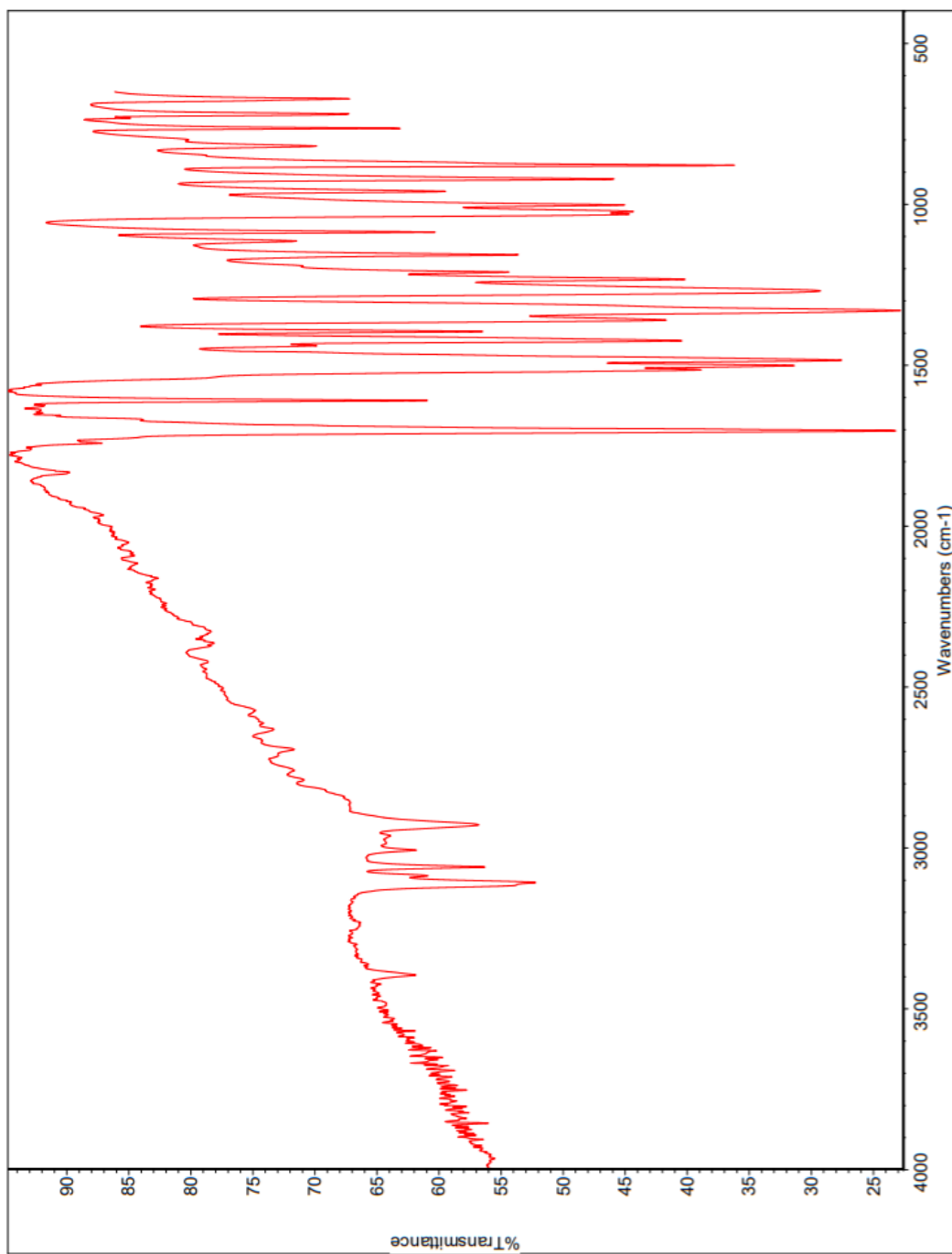
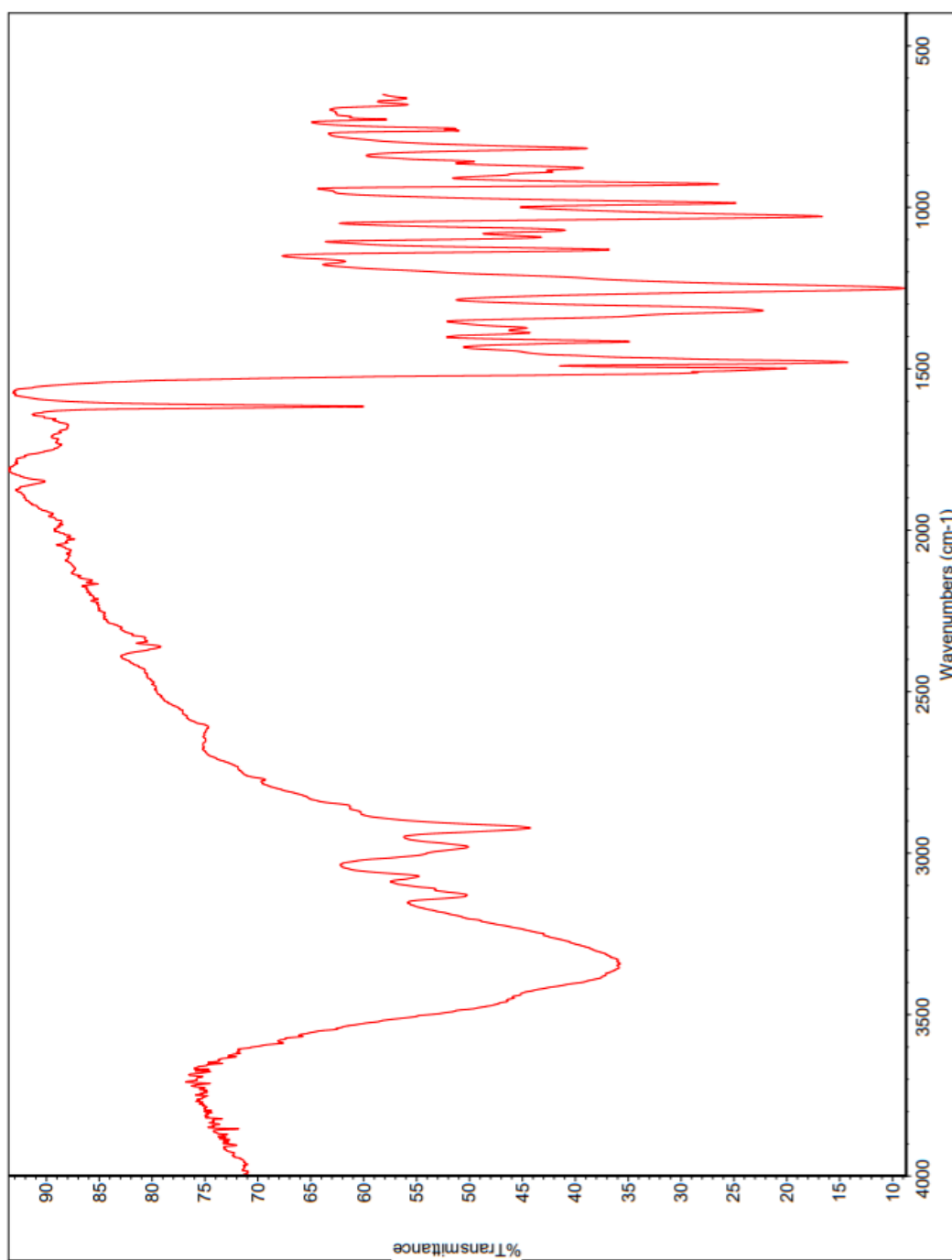**Figure A-20** FTIR spectrum of 4',5'-methylenedioxy-2'-nitroacetophenone (**8**)

Figure A-21 FTIR spectrum of 1-[4',5'-(methylenedioxy)-2'-nitrophenyl]ethanol (**9**)
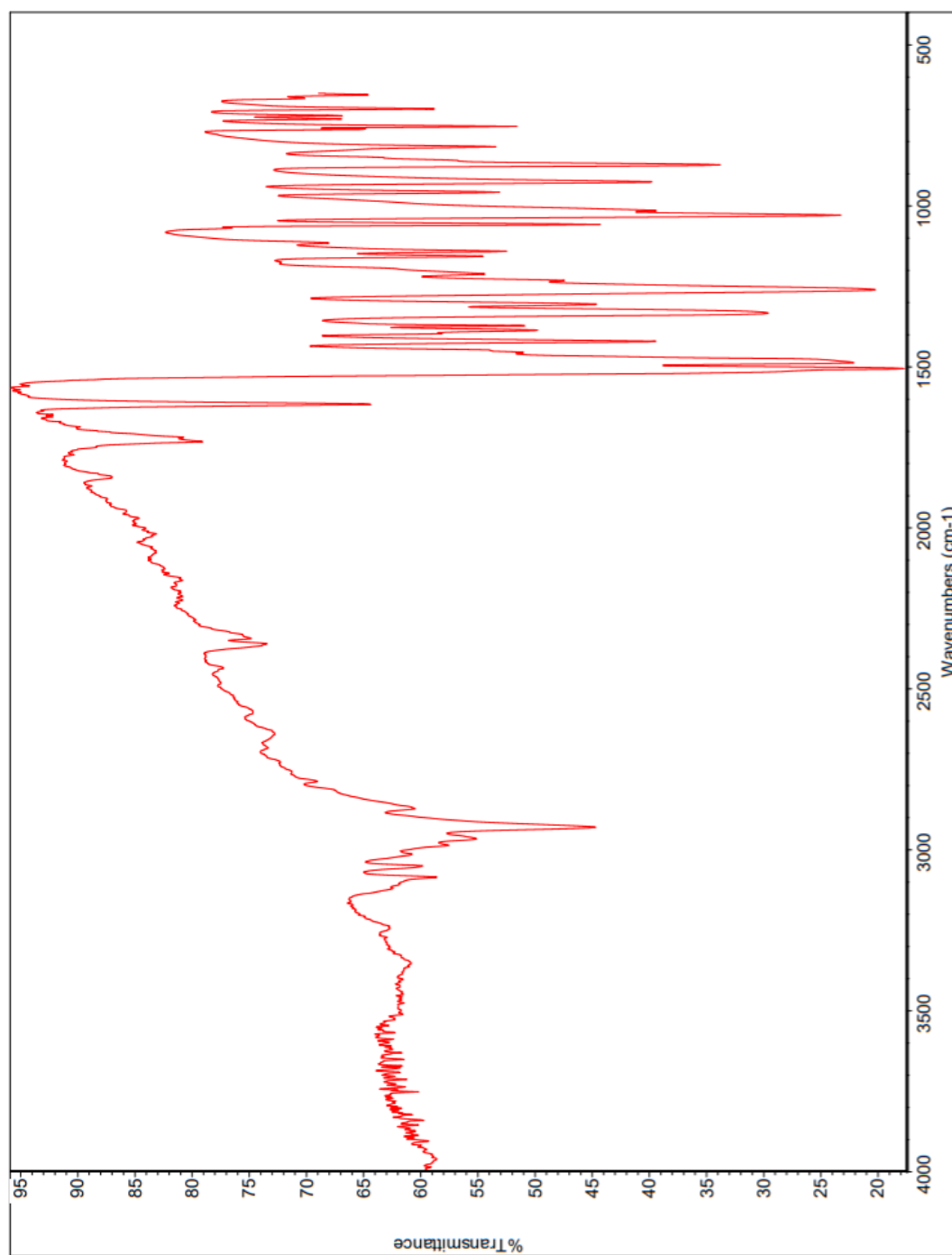
Figure A-22 FTIR spectrum of 1-bromo-1-[4',5'-(methylenedioxy)-2'-nitrophenyl]
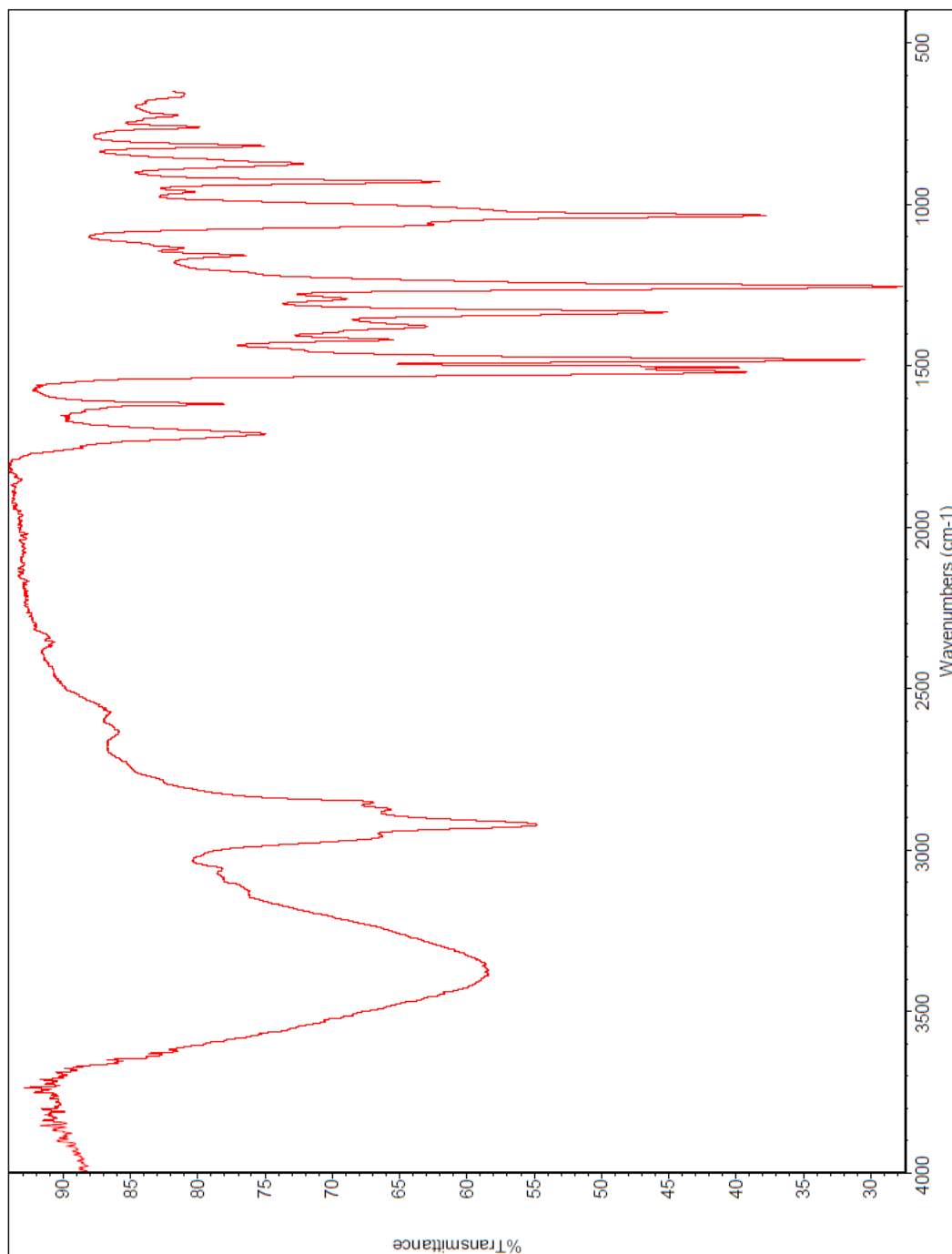
ethanel (**10**)

Figure A-23 FTIR spectrum of -{[1-(6-Nitrobenzo[d][1,3]dioxol-5-yl)ethyl]thio}ethan-1-ol (**11)**

Primer	Length	🌈	Binding Sites	⇅	Tm	Date Added
His-SuMO pHND-OVL F	57-mer		5561 .. 5617	1	67°C	
/sequence = TTTGTTTAACTTTAAGAAGGAGATGTACATATGcatcatcatcatcatcacagcagc 35% GC / 17,508.5 Da						
His-SUMO R	26-mer		6006 .. 6031	↳	60°C	
/sequence = ggatccaccaattcgtttcttctttgtgag 50% GC / 7937.2 Da						
nosigPETase OVL-SUMO F	42-mer		6010 .. 6051	1	71°C	
/sequence = cagagaacagattggtggatcccagaccaatccgtatgcgcg 55% GC / 12,957.5 Da						
Fw_nosigPETase_pET21b_NdeI	29-mer		6032 .. 6051	1	61°C	
/sequence = AAACATATGCAGACCAATCCGTATGCGCG 48% GC / 8879.8 Da						
PETase_S160*_R	20-mer		6398 .. 6417	↳	61°C	
/sequence = ACACCCATGCGGGCAGTATC 60% GC / 6087.0 Da						
PETase_S160*_F	23-mer		6418 .. 6440	1	68°C	
/sequence = GATGGGCTGGtagATGGGGGCG 70% GC / 7281.8 Da						
PETase_TGA_XhoI_R	40-mer		6796 .. 6829	↳	69°C	
/sequence = AAAAACTCGAGTCAggaacagttcgcggtgcgaaatcc 48% GC / 12,356.1 Da						
PETase_TGA XhoI-OVL R	48-mer		6803 .. 6850	↳	74°C	
/sequence = AGCAGCCTAGGTTAATTAAGCCTCGAGTCAggaacagttcgcggtgcg 54% GC / 14,857.7 Da						

Figure A-24 Sequence: M_pNHD1.3 His-SUMO nosigPETase-S160tag.dna
(Circular / 6975 bp) : total 8 Primers

VITA

NAME   Jariya Jitdee

DATE OF BIRTH   30 December 1995

PLACE OF BIRTH   Chom Bueng, Ratchaburi, Thailand

INSTITUTIONS ATTENDED   2014 - Kururatrungsarit school

2018 - B.Sc. (Chemistry), Second Class Honours,

Department of Chemical Technology, Faculty of Science

and Technology, Suan Dusit University

HOME ADDRESS   House No. 23, Village No. 3, Sub-district Rangbua, District

Chombueng, Province Ratchaburi, 70150